Doctoral Dissertation
Doctoral Program in Mechanical Engineering (32.nd cycle)

Offset-Free Model Predictive Control for Active Magnetic Bearings

Luis Miguel Castellanos Molina
* * * * * *

Supervisors
Prof. Andrea Tonoli, Supervisor
Prof. Nicola Amati, Co-supervisor

Referees
Prof. Patrick Keogh, University of Bath
Prof. Jarir Mahfoud, Laboratoire de Mécanique des Contacts et des Structures

Politecnico di Torino
May 17, 2020

I hereby declare that, the contents and organisation of this dissertation constitute my own original work and does not compromise in any way the rights of third parties, including those relating to the security of personal data.

. . . . . .

Luis Miguel Castellanos Molina

Turin, May 17, 2020

Summary

This thesis deals with the study of Offset-Free Model Predictive Control (OF-MPC) for Active Magnetic Bearing (AMB) systems. OF-MPC is a systematic approach to optimally handle the trade-off between control effort and controlled outputs taking into account plant dynamics and constraints. The term "Offset-Free" stands for the possibility to compensate the plant-model mismatch and guarantee zero-offset at steady state based on the external disturbance estimate. A procedure for the overall design is presented and supported by numerical simulations and experimental works conducted in two test rigs: a single-degree-of-freedom AMB system and a more complex cone-shaped AMB system. The results demonstrate that with OF-MPC the coil current limitations are optimally handled and the plant-model mismatch is quantified real-time in terms of disturbance forces. The approach is also effective in guaranteeing stability and rejecting external disturbance forces. The application of OF-MPC is a novel and promising constrained optimal control technique for cone-shaped AMB systems since the main control difficulties: (i) coupling of radial and axial control actions, and (ii) the low force generation capability in axial direction, can be addressed in a clear and systematic way. The results also demonstrate that OF-MPC outperforms Proportional-Integral-Derivative controllers in the compensation of axial external forces. The main contribution of this thesis is the numerical and experimental demonstration of the potentiality of OF-MPC for AMB systems, together with a methodology for its implementation. Furthermore, the control algorithm is described in detail showing how to: reduce the computational burden of the control problem, generate OF-MPC solvers from C code generation tools and design properly the plant state estimator.

Acknowledgements

First of all, I would like to express my gratitude to my dissertation supervisors, Prof. Andrea Tonoli and Prof. Nicola Amati. They have been a constant source of encouragement and insight during my research and helped me with numerous problems and professional advancements.

I would like to thank my friend and research colleague Prof. Boris Vega Lara for his great and catching enthusiasm for control problems. Large thanks go to him for encouraging and long talks about model predictive control. I started loving MPC because of him.

I greatly thank my friend Lester Suárez who introduced me to the LIM laboratory. His vision and daily-life lessons have been valuable to me.

Special thanks go to the staff of the LIM Mechatronics Lab, who maintained a pleasant and flexible environment for my research.

My greatest thanks go to my wife, for her infinite patience and care.

To my parents

Contents

List of Tables

List of Figures

Chapter 1

Introduction

The purpose of this chapter is to introduce the active magnetic bearings technology and a variant of Model Predictive Control (MPC) called Offset-Free MPC (OF-MPC) as a candidate for controlling AMB systems. The main motivations, the goal of the study and the thesis structure are detailed here.

1.1 Active Magnetic Bearings

An Active Magnetic Bearing (AMB) is a mechatronic system that supports a rotating shaft using magnetic levitation. There is no contact between bearing and rotor, and this permits high-speed operation with no lubrication and no mechanical wear. A special advantage of these unique bearings is that the rotordynamics can be controlled actively through the bearings [1]. Some application examples are: turbomolecular pumps, flywheel energy storage systems, turbo blowers, heart pumps and turbo compressors. The number of industrial AMB applications is growing steadily. Figure 1.1 shows a turbocompressor on AMBs.

1.2 Principles of Magnetic Bearing Function

Generating contact free magnetic field forces by actively controlling the dynamics of an electromagnet is the principle which is actually used most often among the magnetic suspensions. Figure 1.2 shows a general schematics of the parts involved in an AMB application. On each controlled degree of motion, a sensor measures the displacement of the rotor from its reference position, a microprocessor as a controller derives a control signal from the measurement, a power amplifier transforms this control signal into a control current, and the control current generates a magnetic field in the actuating magnets, resulting in magnetic forces in such a way that the rotor remains in its hovering position [1].

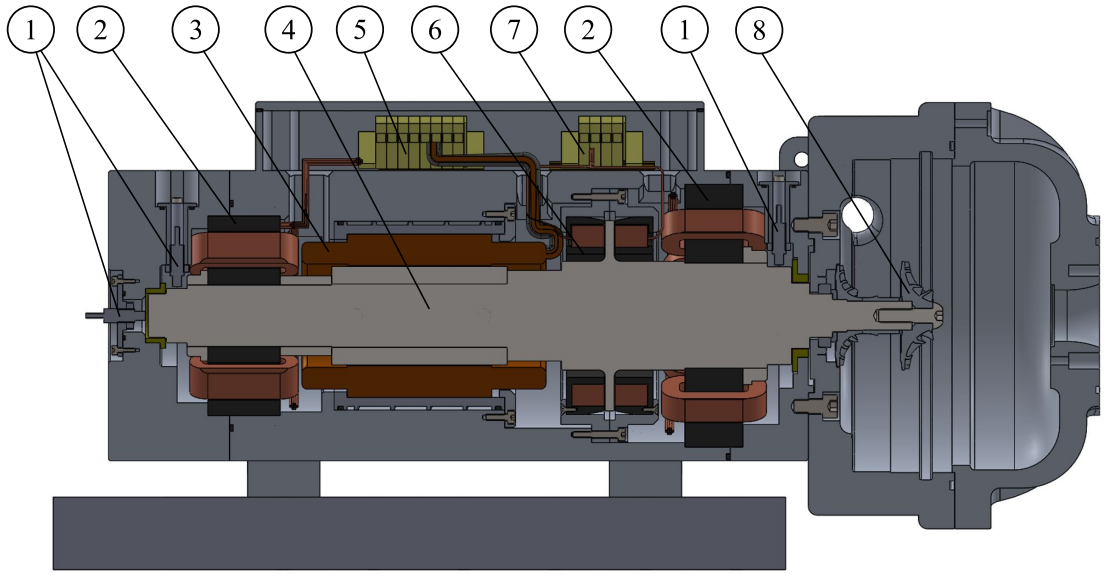

Figure 1.1: Turbo-compressor on AMBs. 1) Displacement sensors. 2) Radial magnetic bearings. 3) Electric motor. 4) Rotor. 5) Strip connector for the AMBs. 6) Thrust magnetic bearings 7) Motor strip connector. 8) Impeller.

An increasingly important part in AMB systems is software. The inherent ability for sensing, information processing and actuation give the magnetic bearing the potential to become a key element in smart and intelligent machines [1] in resonance with the actual needs of digital transformation by integrating automation, software, and cutting-edge technologies. An AMB can be seen today as an intelligent mechatronics system. The reader is invited to visit SIMOTICS (Siemens), MECOS, CALNETIX, SKF, etc. as examples of relevant manufacturers of AMB systems.

1.3 Thesis motivation

1.3.1 Control techniques for active magnetic bearings

AMB systems are strongly nonlinear and unstable in open-loop. There exists a vast literature about linear and nonlinear control solutions that are commonly exploited on these systems. In essence, the goal is to stabilize the rotor position (controlled outputs) at a nominal air gap by manipulating the electromagnetic forces produced by the bearings.

Most applications of AMB systems for rotating machinery are primarily concerned with steady behavior: analysis focuses on response to steady sinusoial loads such as mass unbalance, shaft bow, aerodynamic loads, and sensor noise. Such an approach is even commonly adopted when considering transient phenomena such as compressor surge. Notable exceptions to this include mobile applications (trains, aircraft, vessels)

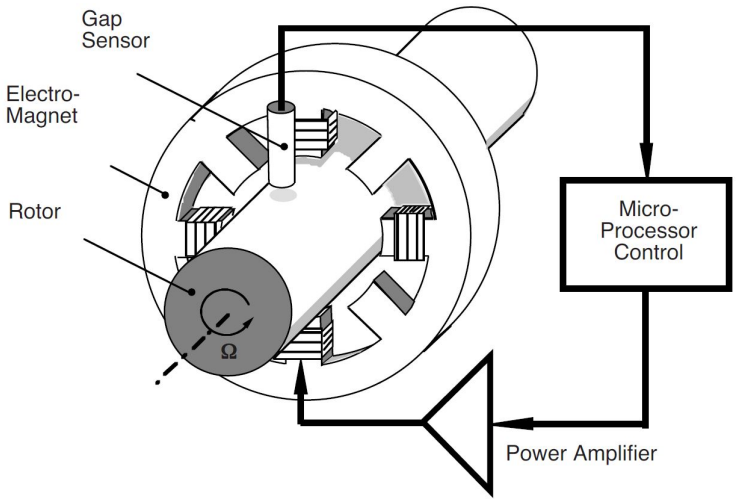

Figure 1.2: Function principle of an active electromagnetic bearing, suspension of a rotor in vertical direction. Image source: reference [1].

i.e., systems subject to extreme impact loading such as underwater naval vessels [2].

The literature contains many detailed application examples where the performance objectives in AMB controller synthesis are elucidated [3, 4, 5, 6],[1, § 12.4]. Generally, the obvious objectives include an adequate stability margin and adequate management of external loads. Given the underlying nonlinear character of AMB systems, a common secondary objective is to maintain operation in an essentially linear regime, avoiding numerous sources of nonlinearity including actuator magnetic saturation, amplifier voltage saturation, and actuator nonlinearity due to large journal displacements [2].

The approach of setting up a decentralized or local feedback control scheme for a rigid body AMB system, is physically well justifiable and features, as one of its most important advantages, control parameters that can be designed solely based on physical considerations by selecting appropriate stiffness and damping values. Despite the fact that this approach utilizes the magnetic bearings in the same way as mechanical springs and dampers without taking further advantage of their numerous capabilities, it has been shown that decentralized control is very applicable to a large number of AMB systems without major deficiencies [1, 7].

The most straightforward and intuitive approach for designing a control law for the rigid rotor in AMBs is by implementing a PID control scheme (locally for each bearing unit and separately for each bearing). However, local PD or PID control can also lead to substantial problems when the AMB rotor system exhibits specific (and common) properties such as sensor non-collocation issues or plant dynamics with large difference between the open-loop eigenvalues. A solution to this deficiency is proposed in references [1, § 8.2.3] and [8] with a decoupled control of parallel and conical modes.

When using decentralized control, the multi-variable nature of the system is not

exploited properly. That is why other feedback control techniques such as Linear-Quadratic-Gaussian (i.e., the combination of a Linear Quadratic Regulator (LQR) and a Kalman filter) and pole-placement controllers have been studied in the AMB literature [9, 10, 11]. However, multi-variable state-feedback controllers are almost always avoided because of (i) potential robustness problems due to uncertainties in the dynamics of the state estimator and (ii) "poor" robustness properties associated to the combination of an estimator with the state feedback controller. The fact is that the stability margins obtained from the LQR formulation are no longer guaranteed when it is combined with a state estimator [12]. Nevertheless, LQR is often used to design decentralized PD/PID controllers from the optimal feedback gain it generates from the trade-off between control efforts and the deviation of the controlled variables. Usually PD/PID generated from LQR gains can guarantee good stability properties [11]. Even when robust control techniques such as μ-Synthesis or H_∞ are preferred [2], an initial stage based on LQR is suggested to establish the loop shape [12]. This is because AMB systems are unstable plants with multiple gain crossover frequencies and these control techniques rely on "confined" model uncertainties which are sometimes difficult to obtain [2]. For a detailed review of control solutions for AMB system the reader is directed to references [13, 14], [1, § 8].

Model predictive control and active magnetic levitation

MPC is a control method that computes the control input of a system by solving an Optimal Control Problem (OCP) in real time. The aim of the OCP is to optimize the trajectory of the system with respect to a cost function that is defined based on economic or performance measures. A MPC controller uses a model of the system to predict its behavior within a finite horizon. When using MPC, the following procedure is executed at each time step:

1. Measure/estimate the current state.
2. Solve the OCP to compute a sequence of control inputs.
3. Apply the first step in the control input sequence to the system.

Model predictive control has had an exceptional history with early intimations in the academic literature coupled with an explosive growth due to its independent adoption by the process industries where it proved to be highly successful in comparison with alternative methods of multivariable control [15]. Its phenomenal success in the process industries was mainly due to its conceptual simplicity and its ability to handle easily and effectively complex systems with hard control constraints and many inputs and outputs [16]. With the advancements of MPC algorithms and controllers' computational power, MPC is increasingly being adopted in other industries such as robotics, automotive and aerospace.

The study of MPC for active magnetic levitation is not new. The benefits of applying linear and nonlinear MPC for active magnetic levitation were demonstrated by many numerical and experimental results in [17, 18, 19, 20, 21, 22] for systems with a single degree of freedom. When using MPC the air gap deviations can be directly written as state constraints together with the limitation of the coil currents and actuator bandwidth (input constraints). Numerical comparisons of MPC with conventional PID controllers are presented by the authors in [23, 24] for flywheel energy storage systems with radial AMBs. Zhao et al. presented a MPC for a flexible rotor on AMBs which effectively stabilizes the rotor-AMB system with remarkably mitigated rotor vibrations in [25]. However, the results are limited to numerical simulations and assuming full state knowledge.

Some of the benefits of applying MPC on AMBs can be summarized as follows:

- MPC is a multivariable control technique. Only one MPC controller design is needed.
- AMB limitations on coil current, actuator bandwidth and air gap deviation can be included from the beginning in the controller design and hence optimally handled every time step.
- Trade-off between actuation effort and rotor displacement can be directly tuned. By selecting a proper objective function, the control performance can be tuned through states and inputs weights of the OCP similarly to the mixed optimization approach (i.e., trade-off between rotor response and use of control effort) in unbalance control [1, § 12.4].
- MPC helps save time during the controller design phase: by enforcing constraints by design, rather than by time-consuming tuning of gains and cumbersome protection logics, MPC can reduce the development and calibration time by a significant amount.

However, in the context of MPC and AMBs, much recent research has focused on preliminary numerical studies and little attention has been paid to the validation through experimental results. The fact is that some difficulties have been encountered when applying MPC on AMBs:

- MPC is computationally expensive even with explicit MPC (the optimal input is obtained from look-up tables generated off-line). Position control in AMBs usually requires a sampling time around $2-5$ kHz depending on the application. Solving the OCP in a deterministic time is not trivial. A fast MPC solver is needed or at least a MPC formulation that leads to faster solutions (i.e., reducing control horizon, removing constraints, etc.).
- Full plant state knowledge. When the states are estimated (MPC + state estimator) the stability margins are not guaranteed. The fact is that a MPC can be properly

designed to guarantee nominal closed-loop stability but when it is combined with a state estimator, special attention must be paid to the closed-loop performance and the quality of the estimate.

- Sensitive to plant-model mismatch. MPC is a model-based control solution and hence the larger the plant-model mismatch, the more deteriorated is the control performance. Integral action must be added to eliminate the steady-state error due to model uncertainties.

Embedding MPC into a target hardware platform. At this point, MPC controllers might be considered computationally expensive control policies compared to other conventional analytical control policies like the linear control policy prescribed by LQR. However, this is not the case in practice, thanks to fast embedded solvers [26, 27, 28] and code generation tools that emit solvers specialized to parametric problems [29, 30, 31]. Nowadays, the feasibility of embedding MPC into a microcontroller is difficult to establish but the truth is that the technological scenario is changing fast. In the context of "fast" MPC and Active Magnetic Levitation, a research gap is identified: **Few experimental results about MPC applications on Active Magnetic Bearings are presented in the literature**. The discussion about the feasibility of embedding a MPC into a hardware platform for AMB systems is still open.

Control design for cone-shaped AMB systems. Typically, an active magnetic suspension exploits three actuation stages, two for the radial and one for the axial control. This standard layout needs a dedicated thrust bearing, which create problems due to the bearing size and weight, and limitations to the maximum rotational speed. The latter is related to magnetic losses and to the possible high values of peripheral velocities of the discs of the thrust bearing. Additionally, the presence of the thrust bearing is the cause of longer shafts with negative consequences for the rotordynamic behavior of the systems. The realization of a more compact and integrated solution can therefore pass through the elimination of the thrust bearing, resorting to only to planes of actuation for the generation of both radial and axial levitation force. This solution can be implemented by using a conical geometry for the pole pieces of the stator and the iron parts of the rotor as shown in Figure 1.3. This configuration can be used in applications where size reduction is an important requirement [32, 33, 34, 35, 14], and is equivalent to common rolling element bearings using conical contact surfaces with combined radial and axial load capability. Although promising, the spread of this solution in industrial applications has been strongly limited by a series of drawbacks, such as the low axial force generation capability and the complex design of the control strategy due to the coupling of the axial and radial control actions [36]. Few works reported in the literature are conducted until the experimental validation of the control strategy. As a matter of fact, in the authors' knowledge, only a few works present a complete analysis with experimental results [37, 38]. A decoupled Proportional-Integral-Derivative PID controllers obtained from a Linear Quadratic Regulator with integral action for

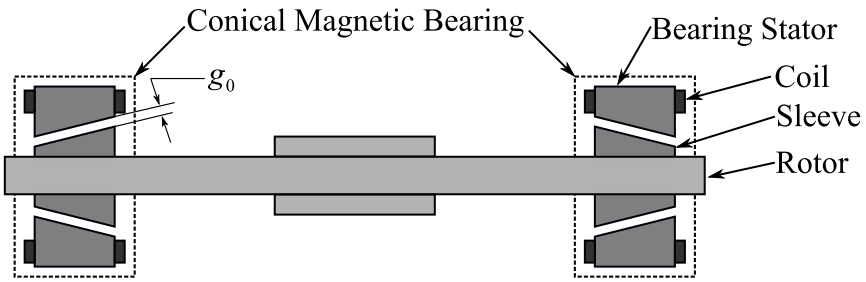

Figure 1.3: Structure of a 5-dof rotor system supported by conical magnetic bearings.

a voltage-controlled cone-shaped AMB system is proposed in [37]. A decentralized solution also based on PID controllers is studied in [38] for a turbo-molecular pump. Numerical analysis for centralized fuzzy controller are presented in [39, 40].

In cone-shaped AMBs, the inherent coupling between the radial and axial control actions, together with the low axial force generation in axial direction and coil currents limitation is difficult to manage when using decentralized control strategies. The current on each electromagnet is the sum of axial and radial control contributions to generate axial and radial restoring forces. Each decentralized controller knows only about the control contribution it produces but nothing about the real amount of current flowing into the coils due to the presence, at the same time, of the axial control contribution. Commonly, the coil current limitations are treated as external saturation blocks and hence not optimally handled. These deficiencies could be overcome by applying centralized constrained optimal control techniques such as Model Predictive Control (MPC). In this context, a research gap is identified: **There is no literature reporting MPC on cone-shaped AMB systems**.

Dealing with model uncertainty. Any engineering model of a physical system has uncertainty. That is, even with the most careful analysis and model calibration process, the physical response of the actual system is expected to deviate from that predicted by the model. The source of this deviation may be traced back to errors in the model, but since the actual errors are *a priori* unknown, they are described as uncertainties [2].

In an AMB system, an obvious source of uncertainty is the linearized properties of the AMB actuator. It is most common to represent the linearized actuator as [1]

$$f \approx -k_s x + k_i i_c \tag{1.1}$$

in which x is displacement of the journal from some nominal operating point, i_c is the control current: the extent to which opposing coil currents differ, and k_s and k_i are linearized actuator properties. These properties are sensitive to the radial air gap length in the AMB which is sensitive to operating temperature and to manufacturing tolerance: it is common for this air gap to have an uncertainty as high as ten percent, leading to 30% uncertainty in k_s and 20% uncertainty in k_i. Static load carried by the AMB also alters

k_s and is commonly substantially uncertain. In flexible rotor systems, modal damping and frequency of flexible modes may be sensitive to assembly (shrink fits) and operating temperature, leading to significant uncertainty in the rotor model. Additionally, gyroscopic coupling will modify rotor flexible modes, making them dependent on rotor spin rate. If this rate is not known precisely (or not incorporated explicitly into controller design) then it may represent a substantial model uncertainty [2].

In general, the "perfect" match between plant and model is rather difficult to obtain due to the nonlinear nature of the magnetic actuators, the uncertainties in the model parameters and external disturbances. In the context of MPC, there is a variant that handles the plant-model mismatch in a systematic way. It is known as Offset-Free Model Predictive Control (OF-MPC) [41, 42, 43, 44, 45]. With OF-MPC the plant model is augmented with a disturbance model to capture the plant-model mismatch. State and input targets are obtained from the estimated disturbance. The states and control inputs are steered to the target equilibrium point to guarantee zero-offset tracking.

Figure 4.4 shows the OF-MPC control scheme. The observer estimates both state and disturbances which are used by the target calculator together with the position reference to obtain the input and state targets. Both target vectors together with the state and disturbance estimates are used to initialize the OF-MPC control problem.

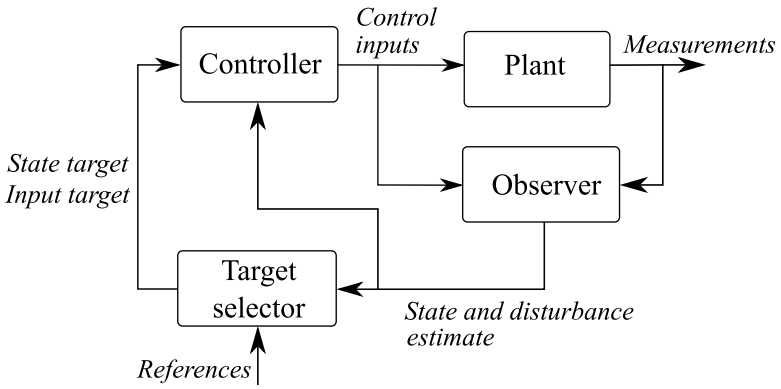

Figure 1.4: OF-MPC control scheme consisting of: controller (OF-MPC problem formulation), Observer (estimates both: original and augmented states), and target selector (produces input and state targets to compensate the plant-model mismatch).

Research motivation in a few words: OF-MPC seems promising for active magnetic bearing systems. As discussed above, an AMB model may deviate from the real plant due to unmodeled dynamics, unknown disturbances, uncertain system parameters or modeling errors. The possibility to optimally handle the inputs and state constraints, together with the plant-model mismatch, is offered by the OF-MPC technique. It guarantees zero-offset tracking adding integral action from the knowledge of the plant-model mismatch, while the controller design is an automated design procedure

based on the trade-off between the control effort and the error in the controlled variables. However, **a methodology for the application of offset-free model predictive control on active magnetic bearings is not addressed in the literature yet**. The fact is that there are infinite choices to formulate an OF-MPC for a magnetic bearing system but a proper implementation might result difficult because OF-MPC (i) requires the selection of an augmented disturbance model to guarantee zero-offset control; (ii) A state estimator must be designed from that augmented model; (iii) An optimal control problem shall be formulated and (iv) an algorithm able to solve the control problem in a deterministic time is required. Figure 1.5 introduces some of the expected stages to be faced in this work.

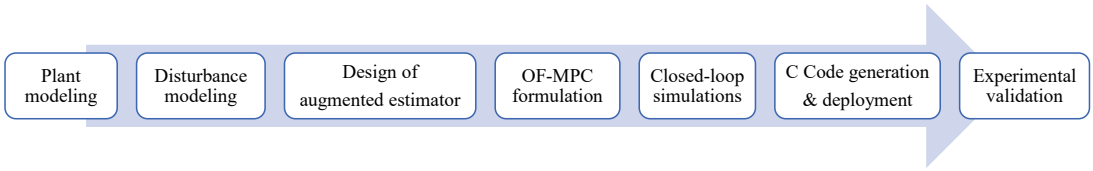

Figure 1.5: Foreseen stages of the methodology. They evolved during the thesis work.

1.4 Objectives and Scope

The primary objective of the work presented in this thesis is the **study of offset-free model predictive control for active magnetic bearing systems**. It is subdivided into more specific objectives as follows:

- Study the general formulation of the OF-MPC control strategy
- Identify an OF-MPC formulation suitable for AMB applications
- Design an augmented model that accounts for the external disturbance and plant-model mismatch
- Design a robust state estimator from the augmented model
- Formulate a custom OF-MPC controller with reduced computational burden to guarantee a deterministic execution time
- Embed the control strategy (OF-MPC + Observer) into a hardware platform
- Validate the performance of the controller in real AMB systems

Scope: The thesis is limited to the linear formulation of OF-MPC. Nonlinear variants [46] are left for future works. The present work is also motivated by the following consideration: OF-MPC is able to handle "persistent" uncertainties whether in the form of additive disturbances, state estimation error or model error. "Fast" varying uncertainties are out of the scope of this work.

1.5 Thesis contribution

- The major contribution of this work is the demonstration of the potentialities of linear OF-MPC on active magnetic bearing systems. A methodology for the overall control design is validated numerically and experimentally. The effectiveness of the control strategy is first evaluated in a single-axis AMB system and later in a more complex cone-shaped AMB system.
- The OF-MPC study presented here, might serve as "application notes" for the real implementation of OF-MPC in cone-shaped AMB systems. In the author's knowledge, there is no literature reporting constrained optimal control solutions for cone-shaped AMB systems. The control algorithm is described in detail showing how to: reduce the computational burden of the control problem, generate OF-MPC solvers from C code generation tools and design properly the plant state estimator.
- OF-MPC resulted in a suitable control solution for AMB plants subject to variable external disturbance forces and for any other system in which the plant input saturation/limitation requires more attention during operation. Note that any other linear control solution such as PD/PIDs, μ-Synthesis can guarantee good stability properties but nothing can be said when the system saturates. However, OF-MPC offers a systematic approach to optimally handle the trade-off between control effort and controlled outputs taking into account both plant dynamics and physical constraints.
- OF-MPC intrinsically offers some insight about the plant operation. This is because it can be formulated to lump the plant-model mismatch together with low-frequency disturbances and load variations into the estimate. That estimate could be interpreted as an engineering quantity for the real-time evaluation of both the plant operation and the quality of the internal model of the controller.

1.6 Dissertation Outline

The work is subdivided into five Chapters. They are independent each other but reading them in appearance order is recommended. They are outlined as follows:

Chapter 2: Linear Offset-Free Model Predictive Control Revisited

This chapter presents the first ingredients of a linear OF-MPC formulation: a plant model, a disturbance model, a state estimator, the target calculation and finally summarizes the OF-MPC design methodology. A resulting quadratic problem for a particular disturbance model is also developed.

Chapter 3: OF-MPC on a Single-Degree-of-Freedom AMB System

This chapter makes reference to the publication [47]. It presents the study of linear Offset-Free Model Predictive Control (OF-MPC) for an Active Magnetic Bearing (AMB) application. It describes the modeling and design of the OF-MPC architecture and its experimental validation for a one degree of freedom AMB system. The effectiveness of the method is demonstrated in terms of the reference tracking performance, cancellation of plant-model mismatch effects, and low-frequency disturbance estimation.

Chapter 4: OF-MPC on a Cone-shaped Active Magnetic Bearing System

With cone-shaped AMBs, the rotor motion is controlled simultaneously in the axial and radial directions by two radial bearings with cone-shaped magnetic core. This configuration eliminates the requirement of a dedicated axial actuator but makes the control more complex than conventional cylindrical AMB solutions due to the coupling of the axial and radial control actions. This chapter presents the benefits of applying Offset-Free Model Predictive Control (OF-MPC) for a cone-shaped AMB system. A procedure for the overall design is presented and supported by the experimental work conducted in a scaled machine that reproduces a turbo-compressor unit in a high-performance aircraft.

Chapter 5: Thesis conclusions and future work

This chapter concludes the thesis work and presents an evolved methodology for the application of OF-MPC in AMB systems. The limitation of this work and future research directions are also outlined.

Chapter 2

Linear Offset-Free Model Predictive Control Revisited

This chapter introduces the linear OF-MPC control solution together with its main ingredients: a linear plant model, a generalized augmented disturbance model, an augmented state estimator, the state and input targets selector, and the OF-MPC problem formulation. A Quadratic Programming (QP) problem that results from a custom OF-MPC formulation is also discussed.

2.1 Introduction

The main concept of Model Predictive Control (MPC) is to use a model of the plant to predict the future evolution of the system. At each time step t a certain performance index is optimized over a sequence of future input moves subject to operating constraints. The first of such optimal moves is the control action applied to the plant at time t. At time $t + 1$, a new optimization is solved over a shifted prediction horizon [41].

Model predictive control ensures stability and allows tracking any reachable target without offset if the system evolves in a deterministic fashion and that the full state (including disturbances) is measured [48]. Nevertheless, the perfect match between plant and model is rather difficult to obtain and the full measurement of state and disturbances is almost impossible. Integral action is used in linear control to ensure that the true system output reaches its desired steady state value, or set point, despite the presence of unaccounted constant disturbances and modeling errors. In the context of MPC, there are several alternative ways in which integral action can be included into a control algorithm. For example, using *certainty equivalence* (CE) principle [48, § 5.5], which consists of designing the control law assuming knowledge of the states and disturbances, and then using their estimates as if they were the true ones when

implementing the controller. The key idea is to include a model for constant disturbances at the input or output of the system and design an observer for the composite model including system and disturbance models. Then the control is designed to reject the disturbance, assuming knowledge of states and disturbance. Finally, the control is implemented using CE. The resulting observer-based closed-loop system has intrinsically the integral action [48]. This control approach is well-known as Offset-Free Model Predictive Control (OF-MPC).

This chapter presents the first ingredients of a linear OF-MPC formulation: a plant model in Section 2.2, and the disturbance model and state estimator in Section 2.3. Section 2.4 presents the target calculation and the OF-MPC problem formulation. The prediction model and the resulting quadratic programming problem for a particular disturbance model is also developed in Section 2.5.

2.2 Plant model

The OF-MPC follows the standard MPC design flow: the model choice, the observer design and the controller design. Consider the discrete-time time-invariant system

$$\begin{aligned} x_m(t+1) &= f(x_m(t), u(t)) \\ y_m(t) &= g(x_m(t)) \\ z(t) &= H y_m(t) \end{aligned} \tag{2.1}$$

where $x_m(t) \in \mathbb{R}^{n_x}$, $u(t) \in \mathbb{R}^{n_u}$ and $y_m(t) \in \mathbb{R}^{n_p}$ are the state, input, measured output vector, respectively. The controlled variables $z(t) \in \mathbb{R}^{n_r}$ are a linear combination of the measured variables. Without any loss of generality H is assumed to have full row rank.

The objective is to design an MPC based on a linear system model of (2.1) in order to have $z(t)$ track $r(t)$ with zero steady-state tracking error. $r(t) \in \mathbb{R}^{n_p}$ is the reference signal, which we assume to converge to a constant i.e., $r(t) \to r_\infty$ as $t \to \infty$.

The MPC scheme will make use of the following linear time-invariant system model of (2.1):

$$\begin{aligned} x(t+1) &= Ax(t) + Bu(t), \\ y(t) &= Cx(t). \end{aligned} \tag{2.2}$$

where $x(t) \in \mathbb{R}^{n_x}$, $u(t) \in \mathbb{R}^{n_u}$ and $y(t) \in \mathbb{R}^{n_p}$ are the state, input, output vector, respectively. It is assumed that the pair $(A,\ B)$ is controllable, and the pair $(C,\ A)$ is observable. Furthermore, C is assumed to have full row rank [41].

2.3 Disturbance model and observer design

To account for plant-model mismatch and disturbances entering the plant, system (2.2) is augmented with a disturbance model. Several disturbance models have been presented in the literature [49, 43, 50, 51, 52]. The generalized augmented disturbance model of [43, 52] is presented here as

$$\begin{aligned} \begin{bmatrix} x(t+1) \\ d(t+1) \end{bmatrix} &= \begin{bmatrix} A & B_d \\ 0_{n_d \times n_x} & I_{n_d \times n_d} \end{bmatrix} \begin{bmatrix} x(t) \\ d(t) \end{bmatrix} + \begin{bmatrix} B \\ 0_{n_d \times n_u} \end{bmatrix} u(t) + w(t), \\ y(t) &= \begin{bmatrix} C & C_d \end{bmatrix} \begin{bmatrix} x(t) \\ d(t) \end{bmatrix} + v(t) \end{aligned} \tag{2.3}$$

where $d(t) \in \mathbb{R}^{n_d}$, $B_d \in \mathbb{R}^{n_x \times n_d}$ and $C_d \in \mathbb{R}^{n_y \times n_d}$. The vectors $w(t) \in \mathbb{R}^{n_x + n_d}$ and $v(t) \in \mathbb{R}^{n_p}$ are zero-mean white-noise disturbances for the augmented state equation and for the output equation, respectively. An observer is designed from (2.3) to estimate both states and disturbances. The observability of the augmented model (2.3) is guaranteed if and only if pair $(C,\ A)$ is observable and

$$\begin{bmatrix} A - I_{n_x \times n_x} & B_d \\ C & C_d \end{bmatrix} \tag{2.4}$$

has full column rank [52]. These observability requirements can restrict the choice of the disturbance model (see [52] for details).

The state and disturbance estimator is designed based on the augmented model as follows:

$$\begin{aligned} \begin{bmatrix} \hat{x}(t+1) \\ \hat{d}(t+1) \end{bmatrix} = \begin{bmatrix} A & B_d \\ 0_{n_d \times n_x} & I_{n_d \times n_d} \end{bmatrix} \begin{bmatrix} \hat{x}(t) \\ \hat{d}(t) \end{bmatrix} + \begin{bmatrix} B \\ 0_{n_d \times n_u} \end{bmatrix} u(t) \\ + \begin{bmatrix} L_x \\ L_d \end{bmatrix} (y_m(t) - C\hat{x}(t) - C_d\hat{d}(t)) \end{aligned} \tag{2.5}$$

where L_x and L_d are chosen so that the estimator is stable.

2.4 The OF-MPC design

In the standard MPC problem formulation, the states and control inputs are usually steered to the equilibrium point. When using the OF-MPC variant, that equilibrium point is replaced by "targets" obtained from a steady-state condition that accounts for the plant-model mismatch. From the observer (2.5) at steady state we have

$$\begin{bmatrix} A - I & B \\ C & 0_{n_d \times n_u} \end{bmatrix} \begin{bmatrix} \hat{x}_\infty \\ u_\infty \end{bmatrix} = \begin{bmatrix} -B_d\hat{d}_\infty \\ y_{m,\infty} - C_d\hat{d}_\infty \end{bmatrix}, \tag{2.6}$$

where $y_{m,\infty}$ and u_∞ are the steady state measured output and input of the system (2.1), x_∞ and $\hat{d}_\infty$ are state and disturbance estimates from the observer (2.5) at steady state, respectively. Denote by $z_\infty = Hy_{m,\infty}$ and r_∞ the tracked measured outputs and their references at steady state, respectively. For offset-free tracking, z_∞ must equal r_∞ and then working on (2.6) we have

$$\underbrace{\begin{bmatrix} A-I & B \\ HC & 0_{n_d\times n_u} \end{bmatrix}}_{A_t} \begin{bmatrix} x_\infty \\ u_\infty \end{bmatrix} = \begin{bmatrix} -B_d\hat{d}_\infty \\ r_\infty - HC_d\hat{d}_\infty \end{bmatrix}. \tag{2.7}$$

As can be appreciated from (2.7), the state and input at steady state depend on $\hat{d}_\infty$. Note that the estimator (2.5) provides $\hat{d}(t)$ at each time step t. Since $\hat{d}(t)$ is known and $\hat{d}(t+1) = \hat{d}(t)$ from (2.3), the best forecast of the steady-state disturbance $\hat{d}_\infty$ is simply considering the estimate persistent i.e., $\hat{d}_\infty = \hat{d}(t)$. Then x_∞ and u_∞ can be obtained from (2.7). Note that x_∞ and u_∞ exist for any $\hat{d}_\infty$ and r_∞ if the matrix A_t has full rank.

The OF-MPC problem formulation is designed as follows

$$\begin{aligned} \min_{\mathrm{u}} \quad & \frac{1}{2}\left(x_N - x_t\right)' P \left(x_N - x_t\right) + \frac{1}{2}\sum_{k=0}^{N-1} \left(x_k - x_t\right)' Q \left(x_k - x_t\right) \\ & + \frac{1}{2}\sum_{k=0}^{M-1} \left(u_k - u_t\right)' R \left(u_k - u_t\right) \end{aligned} \tag{2.8}$$

subj. to

$$\begin{aligned} & x_{k+1} = Ax_k + Bu_k + B_d d_k, \quad k = 0, \ldots, N-1, \\ & d_{k+1} = d_k, \quad k = 0, \ldots, N-1, \\ & u_k = u_t, \quad k = M, \ldots, N-1, \\ & x_k \in \mathcal{X}, \quad k = 1, \ldots, N-1, \\ & x_N \in \mathcal{X}_f, \\ & u_k \in \mathcal{U}, \quad k = 0, \ldots, M-1, \\ & x_0 = \hat{x}(t), \\ & d_0 = \hat{d}(t), \end{aligned} \tag{2.9, 2.10}$$

with the targets u_t, x_t given by

$$\begin{bmatrix} A-I & B \\ HC & 0_{n_d\times n_u} \end{bmatrix} \begin{bmatrix} x_t \\ u_t \end{bmatrix} = \begin{bmatrix} -B_d\hat{d}(t) \\ r(t) - HC_d\hat{d}(t) \end{bmatrix}. \tag{2.11}$$

Matrix Q is positive semi-definite, and matrices P and R are positive definite. At each sampling instant t, the above constrained optimal control problem is solved over a finite time prediction horizon N, using the current observed state of the plant $\hat{x}(t)$.

The optimization yields an optimal control sequence $\boldsymbol{u}(t) = \left\{u_0^*, \ldots, u_{N-1}^*\right\}$ and the first control in this sequence, $u(t) = u_0^*$, is applied to the plant.

From the OF-MPC problem formulation (2.8)-(2.11) we can appreciate that the system steady state relation in (2.11) accounts for the effect of the disturbance on the state evolution ($0 \rightarrow B_d\hat{d}(t)$). Then the states of the original system are moved onto the manifold that cancels the effect of the disturbance in the controlled variables. In some references, the targets are not obtained from (2.11) and a quadratic program that involves the input constraints is used instead [53]. In this way, the input target u_t never violates the inputs constraints of the OF-MPC problem formulation (see, for instance, reference [53]).

2.4.1 Method summary

Figure 2.1 shows the OF-MPC control scheme. The observer estimates both state and disturbances which are used by the target calculator together with the reference vector r to obtain the input and state targets. Both target vectors together with the state and disturbance estimates are used to initialize the OF-MPC control problem (2.8)-(2.10).

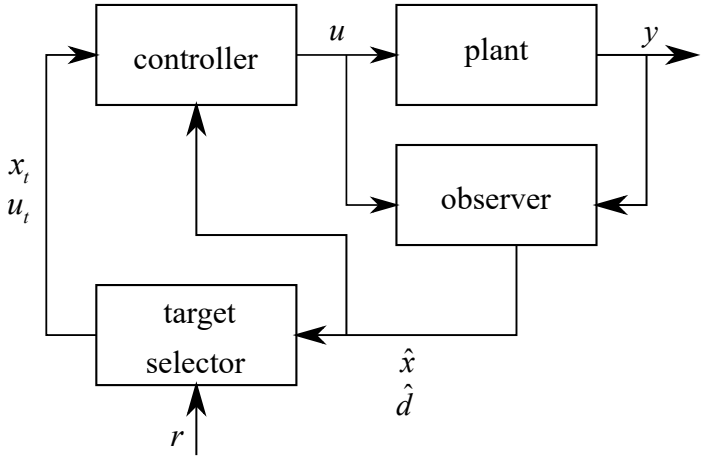

Figure 2.1: OF-MPC control scheme consisting of: controller (2.8)-(2.10), state estimator (2.5), and target selector (2.11).

2.5 OF-MPC as a quadratic programming problem

Since the finite horizon control problem (2.8)-(2.10) contains a quadratic cost function and only linear constraints on the input and output, it can be transformed into a standard *quadratic programming* (QP) problem. Here the *batch* approach [52] is used to rewrite (2.8)-(2.10) into a QP problem.

2.5.1 Objective function handling without inequality constraints

This Section shows how (2.8) can be combined with the equality constraints in (2.10) and then transformed into a standard QP objective function by using the batch approach. The optimal control problem can be solved analytically if the inequality constraints are not considered (i.e., removing the upper and lower limits of inputs and states from the problem formulation). Without loss of generality, it helps one understand the main ingredients of the optimal control input that serves to guarantee offset-free reference tracking.

First the equality constraints are rewritten explicitly to express all future states $x_1, ..., x_N$ as a function of the future inputs $u_0, ..., u_{M-1}$ and disturbances $d_0, ..., d_N$ (if they are known or predicted *a priori*), and using the constraint that $u_k = u_t$ for all $k \geq M$. Then all intermediate states are eliminated by successive substitution to obtain

$$\underbrace{\begin{bmatrix} x_0 \\ \vdots \\ x_N \end{bmatrix}}_{\boldsymbol{x}} = \underbrace{\begin{bmatrix} I \\ A \\ \vdots \\ A^N \end{bmatrix}}_{S^x} x(0) + \underbrace{\begin{bmatrix} 0 & 0 & 0 & 0 & 0 \\ B & 0 & \dots & 0 & 0 \\ AB & B & \ddots & \vdots & \vdots \\ \vdots & \vdots & \ddots & \vdots & \vdots \\ A^{M-1}B & A^{M-2}B & \dots & AB & B \\ A^M B & A^{M-1}B & \dots & A^2 B & AB \\ \vdots & \vdots & \ddots & \vdots & \vdots \\ A^{N-1}B & A^{N-2}B & \dots & \dots & A^{N-M}B \end{bmatrix}}_{S^u} \begin{bmatrix} u_0 \\ \vdots \\ u_{M-1} \end{bmatrix}$$

$$+ \underbrace{\begin{bmatrix} 0 \\ \vdots \\ 0 \\ B \\ AB + B \\ \vdots \\ \sum_{i=0}^{N-M-1} A^i B u_t \end{bmatrix}}_{S^{u_t}} u_t + \underbrace{\begin{bmatrix} 0 & 0 & 0 & 0 \\ B_d & 0 & \dots & 0 \\ AB_d & \ddots & \ddots & \vdots \\ \vdots & \ddots & \ddots & \vdots \\ A^{N-1}B_d & \dots & \dots & B_d \end{bmatrix}}_{S^d} \begin{bmatrix} d_0 \\ \vdots \\ \vdots \\ d_{N-1} \end{bmatrix} \tag{2.12}$$

Then, all future states are explicit functions of the present state $x(0)$, the future disturbances $\boldsymbol{d} = [d_0, ..., d_{N-1}]^T$, the future inputs $\boldsymbol{u} = [u_0, ..., u_{M-1}]^T$ and input target u_t. It is compactly rewritten as

$$\boldsymbol{x} = S^x x(0) + S^u \boldsymbol{u} + S^{u_t} u_t + S^d \boldsymbol{d}. \tag{2.13}$$

By doing the same but at steady state (i.e., when the steady state target x_t and input target u_t are reached) we get

$$\boldsymbol{x}_t = S^x x_t + S^u \boldsymbol{u}_t + S^{u_t} u_t + S^d \boldsymbol{d}_t \tag{2.14}$$

where vector $\boldsymbol{d}_t = [d_t; ...; d_t]$ of length Nn_d and $\boldsymbol{u}_t = [u_t; ...; u_t]$ of length Nn_u stand for the disturbance estimates and inputs at steady state during the prediction horizon. Subtracting (2.13) and (2.14) we get the deviation equation

$$\underbrace{\boldsymbol{x} - \boldsymbol{x}_t}_{\bar{\boldsymbol{x}}} = S^x \underbrace{(x(0) - x_t)}_{\bar{x}} + S^u \underbrace{(\boldsymbol{u} - \boldsymbol{u}_t)}_{\bar{\boldsymbol{u}}} + S^d \underbrace{(\boldsymbol{d} - \boldsymbol{d}_t)}_{\bar{\boldsymbol{d}}} \tag{2.15}$$

which becomes

$$\bar{\boldsymbol{x}} = S^x \bar{x} + S^u \bar{\boldsymbol{u}} + S^d \bar{\boldsymbol{d}} \tag{2.16}$$

Similarly, the objective function (2.8) can be rewritten in vectorial form and with deviation variables as

$$J(\bar{\boldsymbol{x}}, \bar{\boldsymbol{u}}) = \frac{1}{2} \bar{\boldsymbol{x}}' \bar{Q} \bar{\boldsymbol{x}} + \frac{1}{2} \bar{\boldsymbol{u}}' \bar{R} \bar{\boldsymbol{u}} \tag{2.17}$$

where $\bar{Q} = \text{blockdiag}\{\text{Q}, \cdots, \text{Q}, \text{P}\}$, $\bar{Q} \succcurlyeq 0$, and $\bar{R} = \text{blockdiag}\{\text{R}, \cdots, \text{R}\}$, $\bar{R} \succ 0$. Equation (2.16) is substituted into (2.17) to yield

$$\begin{aligned} J(\bar{x}, \bar{\boldsymbol{d}}, \bar{\boldsymbol{u}}) = \frac{1}{2} \bar{\boldsymbol{u}}' \underbrace{(S^{u\prime} \bar{Q} S^u + \bar{R})}_{H} \bar{\boldsymbol{u}} + \bar{x}' \underbrace{(S^{x\prime} \bar{Q} S^u)}_{F} \bar{\boldsymbol{u}} + \bar{\boldsymbol{d}}' \underbrace{S^{d\prime} \bar{Q} S^u}_{Y} \bar{\boldsymbol{u}} \\ + \frac{1}{2} \bar{x}' (S^{x\prime} \bar{Q} S^x) \bar{x} + \frac{1}{2} \bar{\boldsymbol{d}}' S^{d\prime} \bar{Q} S^d \bar{\boldsymbol{d}} + \bar{x}' (S^{x\prime} \bar{Q} S^d) \bar{\boldsymbol{d}} \end{aligned} \tag{2.18}$$

in which the last three terms are independent of the decision variable $\bar{\boldsymbol{u}}$. Then

$$J(\bar{x}, \bar{\boldsymbol{d}}, \bar{\boldsymbol{u}}) \triangleq \frac{1}{2} \bar{\boldsymbol{u}}' H \bar{\boldsymbol{u}} + (\bar{x}' F + \bar{\boldsymbol{d}}' Y) \bar{\boldsymbol{u}} + J_0 \tag{2.19}$$

where J_0 lumps the independent terms. As can be appreciated, the last calculation is equivalent to the elimination of the equality constraints given by the state equations in (2.10) by substitution into the objective function (2.8). The arguments $(\bar{x}, \bar{\boldsymbol{d}})$ are known parameters (see the problem formulation (2.8)-(2.11)). Note that $\bar{\boldsymbol{d}}$ becomes zero when the disturbance estimate is assumed constant and persistent during the prediction horizon i.e., $d_{k+1} = d_k,\ k = 0, ..., N-1$, and $d_0 = \hat{d}(t)$.

Because $\bar{R} \succ 0$, also $H \succ 0$. Thus $J(\bar{x}, \bar{\boldsymbol{d}}, \bar{\boldsymbol{u}})$ is a positive definite quadratic function of $\bar{\boldsymbol{u}}$. Therefore, its minimum can be found by computing its gradient and setting it to zero. This yields the optimal vector of future inputs

$$\bar{\boldsymbol{u}} = -H^{-1}F'\bar{x} - H^{-1}Y'\bar{\boldsymbol{d}}. \tag{2.20}$$

When substituting the deviation variables we have

$$\boldsymbol{u} - \boldsymbol{u}_t = -H^{-1}F'(x(0) - x_t) - H^{-1}Y'(\boldsymbol{d} - \boldsymbol{d}_t) \tag{2.21}$$

where $\boldsymbol{u}(t) = \left\{u_0^*, \ldots, u_{N-1}^*\right\}$. Since only the first control in this sequence, $u(t) = u_0^*$, is applied to the plant (due to the receding horizon principle of MPC), then

$$u_{0,uc}^* = -K(x(0) - x_t) + K_d(\boldsymbol{d} - \boldsymbol{d}_t) + u_t, \tag{2.22}$$

where $K^{n_u \times n_x}$ and $K_d^{n_u \times N n_d}$ are defined as the first n_u rows of the matrices $H^{-1}F'$ and $-H^{-1}Y'$, respectively.

As can be appreciated from (2.22), the input $u_{0,uc}^*$ is obtained every time step based on the knowledge of the actual state $x(0)$ (measured or estimated), the inputs and states targets as well as the disturbances evolution. Since the inequality constraints were not considered, the optimal feedback gains are calculated once and offline. This computationally "cheap" solution may result enough when a cautious controller design approach is desired.

By appropriate selection of the weightings in the objective function (2.8), the resulting K is such that the matrix $(A - BK)$ is Hurwitz, that is, all its eigenvalues have moduli smaller than one [48]. Note that similar to standard linear quadratic regulators, the aggressiveness of the controller depends on the weights selection.

The control input (2.22) includes the future disturbances into the formulation and thus it adds naturally a feedforward compensation to diminish their undesired effects on the controller performance. This is possible because during the formulation of the QP problem, the disturbances $d_0,\ d_1, \ldots$ were treated under the assumption that their time evolution is known or predicted *a priori*. But it is important to remark that this information is not needed to guarantee zero-offset tracking at steady state. In fact, the disturbance is considered persistent ($d_{k+1} = \hat{d}_0,\ k = 1, \ldots, N-1$) in (2.8)-(2.10) and hence $\bar{\boldsymbol{d}} = (\boldsymbol{d} - \boldsymbol{d}_t) = \boldsymbol{0}$.

While the steady state targets guarantees the zero-offset tracking in the controlled variables, there are some restrictions to take into account: (i) The offset-free tracking is guaranteed for a maximum of n_p controlled variables where n_p is the number of measurements and (ii) the offset-free tracking is guaranteed only at steady state.

2.5.2 Adding the inequality constraints to the QP problem

Magnitude and rate constraints such as

$$\begin{aligned} &u_{\min} \leq u_k \leq u_{\max}, k = 0, \ldots, M-1, \\ &x_{\min} \leq x_k \leq x_{\max}, k = 1, \ldots, N-1, \\ &\delta u_{\min} \leq u_k - u_{k-1} \leq \delta u_{\max}, k = 0, \ldots, M-1, \end{aligned} \tag{2.23}$$

are compactly represented by the constraints sets $\mathcal{X}$ and $\mathcal{U}$ in the OF-MPC problem formulation. There exists also a terminal set $\mathcal{X}_f$ in (2.10) that satisfies certain properties and is useful to establish closed-loop stability. The reader is directed to the reference [48, § 5.3.2] to check how all these constraints can be written in the QP problem as linear constraints on $\boldsymbol{u}$ of the form

$$\mathcal{K}\boldsymbol{u} \leq \mathcal{M}(\bar{x}, \bar{\boldsymbol{d}}, \boldsymbol{u}_t). \tag{2.24}$$

Matrices $\mathcal{K}$, $\mathcal{M}$ are obtained in a similar manner as described above for the objective function handling i.e., eliminating intermediate states by successive substitution.

Going back to the QP objective function (2.19) and substituting the deviation variables $\bar{\boldsymbol{u}} = \boldsymbol{u} - \boldsymbol{u}_t$ into it, and then eliminating the terms which are independent of $\boldsymbol{u}$ we get

$$\tilde{J}(\bar{x}, \bar{\boldsymbol{d}}, \boldsymbol{u}, \boldsymbol{u}_t) = \frac{1}{2}\boldsymbol{u}' H \boldsymbol{u} + [\bar{x}' F + \bar{\boldsymbol{d}}' Y - \boldsymbol{u}_t' H]\boldsymbol{u} \tag{2.25}$$

At this point, the OF-MPC problem of minimizing (2.8) subject to the constraints (2.10) can be expressed as the QP problem of finding $\boldsymbol{u}$ by minimizing (2.25) subject to (2.24), that is,

$$\begin{aligned} \min_{u} \quad & \frac{1}{2}\boldsymbol{u}' H \boldsymbol{u} + g(\bar{x}, \bar{\boldsymbol{d}}, \boldsymbol{u}_t)\boldsymbol{u} \\ \text{subj. to} \quad & \\ & \mathcal{K}\boldsymbol{u} \leq \mathcal{M}(\bar{x}, \bar{\boldsymbol{d}}, \boldsymbol{u}_t) \end{aligned} \tag{2.26}$$

Standard numerical procedures (QP algorithms) are available to solve the above optimization problem. Note that the linear term $g(\bar{x}, \bar{\boldsymbol{d}}, \boldsymbol{u}_t)$ as well as $\mathcal{M}(\bar{x}, \bar{\boldsymbol{d}}, \boldsymbol{u}_t)$ are updated every time step before the QP problem (2.26) is solved. When the OF-MPC formulation contains only input constraints (as usual in real applications), $\mathcal{M}$ is fixed and hence its update is not necessary.

2.6 Delta input (δu) MPC formulation

Zero-offset tracking can be also guaranteed when using the δu formulation, also known as incremental formulation [54] or MPC tracking problem [52, § 13.6]. It represents the situation when the system outputs should typically follow the given reference trajectory and the control movement δu is penalized rather than control effort u.

In the δu formulation, the MPC scheme uses the following linear time-invariant system model of the plant

$$\begin{aligned} x(t+1) &= Ax(t) + Bu(t) \\ u(t) &= u(t-1) + \delta u(t) \\ y(t) &= Cx(t) \end{aligned} \tag{2.27}$$

The absolute control value is estimated by the observer, which is expressed as follows

$$\begin{bmatrix} \hat{x}(t+1) \\ \hat{u}(t+1) \end{bmatrix} = \begin{bmatrix} A & B \\ 0 & I \end{bmatrix} \begin{bmatrix} \hat{x}(t) \\ \hat{u}(t) \end{bmatrix} + \begin{bmatrix} B \\ I \end{bmatrix} \delta u(t) + \begin{bmatrix} L_x \\ L_u \end{bmatrix} (y_m(t) - C\hat{x}(t)) \tag{2.28}$$

and the MPC problem is modified to

$$\min_{\delta u_0, \ldots, \delta u_{N-1}} \frac{1}{2} \sum_{k=0}^{N-1} (y_k - r_k)' Q_y (y_k - r_k) + \delta u_k' R \delta u_k \tag{2.29}$$

subj. to

$$\begin{aligned} & x_{k+1} = Ax_k + Bu_k, \quad k = 0, \ldots, N-1, \\ & u_k = u_{k-1} + \delta u_k, \quad k \geq 0, \\ & x_k \in \mathcal{X},\ u_k \in \mathcal{U}, \quad k = 0, \ldots, N-1, \\ & u_{-1} = \hat{u}(t), \\ & x_0 = \hat{x}(t). \end{aligned} \tag{2.30}$$

The control input applied to the system is

$$u(t) = \delta u_0^* + u(t-1). \tag{2.31}$$

The input estimate $\hat{u}(t)$ is not necessarily equal to the actual input $u(t)$. This scheme inherently achieves offset-free control, there is no need to add a disturbance model. This is due to the fact that any plant-model mismatch is lumped into $\hat{u}(t)$. Indeed this approach is equivalent to an input disturbance model ($B_d = B, C_d = 0$). If in (2.30) the measured $u(t)$ were substituted for its estimate, i.e. $u_{-1} = u(t-1)$, then the algorithm would show offset.

In this formulation the computation of a target input u_t and state x_t is not required. A disadvantage of the formulation is that it is not applicable when there is an excess of manipulated variables u compared to measured variables y, since detectability of the augmented system is then lost [52].

2.7 Conclusions

The model predictive control strategy can be cast into OF-MPC to ensure that the true system output reaches its desired steady state value, or set point, despite the presence of unaccounted constant disturbances and modeling errors. To do so, the system model is augmented with a disturbance model that serves to obtain combined state and disturbance estimates via an observer. Those estimates can then be used in the control

algorithm by means of the certainty equivalence principle. The resulting observer-based closed-loop system has integral action.

Two MPC variants that guarantee zero-offset tracking were presented here: The general OF-MPC and delta input (δu) formulations. The (δu) formulation can be seen as a particular case in which the plant-model mismatch is lumped into the control variable while the general OF-MPC formulation (Section 2.4) allows one to "locate" the disturbances by using a more general augmented disturbance model [43]. An informal discussion of the stability properties of the OF-MPC is presented in [55, § 5.3.3].

The OF-MPC controller described in this Chapter is motivated by the following consideration: OF-MPC is able to handle "persistent" uncertainties whether in the form of additive disturbances, state estimation error or model error. "Fast" varying uncertainties, however, are better handled by *tube-based* MPC [55] and other robust MPC variants not mentioned here. The design of robust MPC to deal with "fast" varying uncertainties are out of the scope of this work.

Chapter 3

OF-MPC on a Single-Degree-of-Freedom AMB System

This chapter makes reference to the publication [47]. It presents the study of linear OF-MPC for a single-degree-of-freedom AMB System. The modelling of the system is described together with the design of the OF-MPC in all its parts: general control architecture, disturbance model and observer design, target calculation, and MPC problem formulation. The effectiveness of the control technique is demonstrated in terms of the reference tracking performance, cancellation of plant-model mismatch effects, and low-frequency disturbance estimation.

3.1 Introduction

The adoption of Active Magnetic Bearings (AMBs) in industrial applications has exhibited a steady growth in the last decades because of their remarkable advantages over traditional oil-lubricated bearings due to their contactless nature. This allows tribology and fatigue issues to be avoided, reducing power losses and eliminating oil supply units. Furthermore, AMB systems are characterized by monitoring and diagnostic capabilities, while the high tunability of the control action permits on-line adjustments of the bearing system according to the operating conditions. These and other benefits have favoured the adoption of AMBs in a variety of applications such as kinetic energy storage systems, the oil & gas and vacuum industry, heart pumps, refrigeration compressors and milling spindles [1, 56, 57]. Nowadays, the research effort to refine this technology is focused on several aspects, such as actuator configuration [58, 11, 59], sensing technology [60, 61, 62], the interaction with rotordynamic aspects [63, 64], and the integration of an electric motor with magnetic bearings [65, 66]. The control strategy is typically based on linear or nonlinear control architectures such as PID, H_∞,

μ-synthesis, sliding mode control, LQ, and learning control [67, 68, 69, 70, 71]. Each of these strategies has the main goal of compensating for the inherent unstable behavior of the system and satisfying the demands of performance, robustness, and accuracy. In this scenario, Model Predictive Control (MPC) has gained increasing attention in the last few years and has been implemented in a variety of applications and in different forms to tackle issues of nonlinearities and variability of the operating conditions. A rich literature describes the potentialities of this approach in magnetic levitation [20, 17, 18, 19, 21, 22]. In particular, MPC has shown an improved performance in compensating for gyroscopic effects [72] and revealed properties of good stability and robustness when compared with standard control architectures for the levitation of flywheels [72]. When using MPC for AMBs, the electromagnets' current reference is obtained by solving a finite horizon open-loop optimal control problem either in real-time or offline. The current state of the plant is considered as the initial state at every step of computation. If the actual process and the nominal model match perfectly, this control scheme ensures the stability and allows the tracking of any reachable target without offset. Nevertheless, in AMB systems, the perfect match between plant and model is rather difficult to obtain, mainly because of nonlinear effects that are present in the magnetic actuators [73] and uncertainty in the model parameters [74]. Increasing the model complexity may not be enough to overcome this issue due to the intrinsic difficulty in evaluating or identifying all unknown model parameters. This leads to an almost unavoidable steady-state offset of the closed-loop system. The inclusion of some form of integrative action in the MPC scheme is therefore required to yield Offset-Free Model Predictive Control (OF-MPC). Different approaches have been proposed in the literature to obtain OF-MPC: (a) adding an external integrative action to the tracking error [21]; (b) completing the cost function of the MPC scheme with a term related to the tracking error [18]; (c) adopting the so-called "velocity form linear model" considering the variations between two time-steps of the input and, if needed, of the state [43]; and (d) exploiting a disturbance observer based on an augmented plant model. The last case can be performed with either an "output disturbance model" [75] or an "input disturbance model" [76, 41]. In the last years, these techniques have been intensively studied in terms of their linear and nonlinear formulations [76, 41, 42, 45, 49, 46], as well as in terms of their applications in a variety of real cases. They have shown advantageous properties of stability and robustness [77, 78].

To the author's knowledge, linear OF-MPC based on an "input disturbance model" has not been attempted yet in AMB systems, despite its inherent capability to handle the steady-state offset generated by the plant-model mismatch and by unmeasured nonzero-mean disturbances. Hence, this is the objective of the present study. An additional advantage of the proposed method is to allow a real-time estimation of the low-frequency external disturbances and load variations acting on the AMB system to be obtained. This property is of great importance in applications such as compressors, pumps, and blowers, where the axial load applied to the machine can change significantly according to the operating conditions.

3.2 Single-degree-of-freedom AMB system

The test rig adopted for the experimental validation is a single-degree-of-freedom AMB system presented in Figure 3.1. It consists of a horizontal arm hinged at one extremity with a pivot and controlled at the other extremity by means of a single-axis magnetic bearing with two opposite electromagnets.

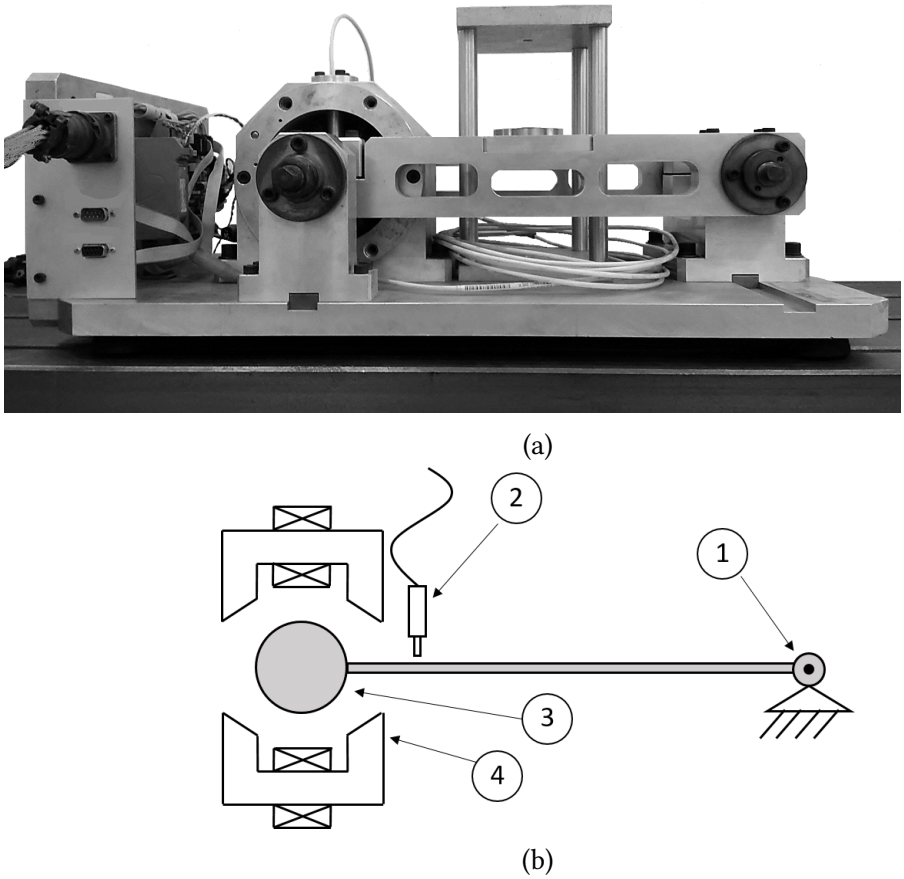

Figure 3.1: Single-degree-of-freedom AMB system. (a) Picture of the test rig.(b) System layout: (1) Pivot; (2) Displacement sensor; (3) Moving mass; (4) Electromagnet.

The length of the arm (320 mm) and the small air gap (0.6 mm) ensure that the circular motion of the mass can be approximated with a pure linear displacement (q). The base plate, connecting the arm and electromagnets' housing, is made from aluminium, and the shaft is steel, while silicon iron laminations are used for the stator and moving part of the magnetic circuit. The displacement of the mass is detected by means of a Bently Nevada Proximitor 3300XL (Minden, NV, USA) eddy current sensor. The currents in the electromagnets are measured by two AMP25 Hall sensors, one per electromagnet. The main electro-mechanical parameters of the plant are listed in Table 3.1.

Table 3.1: Plant parameters

Symbol	Name	Value	Unit
m	Mass	3.41	kg
S	Cross-section area at the air gap	420	mm^2
q_0	Nominal air gap	0.6	mm
n	Number of turns	142	-
R	Coil resistance	0.35	Ω
L_0	Coil nominal inductance	5.8	mH
k_i	Current-force factor	13.65	$\mathrm{N/A}$
k_q	Electromagnet negative stiffness	11.4	$\mathrm{N/mm}$
k_m	Back-electromotive-force factor	13.65	$\mathrm{Vm/s}$

A dSPACE MicroLabBox unit is used to close the feedback loop and for data acquisition. It includes a Freescale QorlQ P5020 real-time processor and a FPGA-PC-dSPACE prototyping platform for rapid control software development. The power stage consists of an H-bridge for each electromagnet with a 20 kHz fixed PWM frequency and a 24 V DC bus voltage.

3.3 Modeling

As is usual in AMB systems, the two electromagnets are operated in differential driving modes, i.e., one electromagnet is driven with the sum of bias and control current $(i_0 + i_c)$, while the other one with their difference $(i_0 - i_c)$. In the closed loop, i_c is set by the position controller, while i_0 is fixed. The system dynamic equilibrium equation is

$$m\dot{v} = f_m(i_c, q) + f_d \tag{3.1}$$

where m is the equivalent mass of the moving parts (including the arm and the moving part of the magnetic circuit), v is its velocity, f_m represents the magnetic actuators' force, and f_d represents an external disturbance force.

Assuming that: the two electromagnets are identical and magnetically uncoupled with each other, no saturation occurs in the magnetic material, the stray flux and eddy current effect are negligible, and the reluctance in the ferromagnetic part is negligible compared to that of the (small) air gap, the nonlinear magnetic force can be expressed as [1]:

$$f_m = \Gamma \left(\frac{(i_0 + i_c)^2}{(q_0 - q)^2} - \frac{(i_0 - i_c)^2}{(q_0 + q)^2} \right) \cos\alpha \tag{3.2}$$

where coefficient $\Gamma = \mu_0 n^2 S$ and $\mu_0 = 4\pi \times 10^{-7}\ \mathrm{H/m}$ is the magnetic permeability of the vacuum; $\alpha = \pi/8$ is the angle of each pole relative to the centerline between the

poles. The error of the predicted force with this modeling approach is within a range of 5%–10% ([1, § 3.1.5]).

In linear AMB, the nonlinear function (3.2) is linearized at the operating point with nominal airgap q_0, as

$$f_m(i_c, q) = k_i i_c + k_q q \tag{3.3}$$

where k_i and k_q are the force-current and force-displacement (or negative stiffness) factors, respectively. The linearization of (3.3) makes the control design easier as it can exploit all tools of linear control theory. Nevertheless, it becomes the first cause of plant-model mismatch, as well as the aforementioned assumptions at the base of the force Equation (3.2). These effects lead to a mismatch of the actual k_i and k_q coefficients relative to their nominal value and the force in Equation (3.3) can be rewritten as

$$f_{m,real}(i_c, q) = (k_i + \epsilon_i) i_c + (k_q + \epsilon_q) q \tag{3.4}$$

where ϵ_i, ϵ_q are the uncertainty on force-current and force-displacement factors, respectively. If this uncertainty is constant as time tends to infinity, (3.4) becomes

$$f^*_m(i_c, q)_\infty = k_i i_{c,\infty} + k_q q_\infty + \epsilon \tag{3.5}$$

in which ϵ lumps both force-factors uncertainties. This mismatch can be combined with low-frequency external disturbance effects into the disturbance term

$$d(t) = \epsilon + f_d(t) \tag{3.6}$$

3.4 OF-MPC design

The augmented model at the base of the OF-MPC controller is given by (3.1), (3.3), and (3.6), and can be expressed with the linear continuous-time state space representation

$$\begin{aligned} \dot{x}(t) &= \begin{bmatrix} 0 & 1 \\ \frac{k_q}{m} & 0 \end{bmatrix} x(t) + \begin{bmatrix} 0 \\ \frac{k_i}{m} \end{bmatrix} u(t) + \begin{bmatrix} 0 \\ \frac{1}{m} \end{bmatrix} d(t) \\ y(t) &= [1\ 0] x(t) \end{aligned} \tag{3.7}$$

where u stands hereinafter for the control current i_c , and the state vector $x(t) = [q(t) v(t)]^T$ includes the displacement $q(t)$ and the velocity $v(t)$ of the moving mass. The linear discrete-time representation

$$\begin{aligned} x(k+1) &= Ax(k) + Bu(k) + B_d d(k) \\ y(k) &= Cx(k) \end{aligned} \tag{3.8}$$

derived from (3.7) is required to apply OF-MPC. Aiming to obtain an offset-free control in the controlled variable y, a disturbance model is required to account for unmeasured low-frequency disturbances caused by plant-model mismatch or from external loads. To this end, the disturbance d is considered a new state to be estimated. The augmented model results in

$$\begin{aligned} \begin{bmatrix} x(k+1) \\ d(k+1) \end{bmatrix} &= \begin{bmatrix} A & B_d \\ 0_{1\times 2} & 1 \end{bmatrix} \begin{bmatrix} x(k) \\ d(k) \end{bmatrix} + \begin{bmatrix} B \\ 0 \end{bmatrix} u(k) + \begin{bmatrix} w_x(k) \\ w_d(k) \end{bmatrix} \\ y(k) &= [C\ C_d] x(k) \end{aligned} \tag{3.9}$$

where $w_x \in \mathbb{R}^2$ and $w_d \in \mathbb{R}$ represent the state noise, and $w_x \in \mathbb{R}^2$ is the output noise. Matrices B_d and C_d represent the effect of the disturbance d on the state and output equations, respectively. If only the disturbance on the output is considered, then B_d is a zero matrix and C_d is nonzero, the integrating disturbance d is only added to the output y, and the resulting formulation is therefore called the output disturbance model. However, considering the interest in turning d into a representation of plant-model mismatch and external disturbance force, the disturbance will not have a direct influence on the output equation (i.e., $C_d = 0$) and the resulting augmented model is called the input disturbance model with $B_d \neq \mathbf{0}$. In this last case, the output equation in (3.9) is not affected by the disturbance d, and hence

$$y(k) = Cx(k) + w_n(k) \tag{3.10}$$

Provided that the system (3.9) is observable since pair (C, A) has full rank, and also guaranteeing that the matrix

$$\begin{bmatrix} A - I_{n_x \times n_x} & B_d \\ C & C_d \end{bmatrix} \tag{3.11}$$

has full column rank [52], the state and the disturbance are estimated by the Kalman filter

$$\begin{bmatrix} \hat{x}(k+1) \\ \hat{d}(k+1) \end{bmatrix} = \begin{bmatrix} A & B_d \\ 0_{1\times 2} & 1 \end{bmatrix} \begin{bmatrix} \hat{x}(k) \\ \hat{d}(k) \end{bmatrix} + \begin{bmatrix} B \\ 0 \end{bmatrix} u(k) + \begin{bmatrix} L_x \\ L_d \end{bmatrix} (y(k) - C\hat{x}(k)) \tag{3.12}$$

where $L_x \in \mathbb{R}^2$ and $L_d \in \mathbb{R}$ are the predictor gain matrices for the state and the disturbance, respectively. They are calculated off-line, solving the Algebraic Riccati Equation as explained in detail in [53, 12]. The variance of the stochastic disturbance sequences w_x (states), w_d (disturbance), and w_n (output) is treated as adjustable parameters of the filter. An increase in the ratio between w_x and w_d makes the filter slower in estimating the disturbance, while an increase in the ratio between w_n and w_d makes the estimator less sensitive to the output noise [53]. The design parameters of the filter are reported in Table 3.2.

Table 3.2: Kalman filter design parameters

Parameter	Value
Variance of $\{w_x\}$	$\begin{bmatrix} 4 & 0 \\ 0 & 4 \end{bmatrix} \times 10^{-10}$
Variance of $\{w_d\}$	1
Variance of $\{w_n\}$	4×10^{-10}
L_x	$\begin{bmatrix} 1 \\ 119 \end{bmatrix}$
L_d	28325

3.4.1 Control system architecture

The objective of the proposed technique is to control the displacement of the moving mass to perform (a) reference tracking with the cancellation of plant-model mismatch effects; and (b) real-time estimation of low-frequency external disturbance, including load variations. The control architecture which is presented in Figure 3.2 is composed of an MPC block running at 5 kHz and generating the current reference u for the actuators. As is usual in standard AMB systems, the current is controlled by two internal PI control loops, one per electromagnet. These inner loops run at 20 kHz. The PI integral time is selected to be equal to the time constant of the RL circuit (i.e., $\tau_i = \tau_{RL} = L_0/R$), and the proportional parameter K_p is set equal to 55 V/A.

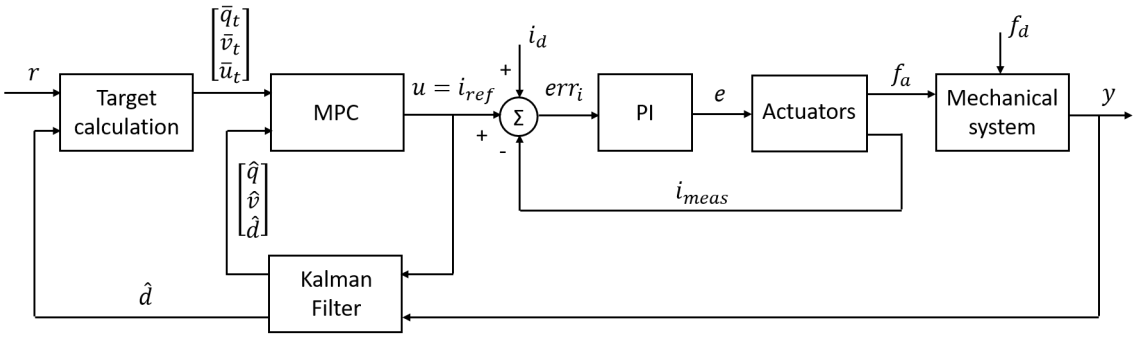

Figure 3.2: Control system architecture.

Taking the MPC current command and the displacement measured by the eddy current sensor as inputs, the Kalman filter (3.12) estimates the displacement ($\hat{q}$), velocity ($\hat{v}$), and disturbance ($\hat{d}$). The latter is provided to the target calculation block together with the position reference (r), in this case equal to 0, to obtain the state and input targets ($\bar{q}_T$, $\bar{v}_T$, $\bar{u}_T$). These and the total set of Kalman filter estimate ($\hat{q}$, $\hat{v}$, $\hat{d}$) are provided to the MPC to determine the current command (u). The control sequence repeated at each sampling time is the following: (a) the state $\hat{x}$ and the disturbance $\hat{d}$ are estimated by the Kalman filter; (b) the target calculation block exploits the reference r and the

estimated disturbance $\hat{d}$ to generate the state and control targets sent to the MPC at the current sampling instant; and (c) the MPC solves a constrained optimization problem, based on the targets and estimations, to get a new optimal control current u_0^*, which is applied to the system during the next sampling period.

3.4.2 Target calculation and MPC problem formulation

For offset-free tracking, at a steady state, the tracked measured output y_∞ must reach its reference r_∞ ($y_\infty = r_\infty$). When substituting the estimated disturbance in (3.9), the augmented model at a steady state is expressed by

$$\begin{bmatrix} A-I & B \\ C & C_d \end{bmatrix} \begin{bmatrix} x_\infty \\ u_\infty \end{bmatrix} = \begin{bmatrix} -B_d\hat{d}_\infty \\ r_\infty - C_d\hat{d}_\infty \end{bmatrix} \tag{3.13}$$

This model is included in the MPC problem formulation to obtain the state and input targets. The OF-MPC problem is formulated as

$$\begin{aligned} \min_u \quad & (x_N - \bar{x}_T)' P (x_N - \bar{x}_T) + \sum_{j=0}^{N-1} [(x_j - \bar{x}_T)' Q (x_j - \bar{x}_T) \\ & + (u_j - \bar{u}_T)' R (u_j - \bar{u}_T)] \end{aligned} \tag{3.14}$$

subj. to

$$\begin{aligned} & x_{j+1} = Ax_j + Bu_j + B_d d_j, \quad j = 0, \ldots, N \\ & x_j \in \mathcal{X}, \quad u_j \in \mathcal{U}, \quad j = 0, \ldots, N-1 \\ & x_N \in \mathcal{X}_f \\ & d_{j+1} = d(j) \\ & x_0 = \hat{x}(0) \\ & d_0 = \hat{d}(0), \end{aligned} \tag{3.15}$$

$$\begin{aligned} & \mathcal{X} = \{x_j \in \mathbb{R}^2 : j = 0, ..., N-1\} \\ & \mathcal{U} = \{u \in \mathbb{R} : -i_0 \leq u_j \leq i_{max}\}, \ j = 0, ..., N-1 \\ & \mathcal{X}_f = \{x_N \in \mathbb{R}^2\} \end{aligned} \tag{3.16}$$

where N is the prediction and control horizon, and the targets $\bar{x}_T$ and $\bar{u}_T$ are given by

$$\begin{bmatrix} A-I & B \\ C & C_d \end{bmatrix} \begin{bmatrix} \bar{x}_T \\ \bar{u}_T \end{bmatrix} = \begin{bmatrix} -B_d d_0 \\ r(t) - C_d d_0 \end{bmatrix} \tag{3.17}$$

In (3.14), Q is a positive semi-definite matrix, and matrices P and R are positive definite and P satisfies the Algebraic Riccati Equation

$$P = A^T PA - (A^T PB)(B^T PB + R)^{-1}(B^T PA) + Q. \tag{3.18}$$

A tailored solver was used for the online execution of the OF-MPC controller. It was obtained by means of the $\mu AO - MPC$ code generation tool [79], which provides C code libraries for the efficient online implementation of MPC problems. The solver is based on an augmented Lagrangian method together with Nesterov's gradient method and guarantees a deterministic execution time [79], since the maximum computation time required by the MPC in the dSpace hardware is about 25 μs. At each sampling instant k, the constrained optimal control problem (3.14)-(3.17) is solved over a finite time prediction horizon N, using the current observed state of the plant $\hat{x}(k)$. The method yields an optimal control sequence $U_0(k) = \{u_0^*, ...u_{N-1}^*\}$, from which the first command $u(k) = u_0^*$ is applied to the plant.

The MPC design parameters adopted in the present case are listed in Table 3.3. The prediction horizon N is selected as the smallest value to obtain a fast-enough response, but guaranteeing the feasibility of the constrained optimal control problem formulation. As is common practice, the value of R is fixed to 1, while Q, i.e., the weight matrix for the state $q(t)$ and $v(t)$, is designed to obtain a reasonable compromise between a sufficiently fast response and low noise amplification. The matrix P is obtained from (3.18).

Table 3.3: OF-MPC design parameters

Parameter	value
N	12
Q	$\begin{bmatrix} 5 \times 10^6 & 0 \\ 0 & 0.1 \end{bmatrix}$
R	1
P	$\begin{bmatrix} 98255756 & 804198 \\ 804198 & 10020 \end{bmatrix}$

A nonlinear version of the proposed method could be investigated to take into account the plant nonlinearity effects [46]. In this case, the design should be conducted considering Equation (3.2) instead of Equation (3.3). The technique would be based on a different solver and on the replacement of the Kalman filter with a nonlinear observer method. The designer should take care of possible issues related to the convergence of the solution and guarantee a deterministic execution time [46].

3.5 Experimental results and discussion

The experimental tests are conducted to validate the system performance in terms of: correctness of the Kalman filter estimation, offset-tracking with the cancellation of

plant-model mismatch, and low-frequency disturbance estimation. The tests are performed with the arm of the AMB system in a vertical direction to avoid the load due to its weight and with a bias current of 0.5 A.

The first test consists of providing a step excitation through the actuators with a disturbance current (i_d in Figure 3.2) of 0.2 A, corresponding to a force of about 3.5 N at a nominal air gap. The obtained results are reported in Figure 3.3. In particular, Figure 3.3a illustrates the nominal force provided to the system (dotted line), the force obtained from (3.2) (dashed line), and its estimate from the Kalman filter (solid line). It can be pointed out that, even with no current disturbance ($t < 0.1$ s), the control output and disturbance estimation values are nonzero, which is caused by the plant-model mismatch. As expected from (3.6), both effects of plant-model mismatch and external disturbances are lumped into a force estimate to move the controller targets and guarantee offset-free tracking. Figure 3.3b illustrates the simulated (dashed line) and experimental (solid line) MPC command: providing the disturbance current i_d , the Kalman filter estimates change, and the controller target is modified to achieve zero offset on the output. Finally, Figure 3.3c reports the comparison between the measured position (solid line) and that estimated from the Kalman filter (dashed line) (the simulation results are not reported in this plot for clarity's sake). The proposed controller is able to recover the effect of the disturbance and reach a null offset in about 0.06 s. The same figure evidences that since the position estimation has low noise (RMS value during 1 $s = 0.79$ μm) with respect to the measurement (RMS value during 1 s $= 1.12$ μm), the signals in the control loop are inherently filtered and clean. The good match between the simulation and experimental results demonstrates the effectiveness of the modeling approach.

The same test is conducted with different amplitudes of excitation to obtain a more exhaustive validation in different operating conditions. Figure 3.4a shows the comparison between the nominal and the estimated disturbance force, and Figure 3.4b displays the corresponding displacement. In this case, the offset due to the plant-model mismatch is removed in post-processing to highlight the correctness of the external disturbance force estimation.

It can be noted that, while the transient response changes considerably because of the nonlinear nature of the plant, at a steady state, the force estimate is still consistent with the current disturbance. This is due to the well-known physical linearization of AMB actuators' characteristics (3.2) taking place when the moving mass is in a centered position ($q = 0$), and both electromagnets are active, ($i_c < i_0$). In these conditions, the current-force characteristic is substantially linear and coefficient k_i does not depend on the new control current value, provided that the moving mass reaches the offset free displacement at the center of the gap.

The next set of tests is performed to evaluate the capability of the proposed method to cancel the plant-model mismatch. As mentioned above, the linear model has been obtained considering a bias current of 0.5 A. If a different value of bias current is set in the experimental tests, the model is not representative of the plant anymore. This

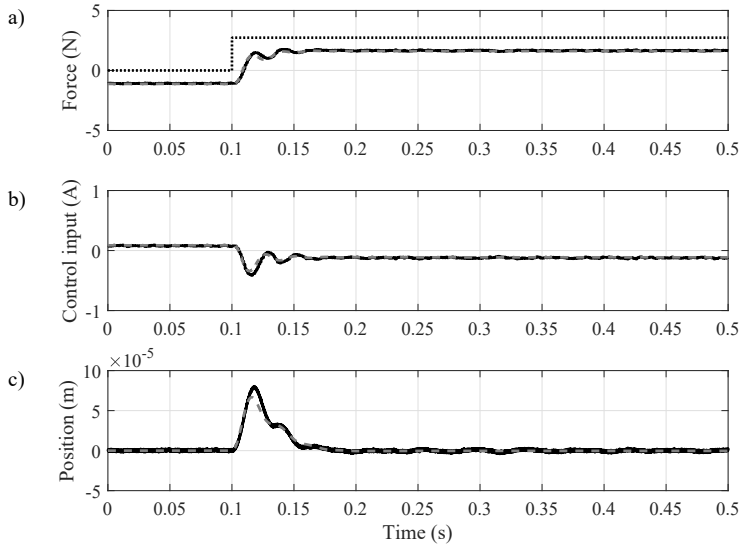

Figure 3.3: Step excitation through the actuators with a current $i_d = 0.25$ A. (a) Nominal force applied to the system (dotted line); force from model simulation (dashed line); force estimated experimentally by the Kalman filter (solid line). (b) MPC command (dashed line: simulation result; solid line: experimental result). (c) Displacement of the mass (solid line: eddy current sensor direct measurement; dashed line: Kalman filter estimation).

plant-model mismatch clearly affects the behavior of simple MPC architectures when no integral action exists, while the proposed OF-MPC method allows this issue to be overcome and, at the same time, the amount of disturbance to be evaluated.

Figure 3.5 illustrates the results of the tests performed by imposing consecutive changes of the bias current from 0.3 A to 0.7 A (d) and comparing the behavior of the displacement of the proposed OF-MPC (a) and of a simple MPC (b) which is based on the same formulation but with targets to the origin (i.e., $\bar{x}_T = 0, \bar{u}_T = 0$, which means no knowledge about plant-model mismatch and disturbance forces). As stated before, both controllers have been designed on the base of a plant model that considers a bias current of 0.5 A. The displacement plot of Figure 3.5a shows that the OF-MPC compensates for the plant-model mismatch effectively, providing, at the same time, an estimation of the disturbance force (c). However, from Figure 3.5b, an offset in the displacement is always present with the MPC controller, even when bias current is the designed one.

The aim of the last set of tests is to evaluate the correctness of the load variation estimation. The tests are performed as illustrated in Figure 3.6 by applying known values of force to the system by means of direct weights (L) acting on the arm by means of a pulley and a piece of string.

Figure 3.7 shows the estimation performance comparing the estimated force (solid

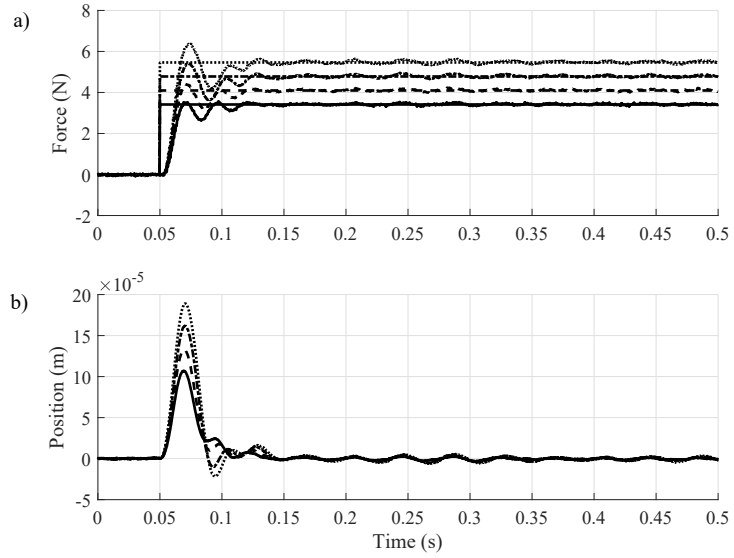

Figure 3.4: Step excitation at different force amplitudes (i_d [A] $= 0.3,\ 0.35,\ 0.4,\ 0.7$). (a) Nominal vs. estimated applied force. (b) Displacement of the mass.

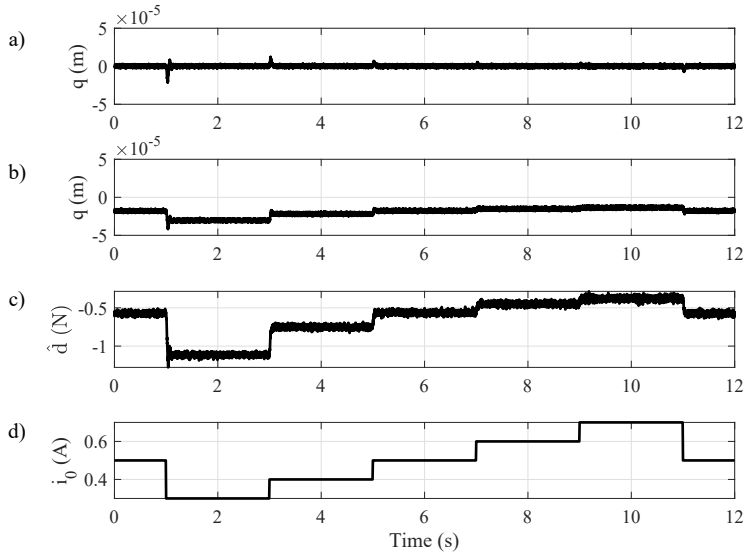

Figure 3.5: Effects of the plant-model mismatch on OF-MPC (a) and MPC (b) architectures. (c) is the estimation of the force equivalent to the plant-model mismatch (obtained only with OF-MPC architecture) and (d) is the variation of bias current provided to the plant.

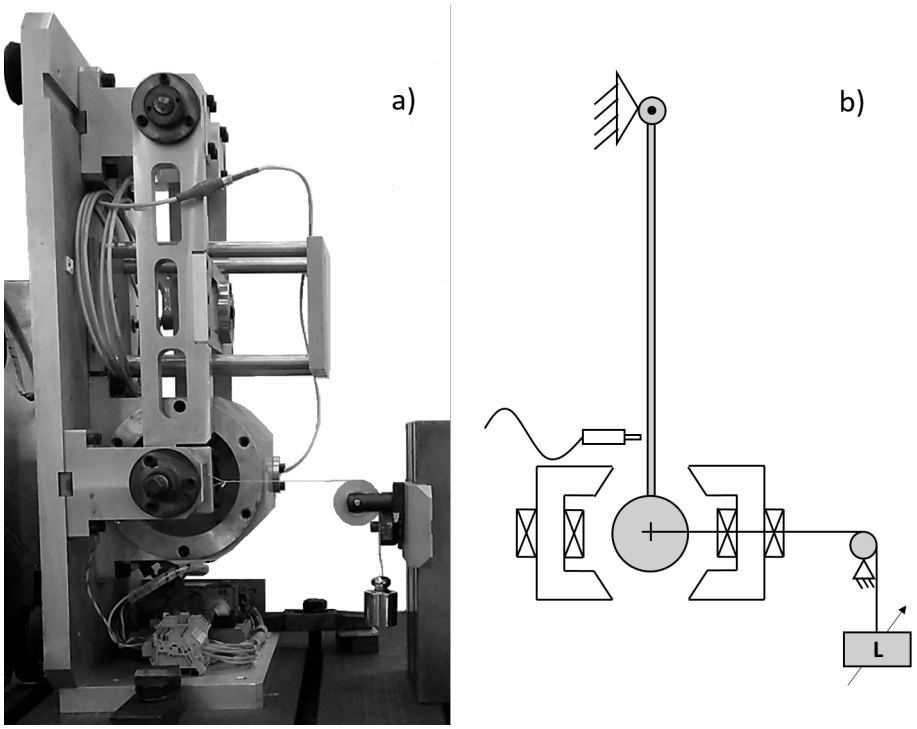

Figure 3.6: Experimental setup for the load variation estimation test. Picture (a) and layout (b) of the setup. L: variable load.

line) with the applied force (dashed line). The precision of the estimation is around $97\ \%$ until the control current is lower than the bias current (0.5 A) and decreases down to $90\ \%$ when one electromagnet is switched off. It is worth noticing that if the disturbance requires switching off one electromagnet (the control current is higher than the bias current), the system is not working in linear differential mode anymore and the electromagnets work in a nonlinear range, even in the nominal position. The force estimation is still acceptable even under these conditions, and this shows the good performance of the proposed strategy, even in a nonlinear operating range.

3.6 Conclusions

In this Chapter, the application of linear Offset-Free Model Predictive Control (OF-MPC) to a single-axis active magnetic bearing system has been presented. The proposed method is based on a disturbance observer with an augmented plant model including an input disturbance estimation. The proposed technique allows the well-known advantages of MPC to be exploited and, at the same time, the effect of plant-model mismatch in the reference tracking to be overcome. This architecture allows the real-time estimation of the low-frequency disturbance applied to the system. This last property is of

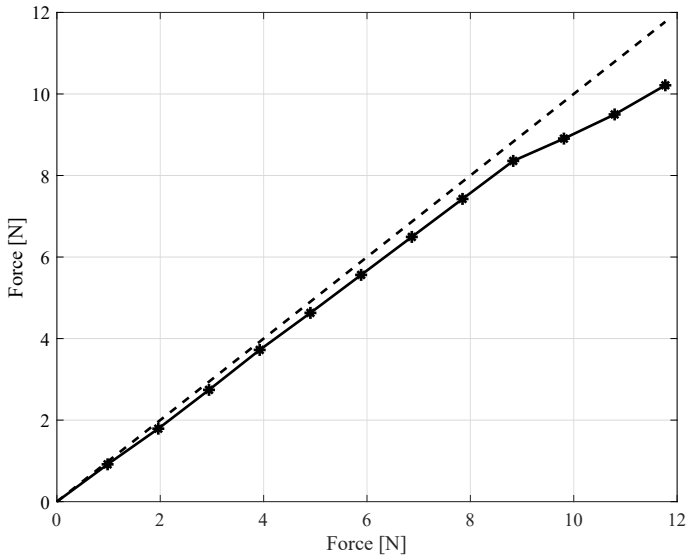

Figure 3.7: Load variation estimation test. Dashed line: real applied force. Solid line: estimated force. The values of the force estimate are referred to the vertical axis.

great interest in industrial applications like compressors and blowers, where keeping the reference position is critical to insuring the system functionality, even when the axial load changes according to the operating conditions. The modeling and control design have been described and validated experimentally for a single-axis AMB system with a set of tests that demonstrate the effectiveness of the approach in terms of reference tracking with the cancellation of plant-model mismatch effects and estimation of low-frequency disturbances and load variations.

Chapter 4

OF-MPC on a Cone-shaped Active Magnetic Bearing System

This chapter presents the study of linear OF-MPC for a cone-shaped AMB System. The modeling of the system is described together with the design of the OF-MPC in all its parts: general control architecture, disturbance model and observer design, target calculation, and the control problem formulation. An OF-MPC variant with reduced control horizon is proposed and implemented in real time. The OF-MPC resulted a promising constrained optimal control technique for cone-shaped AMB since the coupling of axial and radial control actions, together with the coil current limitations can be optimally handled by the controller. The experimental results demonstrate that OF-MPC overcomes decentralized PID controllers in terms of axial disturbance rejection.

4.1 Introduction

With cone-shaped AMBs, the rotor motion is controlled simultaneously in the axial and radial directions by two radial bearings with cone-shaped magnetic core. This configuration eliminates the requirement of a dedicated axial actuator but (i) makes the control more complex than conventional cylindrical AMB solutions due to the coupling of the axial and radial control actions, and (ii) the systems becomes less actuated in axial direction (i.e., low axial force generation capability).

In cone-shaped AMBs, the inherent coupling between the radial and axial control actions, together with the low axial force generation capability and coil current limitations result difficult to manage when using decentralized control strategies. The current on each electromagnet is the sum of axial and radial control contributions to generate axial and radial restoring forces. When using decentralized control, for example, one Proportional-Integral-Derivative (PID) controller for each degree of freedom [38, 37], each controller knows only about the control contribution it produces but nothing about the real current flowing into the coils. It is due to the simultaneous presence of axial

and radial control current contributions in the same coil. Commonly, the coil current limitations are treated as external saturation blocks and hence not optimally handled. No previous study has investigated the low axial force generation capability of these kind of systems in terms of control design.

This Chapter presents the benefits of applying OF-MPC for a cone-shaped AMB system. A procedure for the overall design is presented and supported by the experimental work conducted in a scaled machine that reproduces a turbo-compressor unit in a high-performance aircraft. Firstly, the computational burden associated with the online execution of the OF-MPC is addressed by reducing the control horizon in the problem formulation. The resulting Quadratic Programming (QP) problem is translated to C code using CVXGEN, a C code generator for embedded convex optimization. The OF-MPC is compared with conventional PIDs. The experimental results demonstrate that the OF-MPC outperforms the PID controller when the system is perturbed in axial direction. With OF-MPC, the coil current limitations are optimally handled, and zero-offset tracking at steady state is guaranteed based on the disturbances estimate. The approach is also effective in guaranteeing the stability and robustness according to standards for AMB systems. The plant-model mismatch estimate can be interpreted as an engineering quantity for the real-time evaluation of both the plant operation and the quality of the internal model of the controller.

The work is organized as follows. The plant under study is described in Section 4.2. The nonlinear plant modeling is presented in Section 4.3 and the actuator configuration in Section 4.4. The control strategy is detailed in Section 4.5 together with its main ingredients: a linear plant model, the augmented estimator, the target selector and ends with the analysis of the execution time obtained for different hardware. Some preliminary simulations are used to validate numerically the control strategy and introduce the two main parameters involved in the tuning process of the controller and the estimator. The experimental results are presented in Section 4.7 to demonstrate the effectiveness of the controller and Section 4.8 concludes the work.

4.2 Plant description

The plant under study is a scaled reproduction of a turbo-compressor group of a conditioning unit used in high performance jet aircraft. The conical geometry of magnetic bearings allows to perform a compact design of actuation stage whose composed of only four pairs of electromagnets instead of five of conventional cylindrical solution, resulting of great interest for the application in small machines. Turbine and compressor impellers are simulated by two discs of steel. According to the FEM model of the rotor (not presented here), the first two flexible rotor modes are around $10831\ \mathrm{rad/s}$ and $31331\ \mathrm{rad/s}$, respectively. The corresponding critical speeds are beyond the maximum reachable spin speed, that is equal to $20000\ \mathrm{rpm}$.

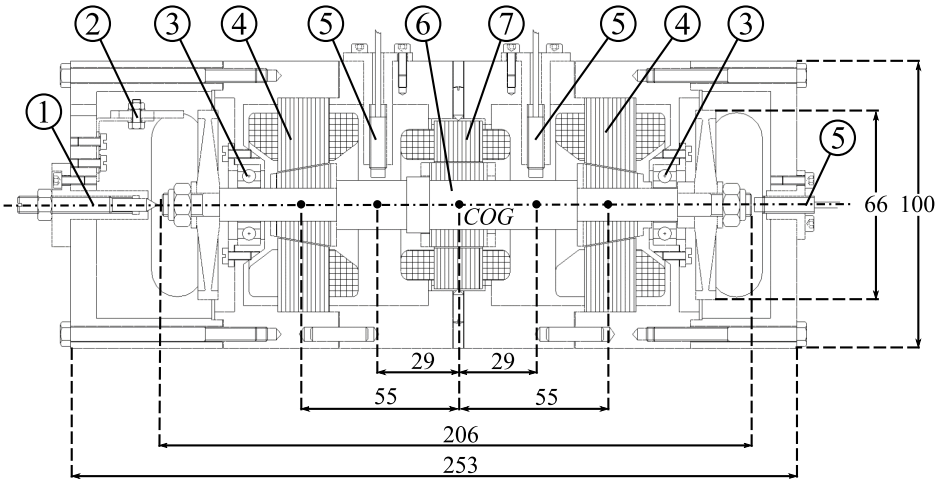

Figure 4.1: Section view of the machine. 1) Centering tip. 2) Spin speed sensor. 3) Landing bearings. 4) Magnetic actuators. 5) Inductive displacement sensors. 6) Rotor. 7) Electric motor. The dimensions are in mm.

4.3 Nonlinear plant modeling

Figure 4.2 shows the electromagnetic forces $(F_1, ..., F_8)$ produced by the eight electromagnets placed on the stator. These forces are generated by varying the coil currents to control the shaft position. Table 4.1 presents the main parameters of the system that are involved in the modeling equations.

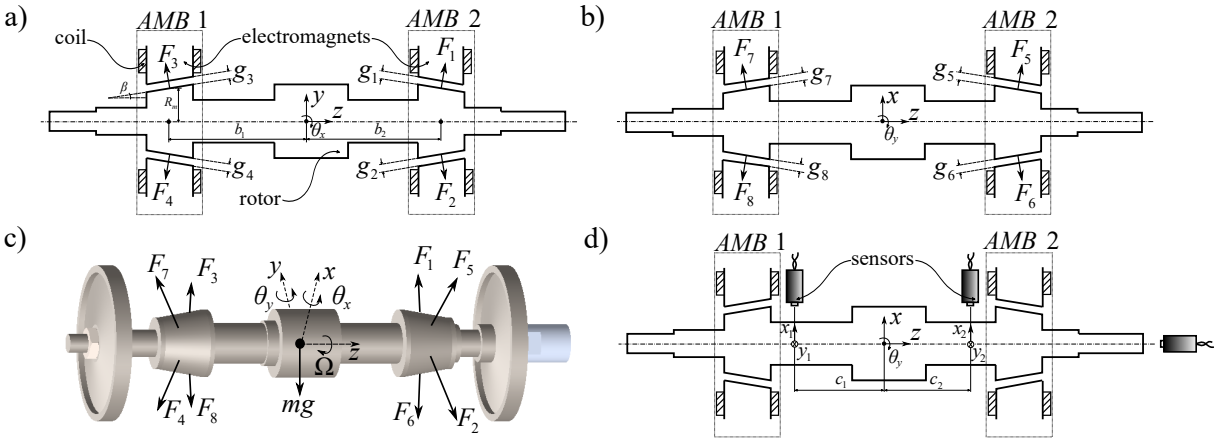

Figure 4.2: Forces on a) Y-Z and b) X-Z planes. c) 3D projection of the motor shaft with the two discs that simulate the turbine and compressor impellers. d) Displacement sensors on $x_{1,2}$ and z directions. Two other sensors are installed in $y_{1,2}$ directions but omitted in the scheme.

Assuming that the rotor is rigid, and considering the gyroscopic effects [80], the

Table 4.1: Plant parameters

Subsystem	Symbol	Name	Value	Unit
Rotor	g_0	Nominal air gap	0.45×10^{-3}	m
	m	Rotor mass	0.755	kg
	J_p	Polar moment of inertia	1.54×10^{-4}	kgm^2
	J_d	Diametrical moment of inertia	31.68×10^{-4}	kgm^2
	β	Inclined angle of the magnetic core	0.98	rad
	b_1	Distance between the radial magnetic bearing (1) and the center of gravity	55×10^{-3}	m
	b_2	Distance between the radial magnetic bearing (2) and the center of gravity	55×10^{-3}	m
	c_1	Distance between the sensor coordinates in bearing (1) and the center of gravity	29×10^{-3}	m
	c_2	Distance between the sensor coordinates in bearing (2) and the center of gravity	29×10^{-3}	m
	R_m	Effective radius	12.4×10^{-3}	m
Actuators	N_t	Coil turns	82	–
	R_{coil}	Coil resistance	0.5	Ω
	L_0	Nominal Inductance	1.2×10^{-3}	H
	S	Cross-sectional pole face area	118×10^{-6}	m^2

equations of motion can be written as

$$m\ddot{z} = (F_1 + F_2 + F_5 + F_6)\sin\beta - (F_3 + F_4 + F_7 + F_8)\sin\beta + F_z \tag{4.1a}$$

$$m\ddot{x} = (F_5 - F_6 + F_7 - F_8)\cos\beta + F_x \tag{4.1b}$$

$$m\ddot{y} = (F_1 - F_2 + F_3 - F_4)\cos\beta + F_y \tag{4.1c}$$

$$\begin{aligned} J_d\ddot{\theta}_x = &[(F_1 - F_2)\,b2 + (F_4 - F_3)\,b_1]\cos\beta + (F_2 - F_1 + F_3 - F_4)\,R_m\sin\beta \\ &- J_p\Omega\dot{\theta}_y + M_x \end{aligned} \tag{4.1d}$$

$$\begin{aligned} J_d\ddot{\theta}_y = &[(F_6 - F_5)\,b2 + (F_7 - F_8)\,b_1]\cos\beta + (F_5 - F_6 + F_8 - F_7)\,R_m\sin\beta \\ &+ J_p\Omega\dot{\theta}_x + M_y \end{aligned} \tag{4.1e}$$

where $F_z,\ F_x,\ F_y$ are generalized disturbance forces acting on $(x,\ y,\ z)$ directions, respectively, and $M_x,\ M_y$ are moments around x-axis and y-axis, respectively; Ω stands for the spin speed; and the electromagnetic forces are given by

$$F_j = K\frac{i_j^2}{g_j^2};\ j = 1, ...,8, \tag{4.2}$$

with the force coefficient $K = \frac{\mu_0 S N^2 \cos\sigma}{4}$ in which $\sigma = \pi/8$ is the angle of each pole relative to the centerline between the poles. The bearing air gaps g_j presented in (4.2)

can be referred to the center of gravity (COG) coordinates involving the geometrical quantities introduced in Figure 4.2 as

$$g_{1,2} = g_0 - z\sin\beta \mp \cos\beta(y + b_2\theta_x) \tag{4.3a}$$
$$g_{3,4} = g_0 + z\sin\beta \mp \cos\beta(y - b_1\theta_x) \tag{4.3b}$$
$$g_{5,6} = g_0 - z\sin\beta \mp \cos\beta(x - b_2\theta_y) \tag{4.3c}$$
$$g_{7,8} = g_0 + z\sin\beta \mp \cos\beta(x + b_1\theta_y). \tag{4.3d}$$

Let $\boldsymbol{\zeta}$ denote the state vector $[z, x, y, \theta_x, \theta_y, \dot{z}, \dot{x}, \dot{y}, \dot{\theta}_x, \dot{\theta}_y]^\intercal$, $\boldsymbol{i}$ the vector of coils currents $[i_1, ..., i_8]^\intercal$ and $\boldsymbol{d}$ the vector of disturbances $[F_z,\ F_x,\ F_y,\ M_x,\ M_y]^\intercal$. When substituting (4.3) into (4.2) and then into (4.1a), the state equations can be compactly written as

$$\dot{\boldsymbol{\zeta}} = \boldsymbol{h}(\boldsymbol{\zeta}, \boldsymbol{i}, \boldsymbol{d}, \Omega), \tag{4.4}$$

which is a condensed nonlinear time-domain representation of the system. All the involved parameters are known and presented in Table 4.1, hence equation (4.4) can be used for numerical simulations of the full plant and for performance evaluation of the controller during the design phase.

4.4 Magnetic bearings actuation

In common AMB systems, the actuation along one axis of control is obtained as the sum of the contributions of two opposite electromagnets. They are typically operated in differential driving mode i.e., one electromagnet is driven with the sum of bias and a control current $(i_0 + i_{cj})$, while the opposite one with their difference $(i_0 - i_{cj})$ [1]. The same principle is applied also for conical AMB in the axial direction. By simple inspection in Figure 4.2, one can see that any positive deviation on z direction from the equilibrium point, might be compensated by increasing forces $F_{3,4,7,8}$ (AMB 1) and decreasing $F_{1,2,5,6}$ (AMB 2). The opposite condition is obtained in the case of negative deviations. Figure 4.3 is the schematic illustration of the control strategy together with the differential driving mode configuration.

Then five control currents $\boldsymbol{u} = [u_z, u_{x_1}, u_{y_1}, u_{x_2}, u_{y_2}]^\intercal$ are used to control the five dofs of the plant. The coil currents can be expressed in terms of control actions along the motion directions as

$$\begin{bmatrix} i_1 \\ i_2 \\ i_3 \\ i_4 \\ i_5 \\ i_6 \\ i_7 \\ i_8 \end{bmatrix} = i_0 + \underbrace{\begin{bmatrix} 1 & 0 & 0 & 0 & 1 \\ 1 & 0 & 0 & 0 & -1 \\ -1 & 0 & 1 & 0 & 0 \\ -1 & 0 & -1 & 0 & 0 \\ 1 & 0 & 0 & 1 & 0 \\ 1 & 0 & 0 & -1 & 0 \\ -1 & 1 & 0 & 0 & 0 \\ -1 & -1 & 0 & 0 & 0 \end{bmatrix}}_{K_u} \begin{bmatrix} u_z \\ u_{x_1} \\ u_{y_1} \\ u_{x_2} \\ u_{y_2} \end{bmatrix}, \tag{4.5}$$

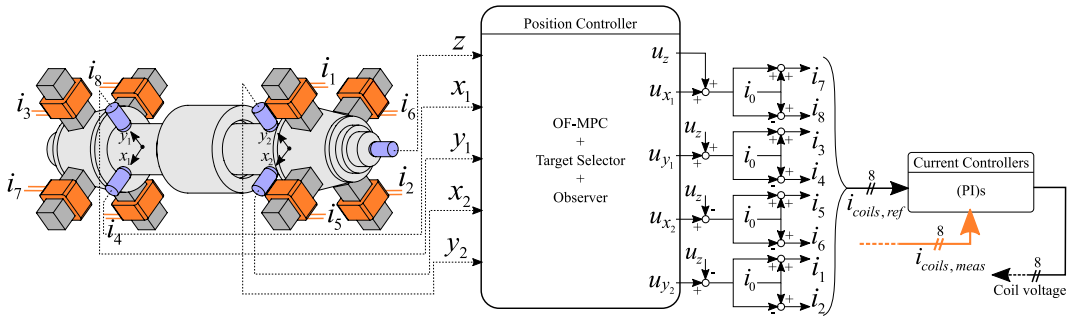

Figure 4.3: Control diagram with the transformation from control to coil currents. The subscript ref stands for *references* and $meas$ for *measurements*.

in which K_u is the transformation matrix between control actions and coil current deviations.

Actuator dynamics

Proportional-Integral (PI) current controllers are designed to speed up the actuators response. All the electromagnets are considered identical and the selected PI integral time τ_i cancels the open-loop time constant of the coils (i.e. $\tau_i = L_0/R_{coil}$. The resulting coil current dynamics can be modeled by the differential equations

$$\dot{i}_j = -\omega_{cl} i_j + \omega_{cl} i_{j,ref}, \; j = 1, ...,8, \tag{4.6}$$

where $i_{j,ref}$ is current reference for coil j and ω_{cl} is the bandwidth of the current loop. The latter can be theoretically defined as $\omega_{cl} = K_p/L_0$ where $K_p = 40$ V/A is the proportional gain. However, from experimental test, the bandwidth resulted around 1 kHz due to voltage saturation. Nevertheless, this dynamics is considered much faster than the mechanical one and then neglected throughout the modeling of the mechanical plant. Therefore, during the modeling phase of the mechanical dynamics it is assumed that the coil current references obtained from (4.5) are the currents flowing into the coils.

4.5 Linear OF-MPC Formulation

Model (4.4) may deviate from the real plant due to unmodeled dynamics, unknown disturbances, uncertain system parameters or modeling errors. Furthermore, the plant under study belongs to an aircraft, with disturbance forces that can change over time due to the aircraft maneuvering. The possibility to optimally handle the plant-model mismatch is offered by the offset-free model predictive control (OF-MPC) whose architecture is represented in Figure 4.4. It guarantees zero offset tracking adding integral action from the knowledge of the plant-model mismatch, while the controller design is

an automated design procedure based on the trade-off between the control effort and the error in the controlled variables. The observer estimates both state and disturbances which are used by the target calculator together with the reference vector r to obtain the input and state targets. Both target vectors together with the state and disturbance estimates are used to initialize the OF-MPC control problem. This Section presents the

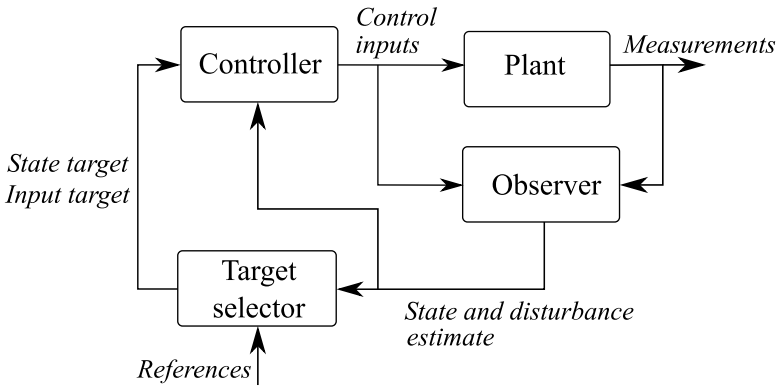

Figure 4.4: OF-MPC control scheme consisting of: controller, state estimator, and target selector.

main ingredients of the OF-MPC strategy: linear plant model, disturbance model, estimator of the augmented model and problem formulation.

4.5.1 Linear model

The nonlinear plant model (4.4) is linearized at nominal air gap g_0 with all the coil currents equal to the bias current $i_0 = 1.5$ A and at standstill operation ($\omega = 0$ rad/s). This linear model will be later adopted in the linear OF-MPC formulation. The linearization is done using Taylor series expansion

$$\dot{\boldsymbol{\zeta}} \doteq \underbrace{\left.\frac{\partial h}{\partial \boldsymbol{\zeta}}\right|_0}_{\bar{A}} (\boldsymbol{\zeta} - \boldsymbol{\zeta_0}) + \underbrace{\left.\frac{\partial h}{\partial \boldsymbol{i}}\right|_0}_{\bar{B}_i} (\boldsymbol{i} - \boldsymbol{i_0}) + \underbrace{\left.\frac{\partial h}{\partial \boldsymbol{d}}\right|_0}_{\bar{B}_d} (\boldsymbol{d} - \boldsymbol{d_0}). \tag{4.7}$$

Denoting the coil current $i_j = i_{cj} + i_0,\ j = 1, ...,8$ and knowing that $\boldsymbol{\zeta} = \boldsymbol{\zeta} - \boldsymbol{\zeta_0}$ since $\boldsymbol{\zeta_0} = \boldsymbol{0}$, equation (4.7) results in

$$\dot{\boldsymbol{\zeta}} = \bar{A}\boldsymbol{\zeta} + \bar{B}_i \boldsymbol{i_c} + \bar{B}_d \boldsymbol{d}, \tag{4.8}$$

where $\boldsymbol{i_c}$ is the vector of the coils current deviations. Expressing the coil current deviations $\boldsymbol{i_c}$ in terms of the control current vector $\boldsymbol{u}$

$$\boldsymbol{i_c} = K_u \boldsymbol{u}, \tag{4.9}$$

equation (4.8) becomes

$$\dot{\boldsymbol{\zeta}} = \bar{A}\boldsymbol{\zeta} + \underbrace{\bar{B}_i K_u}_{\bar{B}}\boldsymbol{u} + \bar{B}_d\boldsymbol{d}, \tag{4.10}$$

with

$$\bar{A} = \begin{bmatrix} 0 & 0 & 0 & 0 & 0 & 1 & 0 & 0 & 0 & 0 \\ 0 & 0 & 0 & 0 & 0 & 0 & 1 & 0 & 0 & 0 \\ 0 & 0 & 0 & 0 & 0 & 0 & 0 & 1 & 0 & 0 \\ 0 & 0 & 0 & 0 & 0 & 0 & 0 & 0 & 1 & 0 \\ 0 & 0 & 0 & 0 & 0 & 0 & 0 & 0 & 0 & 1 \\ 3634 & 0 & 0 & 0 & 0 & 0 & 0 & 0 & 0 & 0 \\ 0 & 58434 & 0 & 0 & 0 & 0 & 0 & 0 & 0 & 0 \\ 0 & 0 & 58434 & 0 & 0 & 0 & 0 & 0 & 0 & 0 \\ 0 & 0 & 0 & 39838 & 0 & 0 & 0 & 0 & 0 & 0 \\ 0 & 0 & 0 & 0 & 39838 & 0 & 0 & 0 & 0 & 0 \end{bmatrix},$$

$$\bar{B} = \begin{bmatrix} 0 & 0 & 0 & 0 & 0 \\ 0 & 0 & 0 & 0 & 0 \\ 0 & 0 & 0 & 0 & 0 \\ 0 & 0 & 0 & 0 & 0 \\ 0 & 0 & 0 & 0 & 0 \\ 6.28 & 0 & 0 & 0 & 0 \\ 0 & 8.90 & 0 & 8.90 & 0 \\ 0 & 0 & 8.90 & 0 & 8.90 \\ 0 & 0 & -111.15 & 0 & 111.15 \\ 0 & 111.15 & 0 & -111.15 & 0 \end{bmatrix},$$

$$\bar{B}_d = \begin{bmatrix} 0 & 0 & 0 & 0 & 0 \\ 0 & 0 & 0 & 0 & 0 \\ 0 & 0 & 0 & 0 & 0 \\ 0 & 0 & 0 & 0 & 0 \\ 0 & 0 & 0 & 0 & 0 \\ 1.32 & 0 & 0 & 0 & 0 \\ 0 & 1.32 & 0 & 0 & 0 \\ 0 & 0 & 1.32 & 0 & 0 \\ 0 & 0 & 0 & 315.66 & 0 \\ 0 & 0 & 0 & 0 & 315.66 \end{bmatrix}.$$

Due to the mathematical complexity of the nonlinear model, the Jacobian matrices $\bar{A}$, $\bar{B}_i$ and $\bar{B}_d$ are obtained using Matlab symbolic tools (see Matlab code in Appendix A.3).

Sensor coordinates

Equation (4.10) is the plant model referred to the COG coordinates $(z, x, y, \theta_x, \theta_y)$. However, in this work, a transformation to the sensor coordinates (z, x_1, y_1, x_2, y_2) is preferred. By inspecting Figure 4.2 d), the displacement sensors installed on the plant fix the sensor coordinates comprised in the equation

$$\begin{bmatrix} z \\ x_1 \\ y_1 \\ x_2 \\ y_2 \end{bmatrix} = \underbrace{\begin{bmatrix} 1 & 0 & 0 & 0 & 0 \\ 0 & 1 & 0 & 0 & c_1 \\ 0 & 0 & 1 & -c_1 & 0 \\ 0 & 1 & 0 & 0 & -c_2 \\ 0 & 0 & 1 & c_2 & 0 \end{bmatrix}}_{T} \begin{bmatrix} z \\ x \\ y \\ \theta_x \\ \theta_y \end{bmatrix}. \tag{4.11}$$

Let $\boldsymbol{q} = [z,\ x_1,\ y_1,\ x_2,\ y_2,\ \dot{z},\ \dot{x}_1,\ \dot{y}_1,\ \dot{x}_2,\ \dot{y}_2,\ \dot{z}]^\intercal$ denote the plant state referenced to the sensor coordinates, then

$$\boldsymbol{q} = \mathcal{T}\boldsymbol{\zeta}, \tag{4.12}$$

in which $\mathcal{T} = blockdiag(T, T)$ is the state transformation matrix from the COG coordinates. When substituting $\boldsymbol{\zeta}$ from (4.12) into (4.10)

$$\dot{\boldsymbol{q}} = \underbrace{\mathcal{T}\bar{A}\mathcal{T}^{-1}}_{\tilde{A}}\boldsymbol{q} + \underbrace{\mathcal{T}\bar{B}}_{\tilde{B}}\boldsymbol{u} + \underbrace{\mathcal{T}\bar{B}_d T^{-1}}_{\tilde{B}_d}\boldsymbol{d}. \tag{4.13}$$

Applying exact discretization to (4.13) with sampling time $T_s = 0.25 \times 10^{-3}$ s we have

$$\boldsymbol{q}(k+1) = A\boldsymbol{q}(k) + B\boldsymbol{u}(k) + B_d\boldsymbol{d}(k) \tag{4.14a}$$

$$\boldsymbol{y} = C\boldsymbol{q}(k). \tag{4.14b}$$

The output equation (4.14b) with $C = [I_{5\times5}\ \mathbf{0}_{5\times5}]$ has been added to turn (4.14) into a discrete-time linear state space representation of the plant under study. It will be used as the internal model of the OF-MPC controller.

4.5.2 Linear augmented model

To guarantee offset-free control of the output $\boldsymbol{y}$ in the presence of plant/model mismatch and/or unmeasured disturbances, the plant model (4.14) is augmented with an integrating disturbance according to the general methodology proposed by Pannocchia and Rawlings [43]. This methodology requires one to add a number of integrating disturbances equal to the number of measured variables in a way that the resulting augmented system is detectable. To this aim infinitely many choices are available. In this work, the so called *input disturbance model* is used. It consists of adding an integrating state $\boldsymbol{d}$ that enters the system at the same place as the inputs $\boldsymbol{u}$. According to [53], several studies have pointed out that such a disturbance model is an appropriate choice

for efficiently rejecting unmeasured disturbances (see [81, 44]). By inspecting equation (4.14), external disturbances are already modeled as unmeasured external forces $\boldsymbol{d}$. The resulting augmented system is presented in discrete-time domain as follows

$$\begin{bmatrix} \boldsymbol{q}(k+1) \\ \boldsymbol{d}(k+1) \end{bmatrix} = \underbrace{\begin{bmatrix} A & B_d \\ 0_{n_d \times n_q} & I_{nd \times nd} \end{bmatrix}}_{A_{aug}} \begin{bmatrix} \boldsymbol{q}(k) \\ \boldsymbol{d}(k) \end{bmatrix} + \underbrace{\begin{bmatrix} B \\ \mathbf{0}_{n_d \times n_u} \end{bmatrix}}_{B_{aug}} \boldsymbol{u} + \begin{bmatrix} \boldsymbol{w}_q(k) \\ \boldsymbol{w}_d(k) \end{bmatrix} \tag{4.15a}$$

$$\boldsymbol{y}_m(k) = [C\ \mathbf{0}_{ny \times nd}] \begin{bmatrix} \boldsymbol{q}(k) \\ \boldsymbol{d}(k) \end{bmatrix} + \boldsymbol{w}_n(k). \tag{4.15b}$$

where $\boldsymbol{w}_q \in \mathbb{R}^{n_q}$ and $\boldsymbol{w}_d \in \mathbb{R}^{n_d}$ represent the state and disturbance noise, respectively; $\boldsymbol{y}_m$ stands for the measurements, i.e., the model output $\boldsymbol{y}$ corrupted by the measurement noise $\boldsymbol{w}_n \in \mathbb{R}^{n_y}$. With some abuse of notation, the added disturbances are named $\boldsymbol{d}(k)$. It means that hereinafter, the estimates $\hat{\boldsymbol{d}}$ will lump not only the real external forces but also the plant-model mismatch. $n_q = 10$, $n_d = 5$, and $n_y = 5$ are the number of states, disturbances and measurements, respectively.

4.5.3 Disturbance estimator and target calculation

If the augmented plant model is detectable, an estimator can be implemented to get the state $\hat{\boldsymbol{q}}(k)$ and the disturbance $\hat{\boldsymbol{d}}(k)$ estimates based on the measurements $\boldsymbol{y_m}$ and inputs $\boldsymbol{u}$. Thus, the current filtered state and disturbance, respectively, are

$$\begin{aligned} \begin{bmatrix} \hat{\boldsymbol{q}}(k+1) \\ \hat{\boldsymbol{d}}(k+1) \end{bmatrix} = &\begin{bmatrix} A & B_d \\ 0_{n_d \times n_q} & I_{n_d \times n_d} \end{bmatrix} \begin{bmatrix} \hat{\boldsymbol{q}}(k) \\ \hat{\boldsymbol{d}}(k) \end{bmatrix} + \begin{bmatrix} B \\ 0_{n_d \times n_u} \end{bmatrix} \boldsymbol{u}(k) \\ &+ \begin{bmatrix} L_q \\ L_d \end{bmatrix} (\boldsymbol{y_m}(k) - C\hat{\boldsymbol{q}}(k)) \end{aligned} \tag{4.16}$$

where $L_q \in \mathbb{R}^{n_q}$ and $L_d \in \mathbb{R}^{n_d}$ are the predictor gain matrices for the state and the disturbance, respectively. They are obtained using the Kalman filter design approach, based on the information of the noise intensities. The disturbance (process noise) $[\boldsymbol{w_q}\ \boldsymbol{w_d}]$, and measurement noise inputs $\boldsymbol{w_n}$ are assumed to be uncorrelated zero-mean Gaussian stochastic processes with covariance matrices W_0 and V_0 given by

$$W_0 = blockdiag(var\{\boldsymbol{w_q}\}, var\{\boldsymbol{w_d}\}), \tag{4.17a}$$

$$V_0 = var\{\boldsymbol{w_n}\}. \tag{4.17b}$$

The variances $var\{\cdot\}$ of $\boldsymbol{w_q}$, $\boldsymbol{w_d}$ and $\boldsymbol{w_n}$ are treated as adjustable parameters. An increase in the ratio between $\boldsymbol{w_q}$ and $\boldsymbol{w_d}$ makes the filter slower in estimating the disturbance, while an increase in the ratio between $\boldsymbol{w_n}$ and $\boldsymbol{w_d}$ makes the estimator less sensitive to the output noise [53]. Even with this general insight of how to tune the variances, the proper selection of them is not trivial and some rules of thumbs are proposed below.

Robustifying the estimator

It is a well known fact that finite time optimal controllers does not necessarily result in closed-loop stable systems. Within the MPC community it is common practice to add a final state constraint and/or a final state penalty in order to obtain guaranteed stability [82, 83]. However, a final question raised by the use of observers combined with MPC is whether or not closed-loop stability is retained when the true states are replaced by state estimates in the control law [48, § 5.7]. In this work, two approaches are suggested to improve the robustness of the system controlled with an OF-MPC + Estimator. The first one, presented by Doyle in [84], is an adjustment procedure for observer-based linear control systems which asymptotically achieves the same loop transfer functions (and hence the same relative stability, robustness, and disturbance rejection properties) as full-state feedback control implementations. The idea is to design the Kalman filter but tuning the process covariance matrix to handle effectively the trade-off between noise rejection and margin recovery in the following form:

$$W(\rho) = W_0 + \rho^2 B_{aug} B_{aug}^\intercal; \quad 0 \leq \rho \leq \infty, \tag{4.18a}$$

$$V = V_0. \tag{4.18b}$$

The scalar parameter ρ serves to tune that trade-off. When $\rho = 0$, the filter will be optimal with respect to the "true" (as modeled) system noise. As ρ increases the filter will do a poorer job of noise rejection but the closed-loop stability margins will improve. The "$_0$" subscripts stands for the noise intensities that are appropriate for the nominal plant.

The second proposed approach to robustify the system performance is using a reduced observer. According to [85, § 8.3], poor passband robustness due to poor state estimation in a full-order state estimator can be to some extent ameliorated by using a reduced-order observer with direct feedthrough of plant outputs [85]. This reduced observer is done by feeding the OF-MPC directly with the measurements $[z,\ x_1,\ y_1,\ x_2,\ y_2]$, together with their rate of variation $[\dot{z},\ \dot{x}_1,\ \dot{y}_1,\ \dot{x}_2,\ \dot{y}_2]$ obtained by discrete differentiation of the measurements. Note that this derivation procedure requires a cut-off filter to avoid noise amplification. In this way, only the disturbance estimate $\hat{\boldsymbol{d}}$ is obtained from (4.16).

Target selector

The augmented model lumps the plant-model mismatch into the external force estimates. If this mismatch persists over time and the desired reference is achieved ($\boldsymbol{y_m}_\infty = \boldsymbol{r}_\infty$) at steady state, then from the estimator we get the steady state relation

$$\underbrace{\begin{bmatrix} A - I & B \\ C & \mathbf{0}_{n_d \times n_u} \end{bmatrix}}_{A_t} \begin{bmatrix} \boldsymbol{q}_\infty \\ \boldsymbol{u}_\infty \end{bmatrix} = \begin{bmatrix} -B_d \hat{\boldsymbol{d}}_\infty \\ \boldsymbol{r}_\infty \end{bmatrix}. \tag{4.19}$$

It means that the state and inputs shall converge to $\boldsymbol{q}_\infty$ and $\boldsymbol{u}_\infty$ at steady state to compensate the plant model mismatch. That is why $\boldsymbol{q}_\infty$ and $\boldsymbol{u}_\infty$ become state and input "target" in the OF-MPC formulation as seen later. Note that $(\boldsymbol{q}_\infty, \boldsymbol{u}_\infty)$ can be obtained from the knowledge of $\hat{\boldsymbol{d}}_\infty$ and $\boldsymbol{r}_\infty$. However, the estimator (4.16) provides $\hat{\boldsymbol{d}}(t)$ at each time step t but $\hat{\boldsymbol{d}}_\infty$ is needed to get the targets. Assuming that the controller action is applied at time t, an anticipative action (preview) on the measured disturbance $\boldsymbol{d}(t)$, $\boldsymbol{d}(t+1)$, $\boldsymbol{d}(t+N+1)$ can be imposed by setting $\boldsymbol{d}(t+k) = \hat{\boldsymbol{d}}(t), \forall\, k = 0; ...; N-1$ and hence $\hat{\boldsymbol{d}}_\infty \equiv \hat{\boldsymbol{d}}(t)$ (causal action, no preview). Then $\boldsymbol{q}_\infty$ and $\boldsymbol{u}_\infty$ can be obtained from (4.19). Note that $\boldsymbol{q}_\infty$ and $\boldsymbol{u}_\infty$ exist for any $\hat{\boldsymbol{d}}_\infty$ and $\boldsymbol{r}_\infty$ if the matrix A_t has full rank.

4.5.4 OF-MPC formulation

A procedure to set the control requirements in frequency domain is proposed in [1, § 12.4] based on a balance between the rotor response and the control effort. The reader can easily understand through examples, how important the mixed optimization (i.e., trade-off between rotor response and use of control effort) is for the unbalance control when $\mathrm{H}_{2,\infty}$ or μ-synthesis control formulations are used. With OF-MPC, the control requirements can be treated in a similar fashion but in time-domain and using quadratic norms. OF-MPC offers a systematic way to optimally handle this trade-off between control effort and controlled outputs taking into account plant dynamics and constraints. The OF-MPC problem is formulated as

$$\begin{aligned}\min_{u} \quad & \frac{1}{2}\left(\boldsymbol{q}_N - \boldsymbol{q}_t\right)^\intercal P \left(\boldsymbol{q}_N - \boldsymbol{q}_t\right) + \frac{1}{2}\sum_{k=0}^{N-1}\left(\boldsymbol{q}_k - \boldsymbol{q}_t\right)^\intercal Q \left(\boldsymbol{q}_k - \boldsymbol{q}_t\right) \\ & + \frac{1}{2}\sum_{k=0}^{M-1}\left(\boldsymbol{u}_k - \boldsymbol{u}_t\right)^\intercal R \left(\boldsymbol{u}_k - \boldsymbol{u}_t\right) \qquad (4.20a)\end{aligned}$$

subj. to

$$\boldsymbol{q}_{k+1} = A\boldsymbol{q}_k + B\boldsymbol{u}_k + B_d\boldsymbol{d}_k, \quad k = 0, \ldots, N-1, \qquad (4.20b)$$

$$\boldsymbol{d}_{k+1} = \boldsymbol{d}_k, \quad k = 0, \ldots, N-1, \qquad (4.20c)$$

$$\boldsymbol{u}_k = \boldsymbol{u}_t, \quad k = M, \ldots, N-1, \qquad (4.20d)$$

$$K_u\boldsymbol{u}_k \leq \boldsymbol{i}_{max}, \quad k = 0, \ldots, M-1, \qquad (4.20e)$$

$$\boldsymbol{q}_0 = \hat{\boldsymbol{q}}(t), \qquad (4.20f)$$

$$\boldsymbol{d}_0 = \hat{\boldsymbol{d}}(t), \qquad (4.20g)$$

with the targets $\boldsymbol{u}_t$, $\boldsymbol{q}_t$ given by

$$\begin{bmatrix} A - I & B \\ C & \mathbf{0}_{n_d \times n_u} \end{bmatrix} \begin{bmatrix} \boldsymbol{q}_t \\ \boldsymbol{u}_t \end{bmatrix} = \begin{bmatrix} -B_d\hat{\boldsymbol{d}}(t) \\ \boldsymbol{r}(t) \end{bmatrix}. \qquad (4.21)$$

Matrices $Q \succcurlyeq 0$ and $R \succ 0$ are used to properly weight the trade-off between the rotor clearance and available bearing capacity. They are selected in such a way that the rotor response consumes 25 % of the available clearance g_0 and, at the same time, for the control effort to be 20 % of the available bearing capacity (in terms of coil current). They are written as

$$Q = C' Q_y C;\ Q_y = diag([\alpha_z\ \alpha_{x_1}\ \alpha_{y_1}\ \alpha_{x_2}\ \alpha_{y_2}]) \frac{1}{(0.25 g_0)^2} I_{n_y \times n_y} \tag{4.22a}$$

$$R = (I_{n_u \times n_u} - diag([\alpha_z\ \alpha_{x_1}\ \alpha_{y_1}\ \alpha_{x_2}\ \alpha_{y_2}])) \frac{1}{(0.20 u_{max}^2)^2} I_{n_u \times n_u}, \tag{4.22b}$$

in which n_u and n_y are the number of inputs and measurements, respectively. The parameters

$$0 \leq \alpha_j \leq 1;\ j = z, x_1, y_1, x_2, y_2$$

are proposed here to tune the aggressiveness of the controller around the nominal control requirement. Note that when $\alpha_j = 0.5$, the trade-off is that one expected from the "nominal" weights. For $\alpha_j \geq 0.5$, the controller becomes more aggressive in "j" direction. The control input weight R involves the maximum control current $u_{j,max}$ which is set to 3.5 A to be consequent with the coil current limitation i.e., $u_{max} + i_0 = i_{max}$ in which $i_0 = 1.5$ A and $i_{max} = 5$ A. Hereinafter, Q_0 and R_0 denote the "nominal" weights on the states and inputs, respectively (i.e., when $\alpha_j = 0.5$).

The inclusion of the terminal penalty with the matrix P selected as the solution of the Discrete Algebraic Riccati Equation (DARE)

$$P = A^\intercal P A - (A^\intercal P B)(B^\intercal P B + R)^{-1}(B^\intercal P A) + Q, \tag{4.23}$$

and together with a terminal constraint (not included here), ensure nominal closed-loop stability [55]. However, these terminal cost and constraints can deteriorate the optimality of the problem and sometimes are avoided in real applications. A terminal constraint is not implemented here to reduce the amount of inequality constraints (as usually done in practical applications of fast MPC). The effects of P on the optimality of the OF-MPC problem will be later analyzed through some preliminary nonlinear simulations.

A prediction horizon of $N = 30$ is selected to cover most of the transient time of the closed-loop response. Note from (4.20a) that a reduction of the control moves (i.e., control horizon $M \leq N$) is applied to limit the computation burden of the optimization problem, as suggested for embedded fast MPC applications. The input signal $\boldsymbol{u}$ is frozen and held constant after prediction time $(M-1)$. The analysis of the controller execution time in a real microprocessor is done later to select the control moves.

Interestingly, note that the relation between *control currents* and *coil currents* are intrinsically considered in the problem formulation through the transformation matrix

$K_u \in \mathbb{R}^{n_{coils},n_u}$ with $n_{coils} = 8$. In conical-shaped AMB systems, the current passing through each coil is a combination of "control efforts" in axial and radial directions. Therefore, each decentralized controller can only limit the control effort it requests but the coil current limitations are implemented separately. When using OF-MPC, the coils current limitations are known by the controller and hence optimally handled.

4.5.5 The OF-MPC controller as a QP problem

By eliminating the state sequence from problem (4.20) using (4.20b)-(4.20d), the optimal control problem (4.20) can be expressed as the convex quadratic programming (QP) problem

$$\min_{\mathbf{u}} \quad \frac{1}{2}\mathbf{u}^\intercal \mathcal{H}\mathbf{u} + [\mathcal{F}^\intercal(\boldsymbol{q} - \boldsymbol{q_t}) - \mathcal{H}^\intercal \mathbf{u}_t]^\intercal \mathbf{u} \tag{4.24a}$$

subj. to

$$\mathcal{K}\mathbf{u} \leq \mathcal{I}, \tag{4.24b}$$

in which $\mathbf{u} = [\boldsymbol{u}_0^*;\ ...;\ \boldsymbol{u}_{M-1}^*]$ is the optimization variable, $\mathbf{u}_t = [\boldsymbol{u_t}; ...; \boldsymbol{u_t}]$ stands for the input targets during the control horizon, $\mathcal{H} \in \mathbb{R}^{Mn_u \times Mn_u}$ is the Hessian matrix and $\mathcal{F} \in \mathbb{R}^{n_q, Mn_u}$. The reader is directed to Section 2.5 for a detailed explanation of how it is done (see also Appendix A.4 for the custom Matlab functions involved in obtaining $\mathcal{H}$ and $\mathcal{F}$). The constraints (4.24b) are obtained writing down (4.20e) for each time step from $k = 0$ to $k = M - 1$ as

$$\underbrace{\begin{bmatrix} K_u & 0 & 0 \\ 0 & \ddots & 0 \\ 0 & 0 & K_u \end{bmatrix}}_{\mathcal{K}} \mathbf{u} = \underbrace{\begin{bmatrix} \boldsymbol{i_{max}} \\ \vdots \\ \boldsymbol{i_{max}} \end{bmatrix}}_{\mathcal{I}}, \tag{4.25}$$

with $\mathcal{K} \in \mathbb{R}^{Mn_{coils} \times Mn_u}$ and $\mathcal{I} \in \mathbb{R}^{Mn_{coils} \times 1}$. Since the matrices defining the dynamics, costs, and constraints in (4.20) do not vary during the execution of the OF-MPC controller (linear time-invariant (LTI) prediction model), the QP matrices in (4.24a)-(4.24b) can be precomputed off-line. Every time step, problem (4.24) is updated with $(\boldsymbol{q},\ \boldsymbol{q_t},\ \boldsymbol{u_t})$ and then solved to get $\mathbf{u}$ but only the input $\boldsymbol{u}_0^*$ is applied to the plant (due to the receding horizon principle of MPC).

As can be seen, applying OF-MPC requires solving the optimization problem (4.24) every time step based on the information of the estimated state and disturbances, and the state and input targets. A well-known technique for implementing fast MPC is to compute the entire control law offline, in which case the online controller can be implemented as a lookup table [86]. This method is named explicit MPC and works well for systems with small state and input dimensions (no more than five), few constraints, and short time horizons [87]. Fortunately, for larger systems, a variety of efficient algorithms already exist to solve a QP problem on-line. However, to the best of the author's

knowledge, the most convenient approach (i.e., explicit or online MPC) to embed the OF-MPC controller for a conical-shaped AMB system is not well defined yet. In this work, an online OF-MPC implementation is proposed using CVXGEN [88, 29] which is a C code Generator for embedded convex optimization. In CVXGEN, the algorithm that solves the QP problem is based on a standard primal-dual interior point method [29, § 5.2]. The CVXGEN code needed to formulate (4.24) is quite simple and freely available for academia [29]. The reader is directed to Appendix A.5 to check the CVXGEN code that corresponds to (4.24) when $M = 2$.

Selecting the control horizon

To limit the computational burden in MPC, it is often useful to limit the control horizon by "blocking" control moves after a certain input horizon M, $1 \leq M < N$ [54].

The larger the control moves M, the longer the computation time needed to solve the embedded QP problem. In fact, Eqs. 4.24a and 4.24b demonstrate how the QP problem dimension is strictly related to M. In this work, a preliminary study was carried out to select the control moves. Benchmarks for three different processors were performed to verify the control implementation feasibility. Table 4.2 presents the execution time needed to solve the OF-MPC for $M = 2, ...,5$.

Table 4.2: Execution time of the OF-MPC

Prediction horizon (M)	NXP (Freescale), QorlQ P5020, 2 GHz Time (ms)	Infineon TC1793, 260 MHz Time (ms)	TMS320F28379D, 200 MHz Time (ms)
2	0.095	0.62	1.83
3	0.213	1.56	-
4	0.392	2.78	-
5	0.645	-	-

Results in Tab. 4.2 indicate that the execution time is a quadratic function of the control moves. The plant under study is linearized with a sampling time $T_s = 0.25$ ms. Hence, the NXP QorlQ P5020 processor could be used for the OF-MPC with control moves up to $M = 3$ without the risk of overruns. However, due to the low-bandwidth mechanical dynamics of the system, larger time steps up to $T_s = 0.8$ ms are sufficient to control the plant. As such, off-the-shelf industrial processors such as the Infineon TC1793 become a feasible solution to implement OF-MPC. In contrast, the computational power of the TI TMS320F28379D processor is outperformed by the complexity of the control task, even with $M = 2$. In the following, we focus on the numerical and experimental validation of the OF-MPC strategy with $M = 2$, since it represents a worst-case scenario for the OF-MPC implementation.

4.6 Preliminary simulations

The OF-MPC performance as well as the the effectiveness of the estimator is studied with some preliminary nonlinear simulations of the plant. The control moves of the OF-MPC is set to $M = 2$ according to the QP execution time obtained in Section 4.5.5.

4.6.1 OF-MPC with full plant state knowledge

The evaluation of the controller is firstly done considering full state knowledge. The controller performance is tuned with the parameter α (see (4.22a)) to "move" the weights around the nominal ones (i.e., Q_0, R_0) and with terminal weight $P = Q$. The linearized plant model (4.14) is used as the internal model of the controller and the plant is simulated with the nonlinear model (4.4). Since the external disturbance are not estimated, the state and inputs targets are set to zero.

Figure 4.5 a) shows x_1 when α varies from 0.1 to 0.5 and with the initial plant state $\boldsymbol{q(0)} = [0,\ -0.2 \times 10^{-3},\ 0,\ 0,\ 0,\ 0,\ 0,\ 0,\ 0,\ 0]^\intercal$ (situation similar to a lift-up of the shaft in x_1 direction). It is evident how the aggressiveness of the controller changes with α. However, note that the coil current is limited to ($i_{max} = 5$ A). That is why the control performance does not change to much for $0.4 \leq \alpha_j \leq 0.5$. Because of the symmetry of the system, similar results (omitted here) are obtained when the same initial air gap deviation is applied on y_1, x_2 or y_2. Figure 4.5 b) shows the dynamics on the axial direction (z) for different values of α. Note that the coil currents also saturate when the shaft is steered to the nominal air gap in axial direction.

When repeating the same simulation, but with P as the solution of the DARE (4.23) the optimality of the problem is heavily deteriorated as shown in Figure 4.5 c) and d). Even if the time domain response appeared to be unaffected, the possibility to tune the control performance varying α is no longer possible. This result suggests not to use P as the DARE solution and set $P = Q$ instead. The closed-loop stability will be analyzed through the experimental results.

It can be seen that for position deviations around or larger than 0.2 mm (about 50 % of the clearance g_0) the coil currents saturate. This makes more interesting the application of any constrained optimal control such as the proposed OF-MPC approach, since these actuator limitations can be easily incorporated into the control problem formulation as inequality constraints.

4.6.2 Full simulation. OF-MPC + Estimator + target selector

As already seen in Figures 4.5 a) and c), there exists an offset on x_1 at steady state as well as a steady state control action $u_{x_1,\infty}$ that differs from zero. This is because the controller is compensating the rotor weight. An integral action is required to compensate this and any other external force affecting the plant in a proper manner. This is precisely what OF-MPC does in a systematic way. An augmented estimator is needed

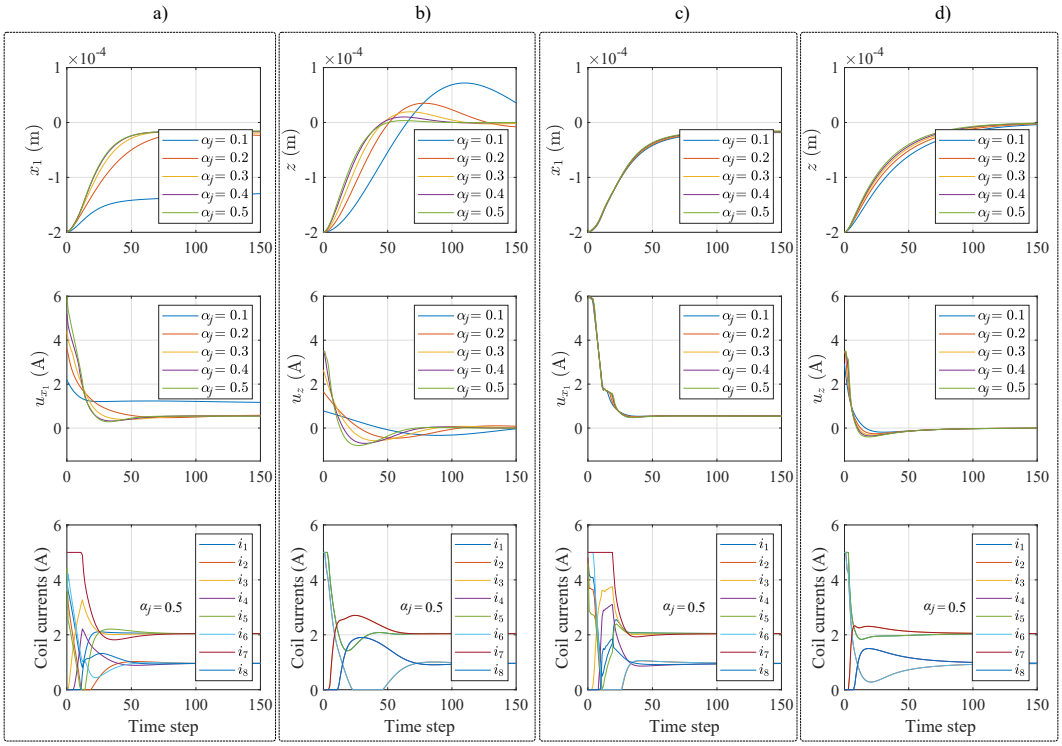

Figure 4.5: Lift-up simulation with the OF-MPC controller and assuming full state knowledge. a) Transient response of $x1$ with $P = Q$ b) Transient response of z direction with $P = Q$, c) Transient response of $x1$ with $P = \text{DARE}$ and d) Transient response of z with $P = \text{DARE}$. ($\alpha_j \equiv \alpha_{z,x_1,y_1,x_2,y_2}$).

to get not only the plant states but also the external disturbances. These estimates are passed to the target calculation to get the state and inputs targets needed to reach zero offset tracking.

Regarding the estimator design: the noise in the displacement measurements $\boldsymbol{w_n}$ is set to 5×10^{-6} m and the process noise $\boldsymbol{w_q}$ is assumed to be zero (i.e., perfect plant model only perturbed by $\boldsymbol{d}$) and hence the process noise together with the plant-model mismatch will be lumped into the external force estimates $\hat{\boldsymbol{d}}$. It is similar to think about $\boldsymbol{d}$ as a colored noise [89, § 7.2] added to the plant model. Since $var\{\boldsymbol{w_q}\}$ is fixed, $var\{\boldsymbol{w_d}\}$ is used to tune how fast the disturbance $\hat{\boldsymbol{d}}$ is estimated and the parameter ρ is used for the trade-off between noise rejection and margin recovery (see Section 4.5.3). Table 4.3 shows the assumed nominal noise intensities, and also the resulting predictor gains when $\rho = 1$.

Lifting up phase

Figure 4.6 shows a lift-up simulation of the plant but this time with full state estimation. Note that also the external forces and moments are estimated and put into

Table 4.3: Kalman filter design parameters

Parameter	Value
ρ	1
$var\{\boldsymbol{w_q}\}$	$\mathbf{0}_{n_q \times n_q}$
$var\{\boldsymbol{w_d}\}$	$0.01^2 I_{n_d \times n_d}$
$var\{\boldsymbol{w_n}\}$	$(5 \times 10^{-6})^2 I_{n_y \times n_y}$
L_q	$\begin{bmatrix} 0.39 & 0 & 0 & 0 & 0 \\ 0 & 0.54 & 0 & 0.12 & 0 \\ 0 & 0 & 0.54 & 0 & 0.12 \\ 0 & 0.12 & 0 & 0.54 & 0 \\ 0 & 0 & 0.12 & 0 & 0.54 \\ 262.0 & 0 & 0 & 0 & 0 \\ 0 & 479.22 & 0 & 179.24 & 0 \\ 0 & 0 & 479.22 & 0 & 179.24 \\ 0 & 179.24 & 0 & 479.22 & 0 \\ 0 & 0 & 179.24 & 0 & 479.22 \end{bmatrix}$
L_d	$\begin{bmatrix} 1639.0 & 0 & 0 & 0 & 0 \\ 0 & 1011.30 & 0 & 1011.30 & 0 \\ 0 & 0 & 1011.30 & 0 & 1011.30 \\ 0 & 0 & -1144.5 & 0 & 1144.5 \\ 0 & 1144.5 & 0 & -1144.5 & 0 \end{bmatrix}$

the disturbance $\boldsymbol{d}$. As expected, the main disturbance is precisely the rotor weight which is distributed in x and y axes due to the $45°$ inclination of the bearings (see that $\hat{F}_{x_\infty} \approx \hat{F}_{y_\infty} = \frac{\sqrt{2}}{2} mg$) while no external disturbances are present on $(z,\ \theta_x,\ \theta_y)$ directions. The inputs and state targets are then calculated and passed to the controller to guarantee an offset-free reference tracking at steady state. One of the main advantages of OF-MPC for magnetic bearings applications is the way in which the plant-model mismatch in handled. The linear plant model does not know about the existence of the weight force or any other disturbance but it is however quantified into $\boldsymbol{d}$ and hence compensated. Any force acting on each dof is lumped into the estimates. The integral action that OF-MPC produces is based on these estimates which in some extent, represent how far the linear internal model of the OF-MPC is from the actual operation of the plant. However, it is important to remark that the estimates $\hat{\boldsymbol{d}}$ are not an accurate representation of external forces because $\boldsymbol{d}$ lumps both model uncertainties and real external forces.

Impact test

The plant state as well as the control inputs obtained from a simulation of impact forces applied on z, x and y are presented in Figure 4.7. The test has been conducted

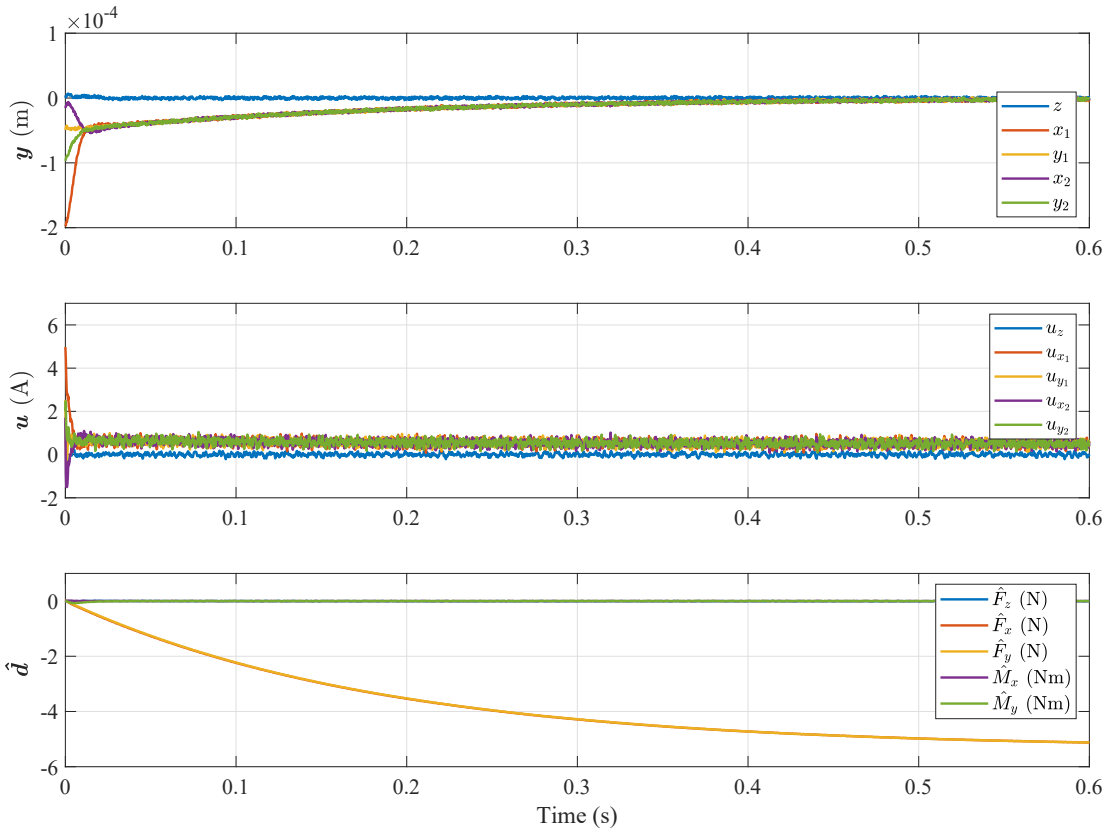

Figure 4.6: Lift-UP response with arbitrary initial sates and assuming a noise measurement about 5×10^{-6} m. The disturbance $\hat{\boldsymbol{d}} \neq \mathbf{0}$ because the rotor weight compensation.

imposing a random noise $|\boldsymbol{w_n}| \leq 5 \times 10^{-6}$ m on each measurement channel. An impact test is applied on z direction at time ($t = 0.025$ s), on x direction at time ($t = 0.1$ s) and on y at time ($t = 0.15$ s). The OF-MPC has been set with $\alpha_{z,x_1,y_1,x_2,y_2} = 0.2$. The comparison of $\boldsymbol{q}$ with its estimates $\hat{\boldsymbol{q}}$ demonstrates that: the observer has been properly designed, good enough damping characteristic of the closed-loop response is appreciated, and the control inputs (which are translated to coil current references) resulted not to much affected by the measurement noise.

The same impacts are applied again in Figure 4.8 but this time without robustifying the observer i.e., observer designed with $\rho = 0$. It shows how the quality of the estimates deteriorates and hence, an undesired closed-loop control performance is obtained. The poor estimation of the states could be ameliorated by assuming some process noise $\boldsymbol{w_q} \neq 0$ and then use the ratio between $\boldsymbol{w_q}$ and $\boldsymbol{w_d}$ for tuning. However, achieving good stability properties with this approach may become more difficult than just using ρ as explained in Section 4.5.3.

As already stated, the trade-off between noise rejection and margin recovery is directly handled by varying ρ. The concern now is that if ρ is increased. In fact, the

estimator will do a poorer job of noise rejection as appreciated in Fig 4.9 when $\rho^2 = 10$. Note how the control input $\boldsymbol{u}$ is much more influenced by the measurement noise than the previous simulations in Figs. 4.7 and 4.8.

By inspecting Figs. 4.8, 4.7, 4.9, is it evident the effectiveness of ρ as a design parameter. The apparent practical value of this procedure is that it gives a simple way of trading off between noise rejection and margin recovery [84].

The simulations presented α (for the OF-MPC) and ρ (for the estimator) as the main parameters involved in tuning the closed-loop performance. Due to the separation principle, both the OF-MPC controller and the estimator can be designed separately. Surprisingly, when the terminal weight P equals the DARE solution the optimality of the problem deteriorated considerably. That is why hereinafter, the terminal weight will equal the state weight Q. Since the OF-MPC formulation does not have the ingredients to guarantee nominal closed-loop stability, the resulting control performance will be analyzed more in depth later on throughout the real experiments.

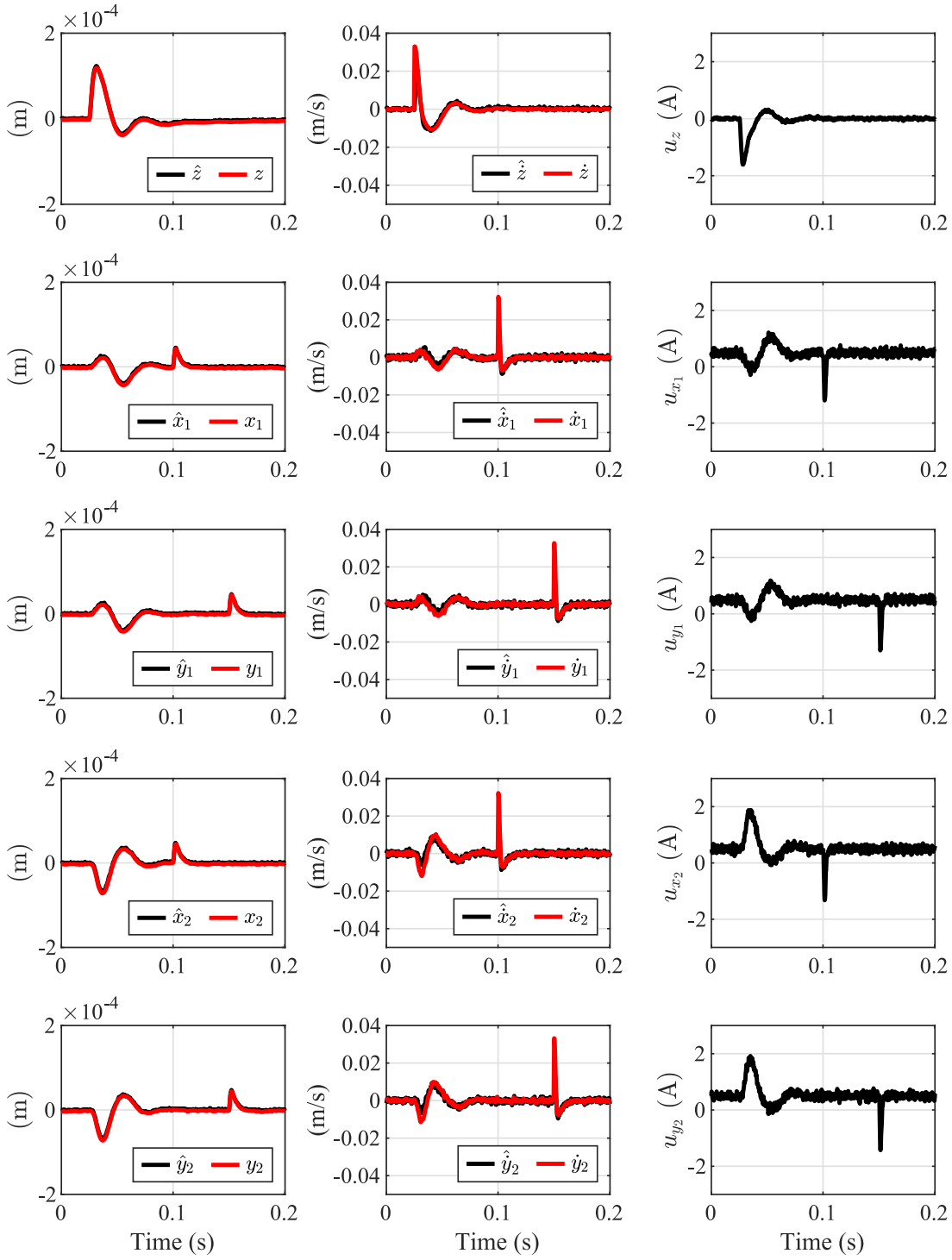

Figure 4.7: Impact test simulation with the estimator obtained for $\rho = 1$. An impact test on z direction at time ($t = 0.025$ s), on x at time ($t = 0.1$ s) and on y direction at time ($t = 0.15$ s). A random noise $|\boldsymbol{w_n}| \leq 5 \times 10^{-6}$ m has been imposed on each measurement channel.

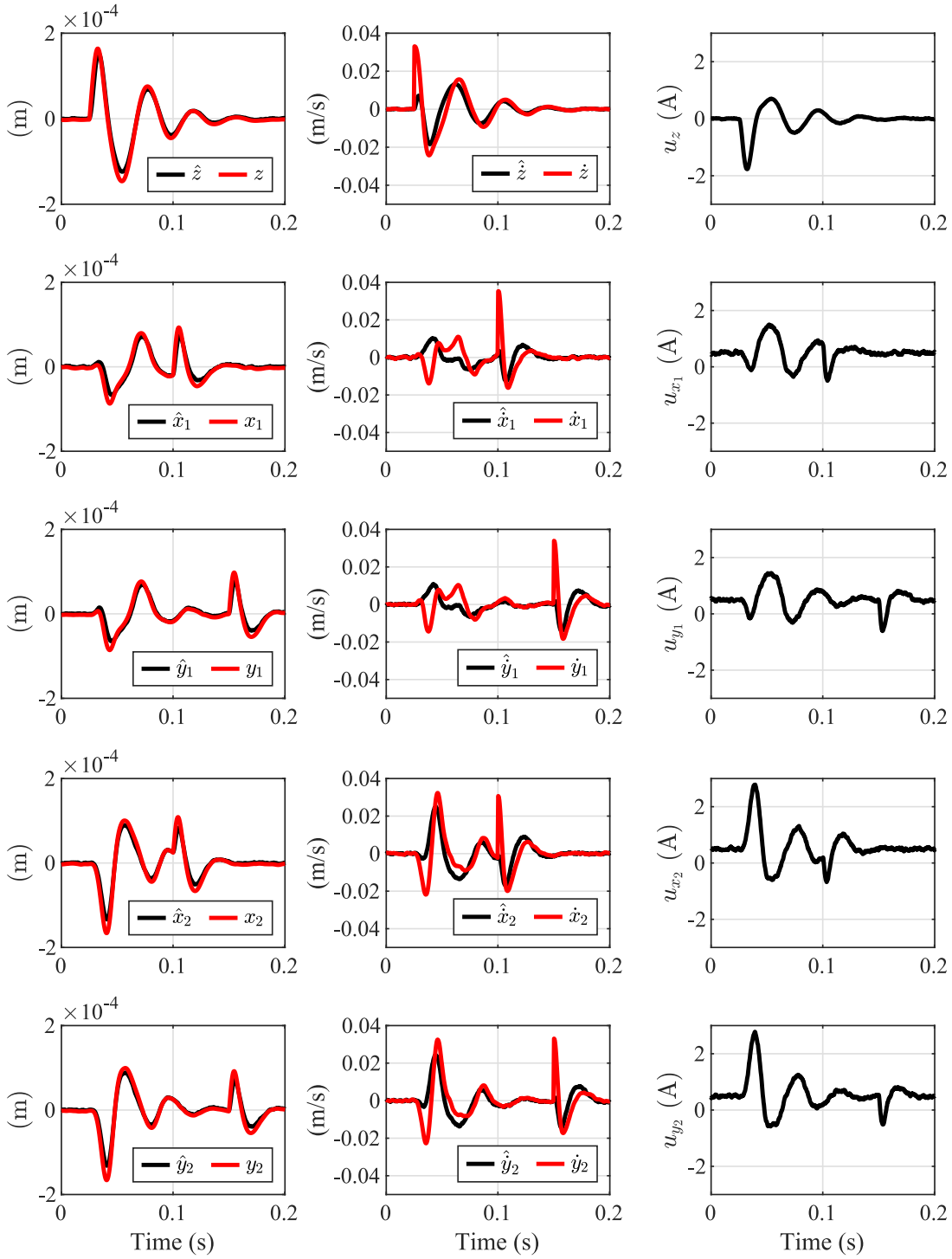

Figure 4.8: Impact test simulation. OF-MPC set with $\alpha_j = 0.2$ and observer designed from the knowledge of nominal noise intensities (i.e., $\rho = 0$).

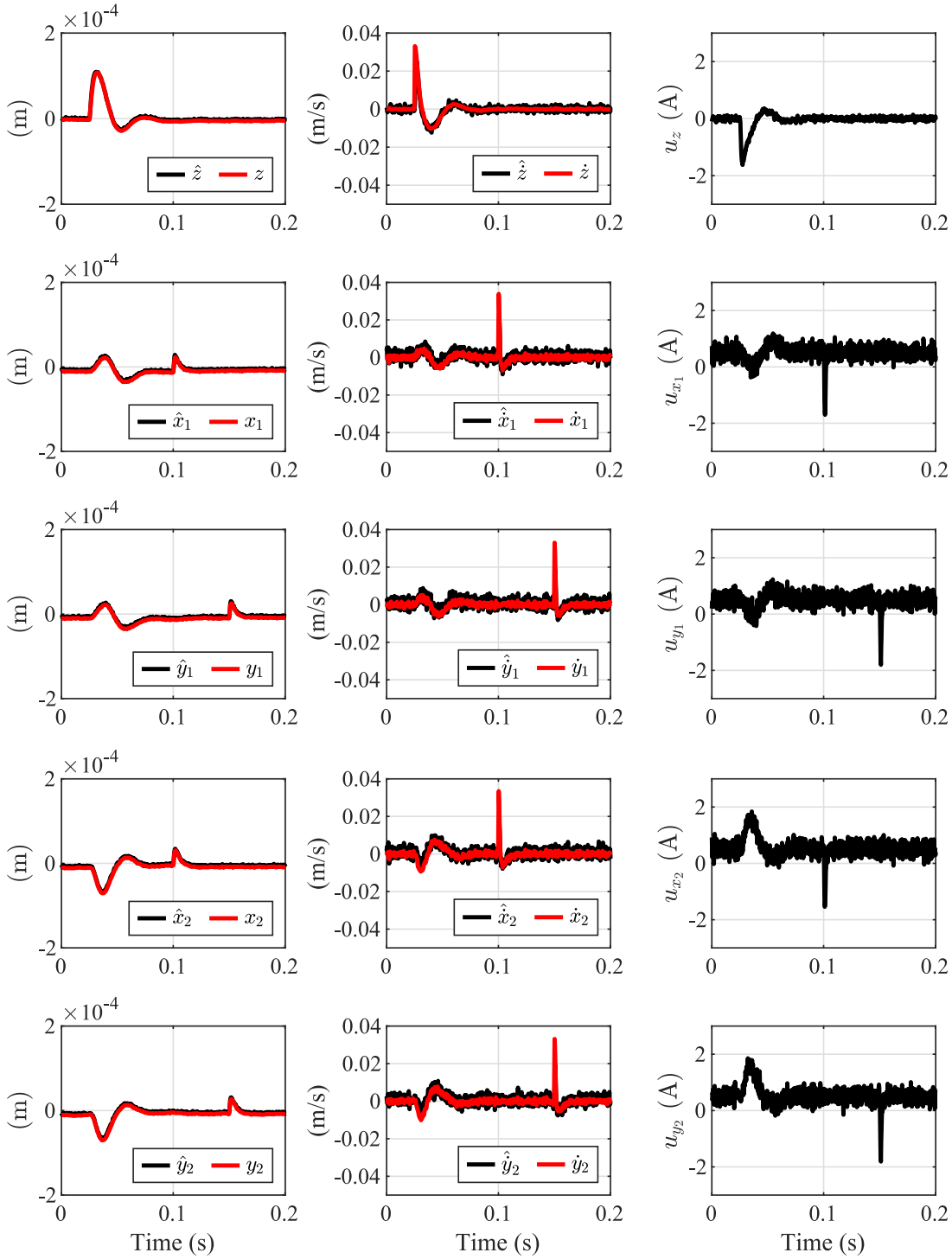

Figure 4.9: Impact test simulation but this time with a poor noise rejection. Observer designed with $\rho^2 = 10$.

4.6.3 Comparison of OF-MPC with decentralized PID controllers

One of the main drawbacks of conical-shape AMB is the low axial force generation capability. The compensation of disturbance forces in axial direction can result difficult to attain when decentralized controllers are used. However, when using OF-MPC the maximum coil current saturation are known and optimally handled by the controller. A comparison of OF-MPC with decentralized PID controllers is presented here.

A control action given by a constant state feedback gain can be obtained by eliminating the inequality constraints from the QP formulation (4.20), and solving the optimal problem just once and off-line. It is done here to show also that the OF-MPC approach serves as a reference to design decentralized controllers for conical-shaped active magnetic bearings. This controller can be seen as a computationally cheap variant useful when the OF-MPC optimal control problem can not be solved in a deterministic time. Because $R \succ 0$, also $\mathcal{H} \succ 0$ thus (4.24a) is a positive definite quadratic function of $\mathbf{u}$. Therefore, its minimum can be found by computing its gradient and setting it to zero

$$\mathbf{u} = -\mathcal{H}^{-1}\mathcal{F}^{\intercal}(\boldsymbol{q}(0) - \boldsymbol{q}_t) + \mathbf{u}_t \tag{4.26}$$

where $\mathbf{u}(t) = \left\{\boldsymbol{u}_0^*, \ldots, \boldsymbol{u}_{M-1}^*\right\}$. Since only the first control in this sequence, $\boldsymbol{u}(t) = \boldsymbol{u}_0^*$, is applied to the plant, then

$$\boldsymbol{u}_{0,uc}^* = -K(\boldsymbol{q}(0) - \boldsymbol{q}_t) + \boldsymbol{u}_t, \tag{4.27}$$

where $K^{n_u \times n_q}$ is defined as the first n_u rows of the matrices $\mathcal{H}^{-1}\mathcal{F}'$. The control action (4.27) can be interpreted as an unconstrained discrete-time optimal controller obtained over a finite horizon. If the resulting K is such that the matrix $(A-BK)$ is Hurwitz, that is, all its eigenvalues have moduli smaller than one [48], hence the plant is closed-loop stable. The terms $\boldsymbol{u}_t$ is nothing but a small integral action added from the knowledge of the plant-model mismatch.

For example, with $\alpha_{z,x_1,y_1,x_2,y_2} = 0.2$, the corresponding matrices $\mathcal{H}$, $\mathcal{F}$ of the QP problem are calculated once and then the state feedback gain results

$$K = \begin{bmatrix} 9911 & 0 & 0 & 0 & 0 & 49 & 0 & 0 & 0 & 0 \\ 0 & 21390 & 0 & 3575 & 0 & 0 & 79 & 0 & 9 & 0 \\ 0 & 0 & 21390 & 0 & 3575 & 0 & 0 & 79 & 0 & 9 \\ 0 & 3575 & 0 & 21390 & 0 & 0 & 9 & 0 & 79 & 0 \\ 0 & 0 & 3575 & 0 & 21390 & 0 & 0 & 9 & 0 & 79 \end{bmatrix}.$$

Note that the state vector $\boldsymbol{q}$ is composed by the five controlled displacements and their derivatives: $\boldsymbol{q} = [z,\ x_1,\ y_1,\ x_2,\ y_2\ \dot{z},\ \dot{x}_1,\ \dot{y}_1,\ \dot{x}_2,\ \dot{y}_2]^{\intercal}$ and note that the term $(\boldsymbol{q}(0) - \boldsymbol{q}_t)$ represents the displacement errors and the error derivatives (because by definition, $\boldsymbol{q}_t$ stands for the steady state references), therefore decentralized PD controller gains (K_p: proportional gain; K_d: derivative gain) can be extracted from K as presented in Table 4.4. A cut-off derivative filter, with a time constant τ_f about ten times lower than the derivative time was added to each PD controller.

Table 4.4: Decentralized PD controllers ($\alpha_{z,x_1,y_1,x_2,y_2} = 0.2$)

Controller	K_p (A/m)	K_d (A/m/s^2)	$1/\tau_f$ (s^{-1})
$\mathrm{PD_z}$	9911	49	2000
$\mathrm{PD_{z,x_1,y_1,x_2,y_2}}$	21390	79	2500

Figure 4.10 shows the control layout of both decentralized and OF-MPC controllers. This time, the plant state needed by the OF-MPC is directly obtained from the measurements. This makes fair the comparison because the Kalman filter dynamics will not affect the control loop shape. The plant state is composed by the measurements $[z,\ x_1,\ y_1,\ x_2,\ y_2]$, together with their rate of variation $[\dot{z},\ \dot{x}_1,\ \dot{y}_1,\ \dot{x}_2,\ \dot{y}_2]$. The latter are filtered with the same cut-off derivative filter presented in Table 4.4 for the decentralized controllers.

As seen in Figure 4.10 b), a small integral action $\boldsymbol{u_t}$ is added to the PD actions to guarantee zero-offset tracking from the knowledge of the plant-model mismatch. The decentralized control results in PID controllers, one for each degree of freedom of the plant.

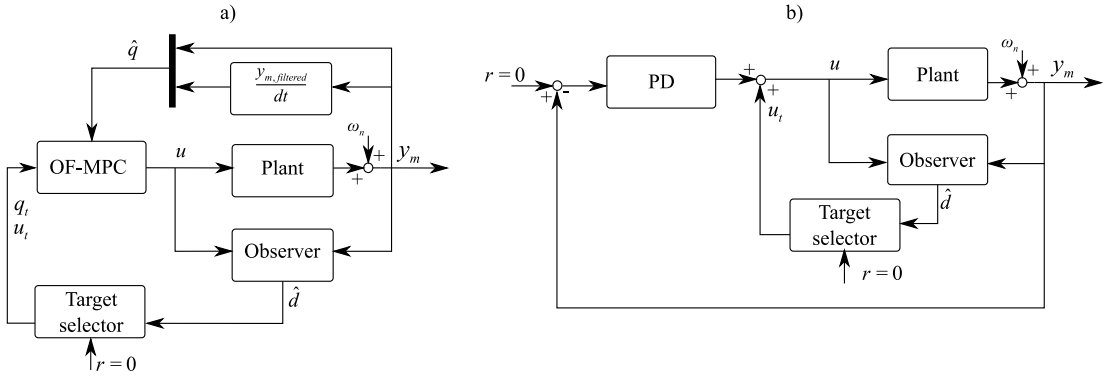

Figure 4.10: a) OF-MPC with a reduced observer i.e., only the disturbance estimates $\hat{\boldsymbol{d}}$ are obtained from the observer, $\hat{\boldsymbol{q}}$ is obtained directly from the measurements. Layout b): Control scheme with PID controllers. The integral action is identical in both OF-MPC and decentralized controllers.

Figure 4.11 shows the results from impact tests in axial direction. The plant has been simulated by the nonlinear system of equations (4.4). A saturation stage limits the coil currents when PIDs controllers are used (i.e., $0 \leq i_{coils} \leq 5$ A). The upper saturation is not necessary in the OF-MPC case because the upper limit values of coil currents are already known by the controller (see problem formulation: Eq. (4.20e)). As can be appreciated, the system responds quite similar when low impacts are applied: a) OF-MPC and b) PIDs. But note in c) and d) that the coil currents saturate when a higher impact is applied and therefore, larger air gap deviations are obtained. With the PIDs the air gap deviation are considerably higher that ones from the OF-MPC. The

fact is that OF-MPC handles much better the coil current saturation together with the trade-off between control effort and air gap deviations. This interesting benefits from applying OF-MPC is later confirmed by the experimental results.

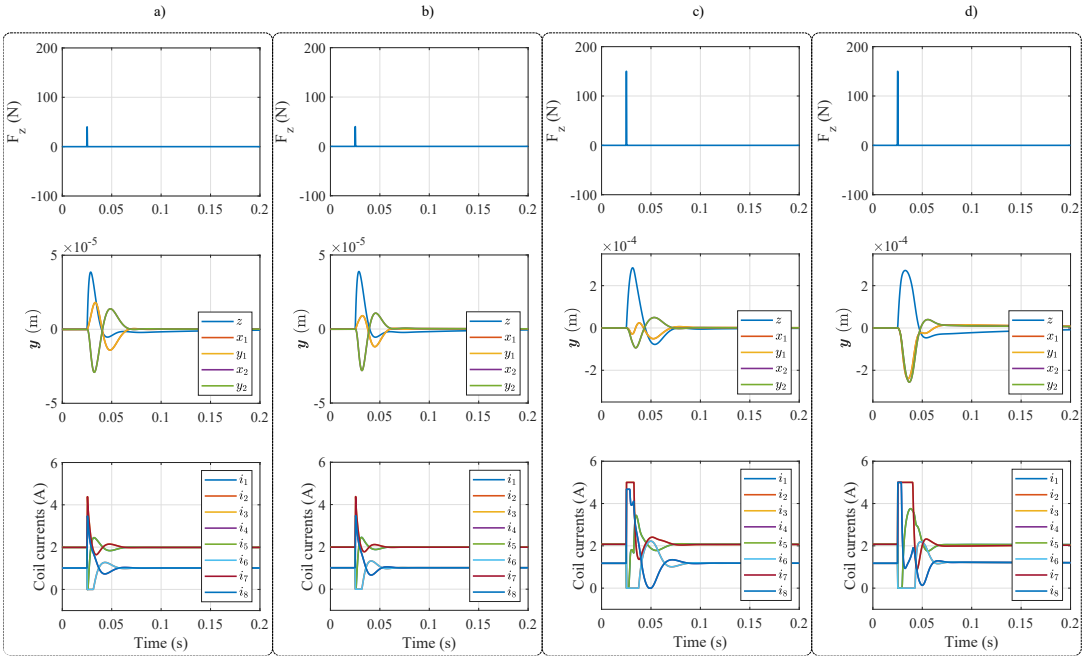

Figure 4.11: Simulation of an impact in axial direction. A low impact is applied in a) with an OF-MPC controller and b) with PIDs. The responses to larger impacts are presented in c) for OF-MPC and in d) for PIDs. Both the controllers are designed with $\alpha_{x_1,y_1,x_2,y_2} = 0.2$ and $\alpha_z = 0.4$. The rotor deviates much more when PIDs are used and the upper coil current limitations are reached.

4.7 Experimental results and discussion

Some experimental tests are conducted to validate the OF-MPC strategy in the test rig. Firstly, the lifting-up phase is presented to assess the controller in one of the most critical transient behavior of the system. Secondly, output sensitivity tests are conducted to evaluate the control performance for different configurations of α_j (OF-MPC tuning parameter) and ρ (Observer tuning parameter). Finally, the disturbance rejection properties of OF-MPC is compared with PIDs in axial direction i.e., the axis with lowest force generation capability of the plant.

4.7.1 Test rig description

Figure 4.12 shows the plant under study together with other components needed for the experimental test. A connection layout of the main components in the test bench is depicted in the diagram 4.13. Inside the control unit, a centralized position controller that runs at 4 kHz receives the air gap information from the displacement sensors and set the corresponding current reference for each electromagnet. Inner PI current controllers set the coils voltages by varying the PWM duty cycle on each power amplifier. The sampling frequency of the ADC module is triggered by the PWM carrier at $20\ \mathrm{kHz}$. The power amplifier is composed by eight of-the-shelf H-bridges in locked-antiphase operation i.e., $(0 \leftrightarrow 100)\ \%$ of duty cycle corresponds to $(-30 \leftrightarrow 30)\ \mathrm{V}$ in the AMB coils. A two-pole induction motor is controlled with a variable-frequency driver to spin the compressor up to the maximum reachable spin speed $\Omega = 20000\ \mathrm{rpm}$.

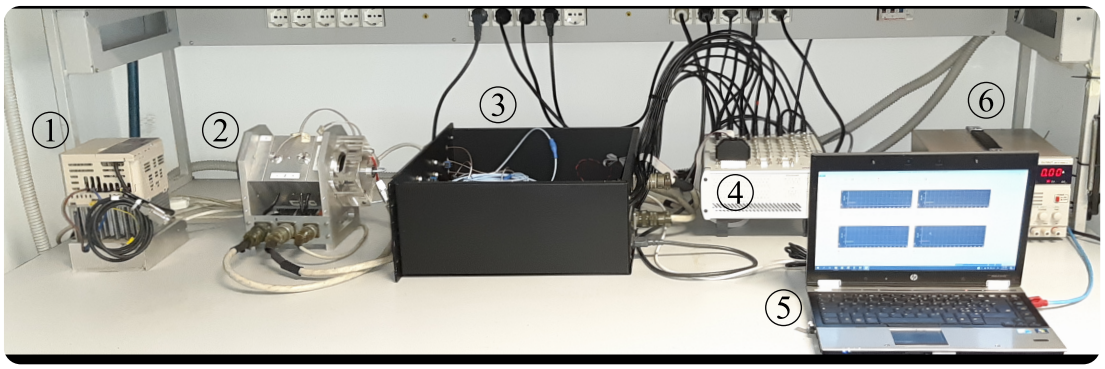

Figure 4.12: Test bench. (1) Motor driver, (2) Turbo-compressor on conical AMBs, (3) Power amplifier and sensor conditioning, (4) Control Unit: dSPACE MicroLabBox, (5) PC, (6) Power supply.

4.7.2 Lifting-up

Let remark that the plant under study belongs to an aircraft which means that the rotor will lift up many times from any initial condition (in contact with the back-up ball

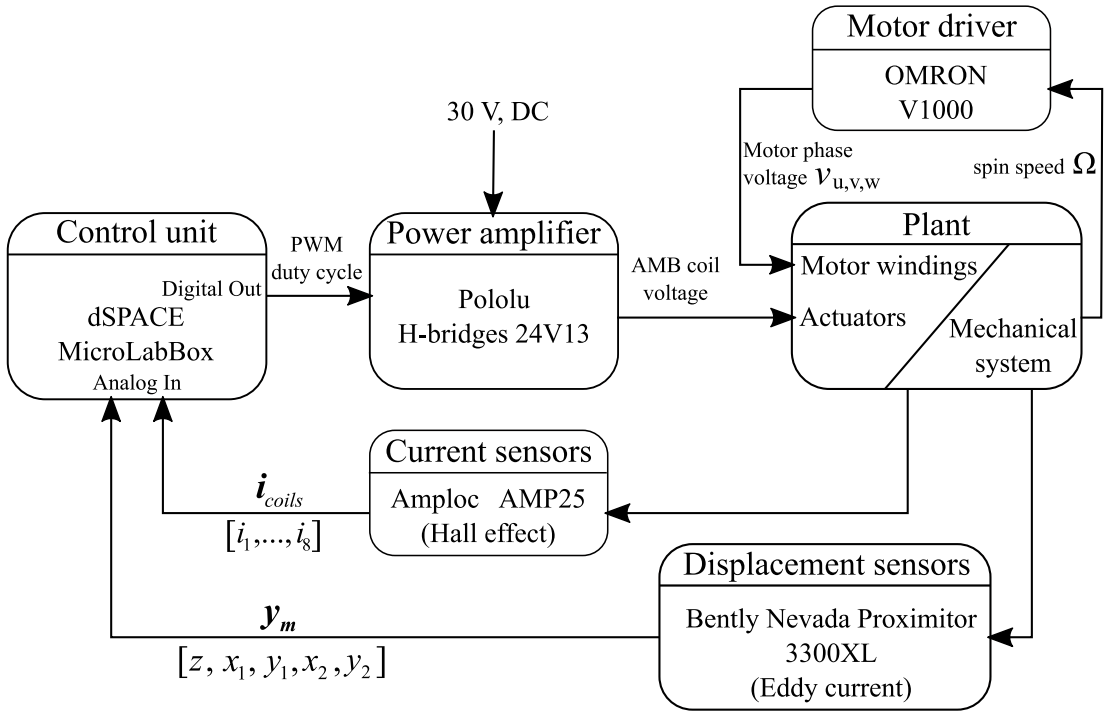

Figure 4.13: Overall layout of the test bench.

bearings) to the nominal air gaps g_0 ($\boldsymbol{q} = \mathbf{0}$). Before the shaft lifts up, the coils current controllers are switched on and a bias current $i_0 = 1.5$ A is imposed on each coil. Then the position controller (OF-MPC + estimator + target selector) is activated to steer the shaft to the nominal air gap as presented in Figure 4.14. By inspecting 4.14, one can say that the transient response resulted well damped and the coil current saturation is optimally handled by the controller. The plant behavior during this phase is highly nonlinear but a linear OF-MPC formulation resulted enough to steer the shaft properly. The target selector produces inputs targets based on the estimates to compensate the plant-model mismatch. In essence, this compensation produces an integral action and hence zero-offset tracking is reached at steady state. The steady state disturbances are not an accurate representation of the weight forces because there exist some part of the estimates that represent the plant-model mismatch. Note that the disturbance estimate $\hat{\boldsymbol{d}}$ lumps the weight force as expected from previous simulations (see Figure 4.6) but now the steady state estimate resulted slightly higher. This is because there are some uncertainties associated to the linear model parameters (force coefficients), actual air gaps on the plant, system geometry, etc. that result in plant-model mismatch and then lumped into $\boldsymbol{d}$ as external forces. To some extent, the disturbance estimate gives one some insight about the plant operation and the internal model of the controller.

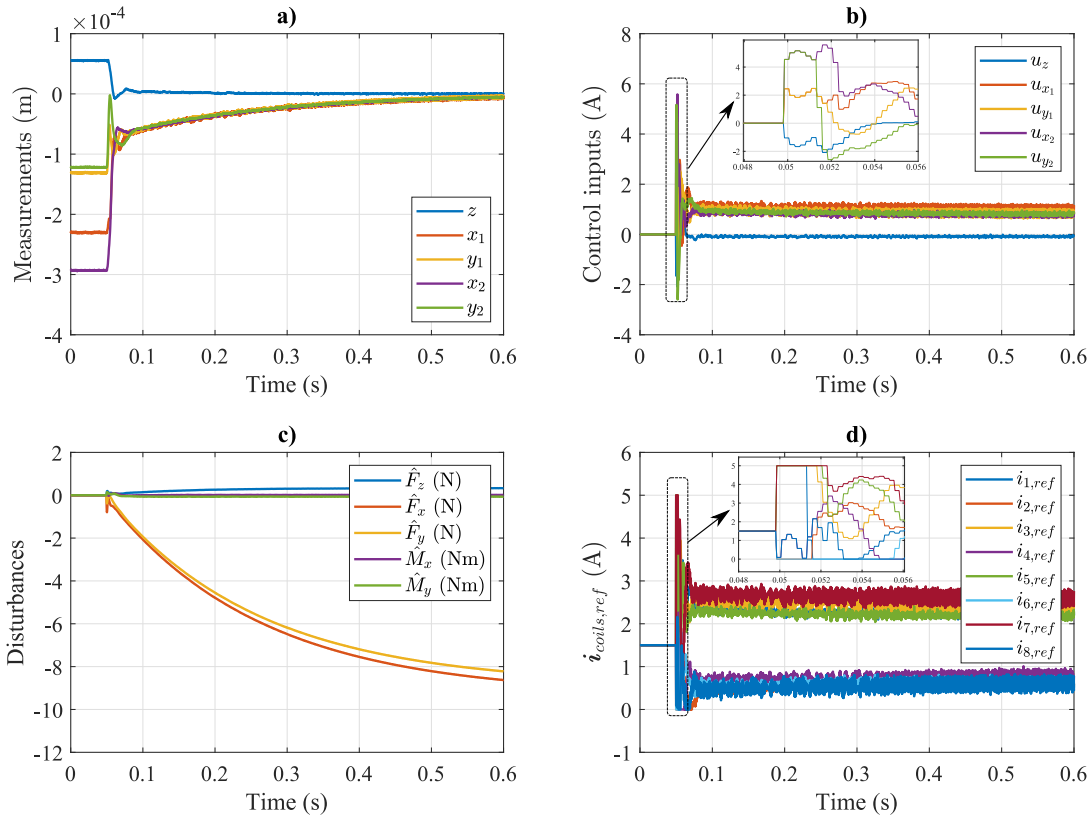

Figure 4.14: Transient response when the plant lifts-up. Control aggressiveness is set to $\alpha_j = 0.2$ and state estimator is set with $\rho^2 = 1$.

4.7.3 Evaluation of the closed-loop performance

Output sensitivities are obtained experimentally by implementing a dual channel Fast Fourier Transforms (FFT) analysis as suggested in the ISO 14839-3:2006 [90]. A sweep noise is injected on each measurement channel (one by one) and then both the injected noise and the corrupted output measurement are recorded. Repeating this process for each channel (z, x_1, y_1, x_2, y_2) and denoting $\boldsymbol{w_n} = [w_{n_z}, w_{n_{x_1}}, w_{n_{y_1}}, w_{n_{x_2}}, w_{n_{y_2}}]^\intercal$, the output sensitivity functions can be expressed as

$$
\begin{aligned}
S_z(f) &= \frac{z(f)}{w_{n_z}(f)}, \\
S_{x_1}(f) &= \frac{x_1(f)}{w_{n_{x_1}}(f)}, \; S_{y_1}(f) = \frac{y_1(f)}{w_{n_{y_1}}(f)}, \\
S_{x_2}(f) &= \frac{x_2(f)}{w_{n_{x_2}}(f)}, \; S_{y_2}(f) = \frac{y_2(f)}{w_{n_{y_2}}(f)}.
\end{aligned} \tag{4.28}
$$

The output sensitivity functions $\mathcal{S} = \{S_z,\ S_{x_1},\ S_{y_1},\ S_{x_2},\ S_{y_2}\}$ are used as the indicator of closed-loop performance. The main advantage of considering $\mathcal{S}$ is that since one ideally wants $\mathcal{S}$ small, it is sufficient to consider just the magnitude $|\mathcal{S}|$; that is, there is no need to worry about the phase [12] to asses the control performance.

The output sensitivity functions are then obtained for different control requirements and estimator configurations (i.e., varying α_j and ρ). Figure 4.15 shows how the aggressiveness of the controller changes for $\alpha_j = \{0.2,\ 0.5,\ 0.8\}$ and $\rho = 1$. The low-frequency disturbance rejection deteriorates considerably when $\alpha_j = 0.2$. It improves with $\alpha_j = 0.5$ and $\alpha_j = 0.8$ but better noise attenuation is achieved with $\alpha_j = 0.5$. It can be said in general that the best trade-off between disturbance rejection and noise attenuation is obtained with $\alpha_j = 0.5$. Nevertheless, all pick values of the sensitivity functions are within zone A [90] (i.e., $|\mathcal{S}|_{max} < 9.5$ dB) and then considered acceptable for unrestricted long-term operation.

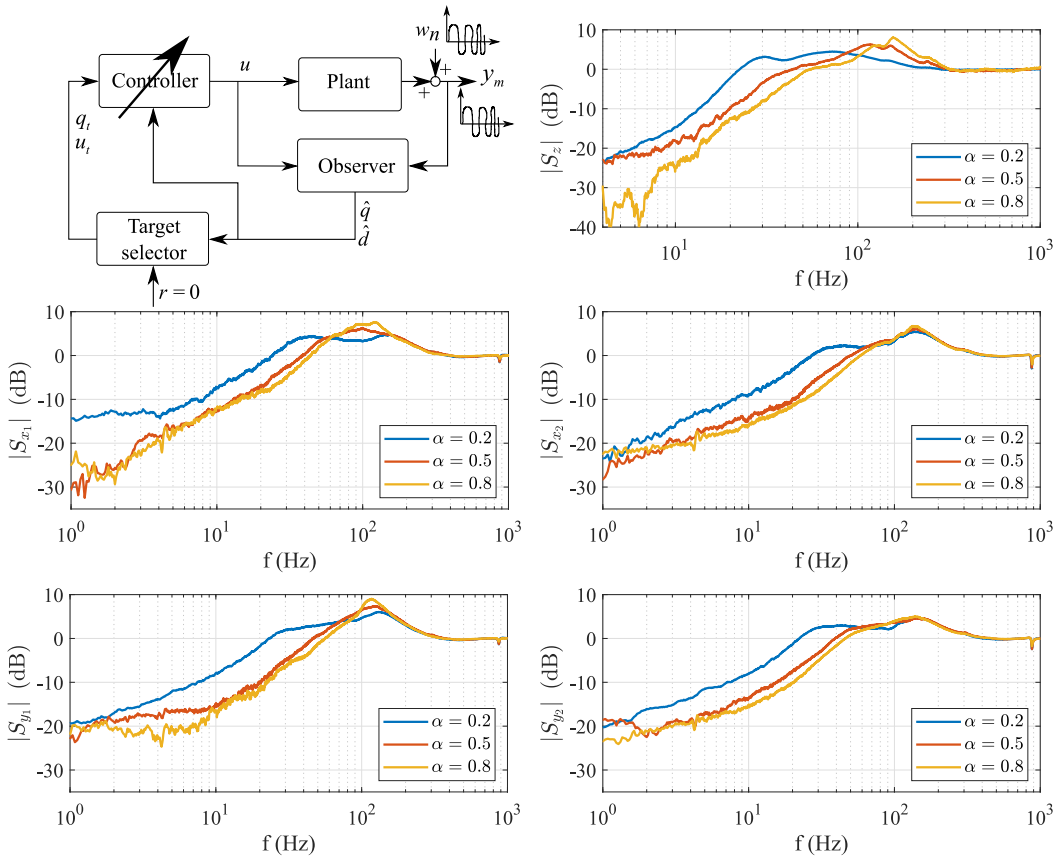

Figure 4.15: Output sensitivities on z, x_1, y_1, x_2 and y_2 with $\rho = 1$ but varying the controller aggressiveness through $\alpha_{z,x_1,y_1,x_2,y_2} \equiv \alpha$. Each test is performed independently on each measurement channel by injecting a sweep noise with a frequency that varies from 0.1 Hz to 1 kHz and amplitude 10×10^{-6} m.

The quality of the estimator is checked by varying ρ in Figure 4.16 and fixing the

controller aggressiveness with $\alpha_j = 0.2$. Considering that all the experimental data have been post-processed with the same smoothness, it is evident that the estimator does a poorer job of noise rejection when ρ increases but the closed-loop stability margins improve (lower pick values of $|\mathcal{S}|$). In some extent, by increasing ρ, the estimates becomes less dependent on the controller outputs $\boldsymbol{u}$ and more on the measurements. This approach makes the loop shape less affected by the estimator. However, note that increasing ρ can deteriorate the noise rejection. The closed-loop performance is

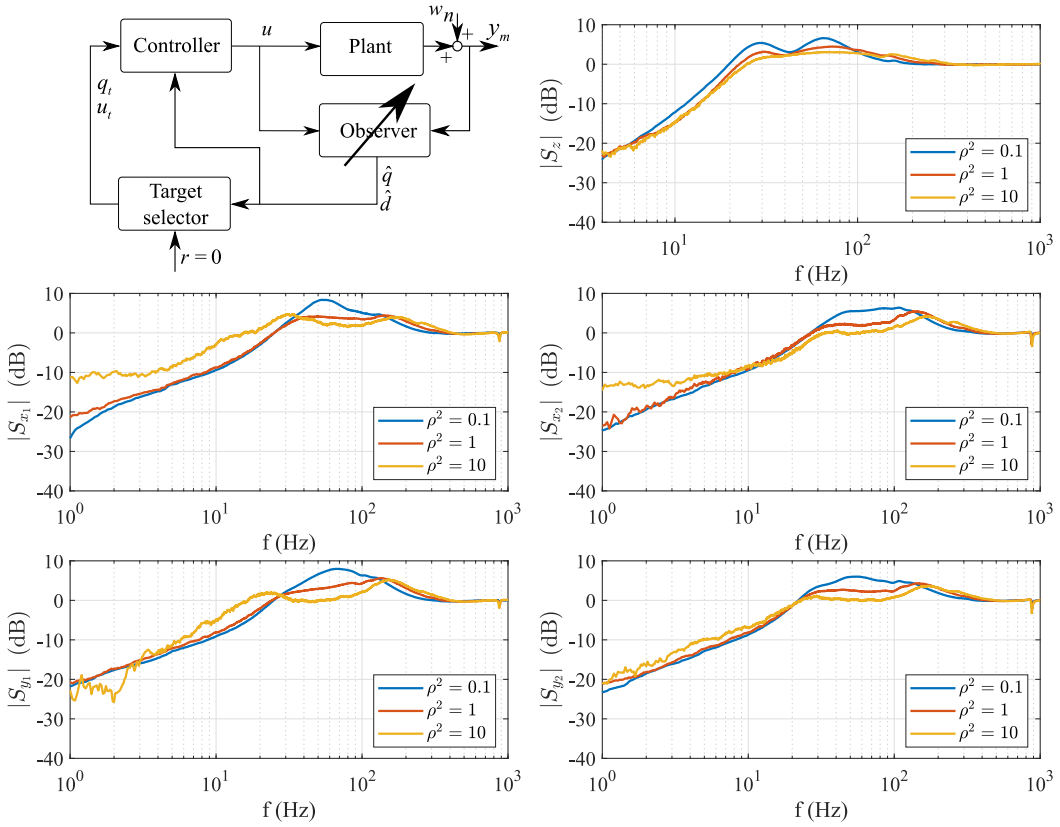

Figure 4.16: Output sensitivities on z, x_1, y_1, x_2 and y_2 with $\alpha_j = 0.2$ but changing the estimator with ρ. Each test is performed independently by injecting a sweep noise that varies from 0.1 Hz to 1 kHz with amplitude 10×10^{-6} m on each measurement channel.

checked again but with a more aggressive controller ($\alpha_j = 0.5$) and varying ρ in Figure 4.17. The control performance improves increasing ρ but at some point it deteriorates because of low noise rejection (when $\rho^2 = 10$). From the experimental results, the best trade-off between disturbance rejection and noise attenuation is achieved with the pair ($\alpha_j = 0.5$, $\rho^2 = 1$). In general, from the experimental results one can say that the aggressiveness of the controller is tuned around the nominal control requirements by changing α_j; and ρ serves for trading-off the noise rejection and margin recovery. It is important to remark that similar to Linear Quadratic Gaussian (LQG) control design,

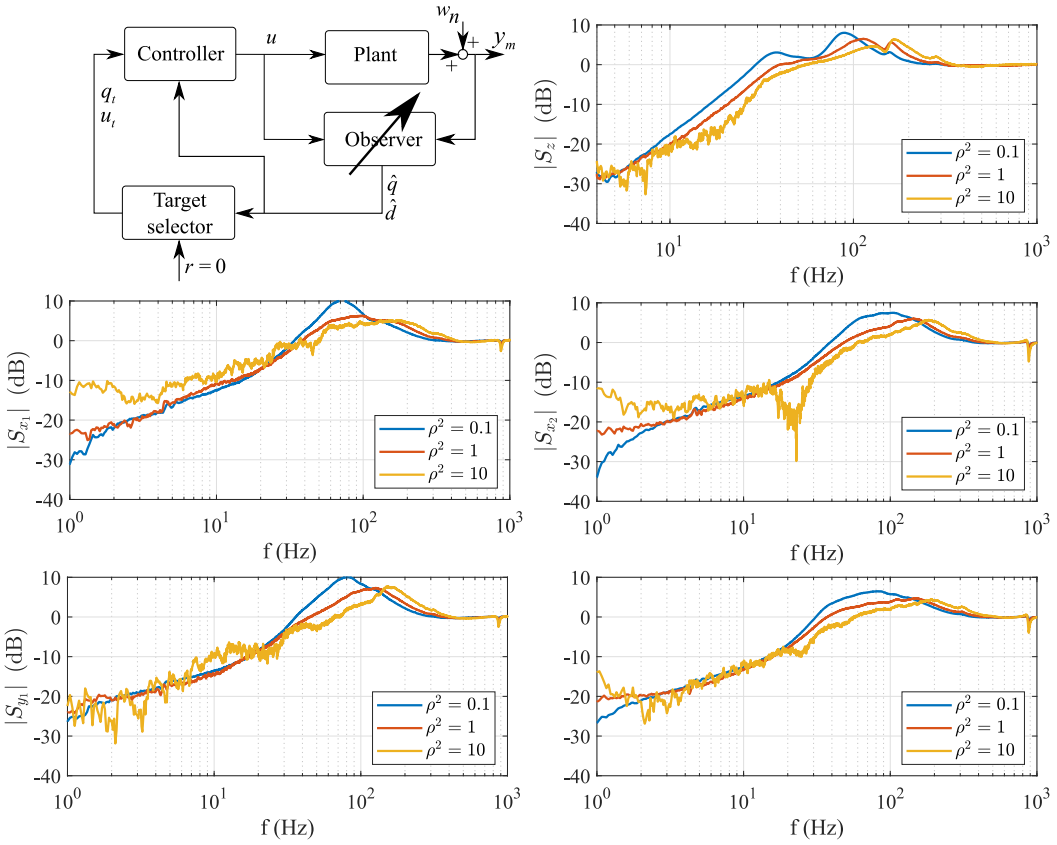

Figure 4.17: Output sensitivities on z, x_1, y_1, x_2 and y_2 with $\alpha_j = 0.5$ but changing the estimator with ρ. Each test is performed independently by injecting a sweep noise that varies from 0.1 Hz to 1 kHz with amplitude 10×10^{-6} m on each measurement channel.

the Separation Theorem or Certainty Equivalence Principle applies here. It consist of first determining the optimal control law i.e., the OF-MPC design. Then the estimator design is done as a next step but without any dependence on the controller design. However, when putting the OF-MPC and the observer together, there are no guaranteed stability margins. Some tips to tune the OF-MPC + estimator can be resumed as follows:

- Initiate the nominal controller ($\alpha_j = 0.5$) and check its feasibility throughout preliminary simulations assuming full state knowledge and no measurement noise.
- Design the augmented estimator as a Kalman filter by setting $var\{\boldsymbol{w_n}\}$ from the sensor noise information, $var\{\boldsymbol{w_q}\} = \mathbf{0}$ ("perfect" model) and $\rho = 0$ (nominal noise information). The variance of the augmented state $var\{\boldsymbol{d}\}$ is used to regulate how fast the external disturbances are estimated. Faster the convergence of these estimates (with high values of $var\{\boldsymbol{w_d}\}$), larger the controller integral action. This is because the OF-MPC targets are calculated from the disturbance

estimate.

- Robustify the closed-loop response by increasing ρ ($0 \leq \rho \leq \infty$) till a desired performance is achieved.
- It is a model-based control design approach. Therefore, if a desired closed-loop behavior is not achieved following the above steps, the quality of the linear plant model should be revised.

4.7.4 Comparison of OF-MPC with PIDs

PID are generated from the OF-MPC formulation as explained in Section 4.6.3 (see also both OF-MPC and PID control schemes in 4.10). The reduced observer is that presented in Table 4.3. A comparison of the output sensitivities when using PID and OF-MPC controllers is presented in Figure 4.18 for ($\alpha_{z,x_1,y_1,x_2,y_2} = 0.2$). The test is performed is such a way that the rotor moves in the vicinity of the nominal air gap and with no saturation in the control actions. Both controllers perform quite similar and hence one can say that computationally cheap decentralized controllers can be designed from the OF-MPC formulation if needed. However, notable differences between OF-MPC and decentralized PIDs are described below in presence of axial disturbances.

Impact test in axial direction

One of the main drawbacks of conical-shape AMB systems is the low axial force generation capability. Notable differences in the transient response are obtained when using PIDs or OF-MPC controllers and the coil current limits are reached. To compare the OF-MPC and the PIDs when the system reacts to an axial disturbance force, the axial control action is modified to

$$u_{z,disturbed} = u_z + u_{d,z},$$

where $u_{d,z}$ is a disturbance current used to perturb the plant in axial direction. Figures 4.19, 4.20 and 4.21 show transient responses for two levels of axial disturbance forces and different aggressiveness of the controllers. They are discussed below.

With $\alpha_{z,x_1,y_1,x_2,y_2} = 0.2$, the controllers are not so aggressive and similar transient behavior is obtained when $u_{d,z,max} = 4$ A; see Figures 4.19, a) and b). However, with a larger axial disturbance $u_{d,z,max} = 5$ A in Figures 4.19: c) and d), the OF-MPC system produces a more contained overshoot (about 56 %) when compared to the PID variant.

As expected, with a more aggressive control action in the axial direction (i.e., $\alpha_z = 0.4$), the axial deviations in Figures 4.20 a) and b) halved those in the previous test 4.19 a) and b). However, the radial deviations were severely affected, with the PID variant being noticeably worse than OF-MPC. A comparison between Figures 4.20 a) and b) shows that the maximum deviations when using PIDs resulted 50 % and 20 % larger than OF-MPC ones in (x_1, y_1) and (x_2, y_2), respectively. Also, the upper coil current saturation

lasts for a longer time interval when using PIDs. Thus, OF-MPC offers a more favorable saturation handling by intrinsically taking it into account and considering the trade-off between control efforts and air gap deviation. When a large-amplitude disturbance signal is applied, the PID-controlled plant response presented in Figure 4.20 d) reached a critical condition because the shaft almost reached a mechanical impact condition with the back-up ball bearings (radial deflection of $0.22\ \mathrm{mm}$). A more favorable behavior was obtained with the OF-MPC, where the overall displacement of the rotor did not exceed $0.15\ \mathrm{mm}$.

Figure 4.21 shows that OF-MPC outperforms PIDs also when the radial aggressiveness is increased to $\alpha_{x_1,y_1,x_2,y_2} = 0.3$. With OF-MPC, in Figure 4.21 a), the maximum radial deviations were attenuated to $70\ \%$ of those with PIDs in Figure 4.21 b). For a larger disturbance, the radial air gap deviations with PIDs in Figure 4.21 d) almost doubled those with OF-MPC in Figure 4.21 c).

It is more evident how OF-MPC outperforms PIDs when the control aggressiveness is increased as seen in Figures 4.21 c) and d). When using PIDs, the radial air gap deviations almost doubled those ones obtained with the OF-MPC.

For both OF-MPC and PID control techniques, the implementation of more aggressive control actions was not experimentally feasible because the measurement noise is fed back into the control loop by the compensators. This effect is evident when inspecting the coil current reference waveforms, as the noise tends to be directly proportional to the control aggressiveness α_j. In the particular case of the OF-MPC, this issue can be addressed with a full-state estimation, as presented in Secs. 4.7.2 and 4.7.3. In such case, the trade-off between noise rejection and margin recovery can be handled effectively by tuning through repeated experiments the parameter ρ from Eq. (4.18a).

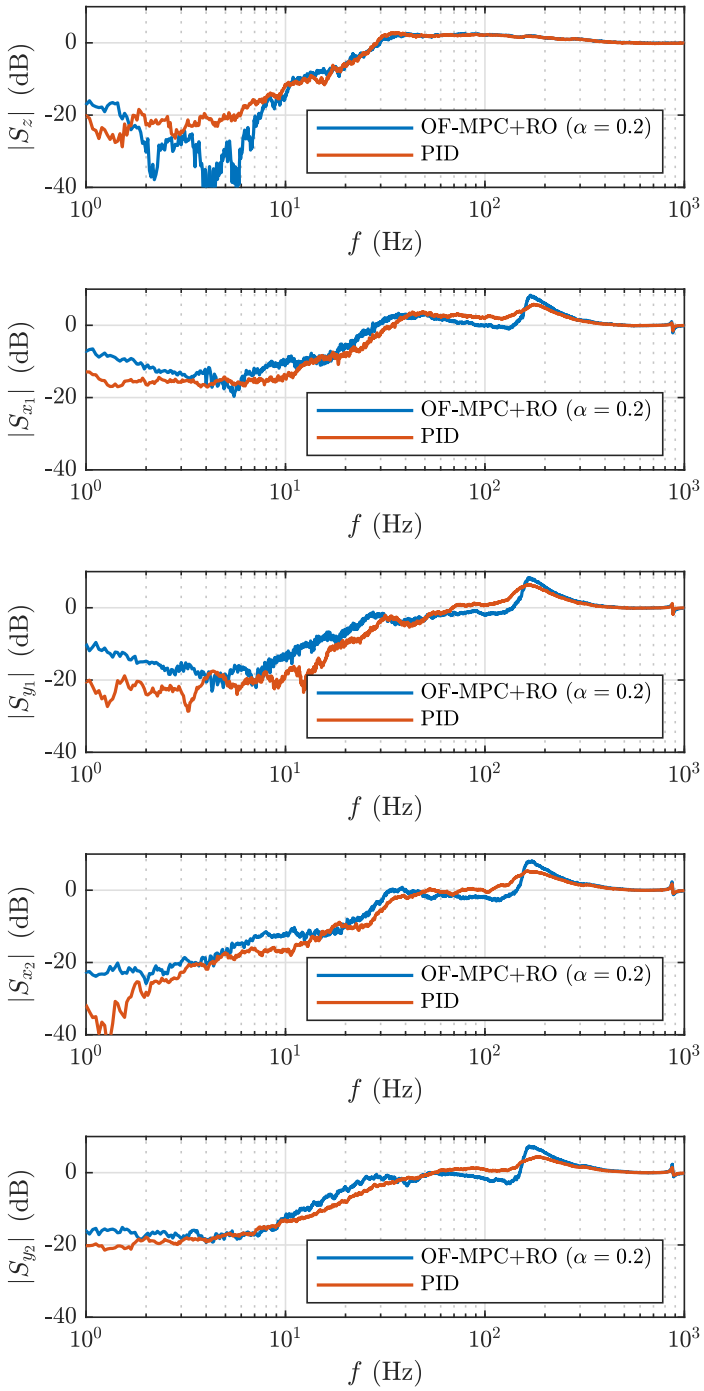

Figure 4.18: Output sensitivities on z, x_1, y_1, x_2 and y_2 from a comparison of the OF-MPC + reduced observer (RO) with decentralized PID controllers. Each test is performed independently on each measurement channel by injecting a swept sine noise with a frequency that varies from 0.1 Hz to 1 kHz with amplitude 10×10^{-6} m on each measurement channel.

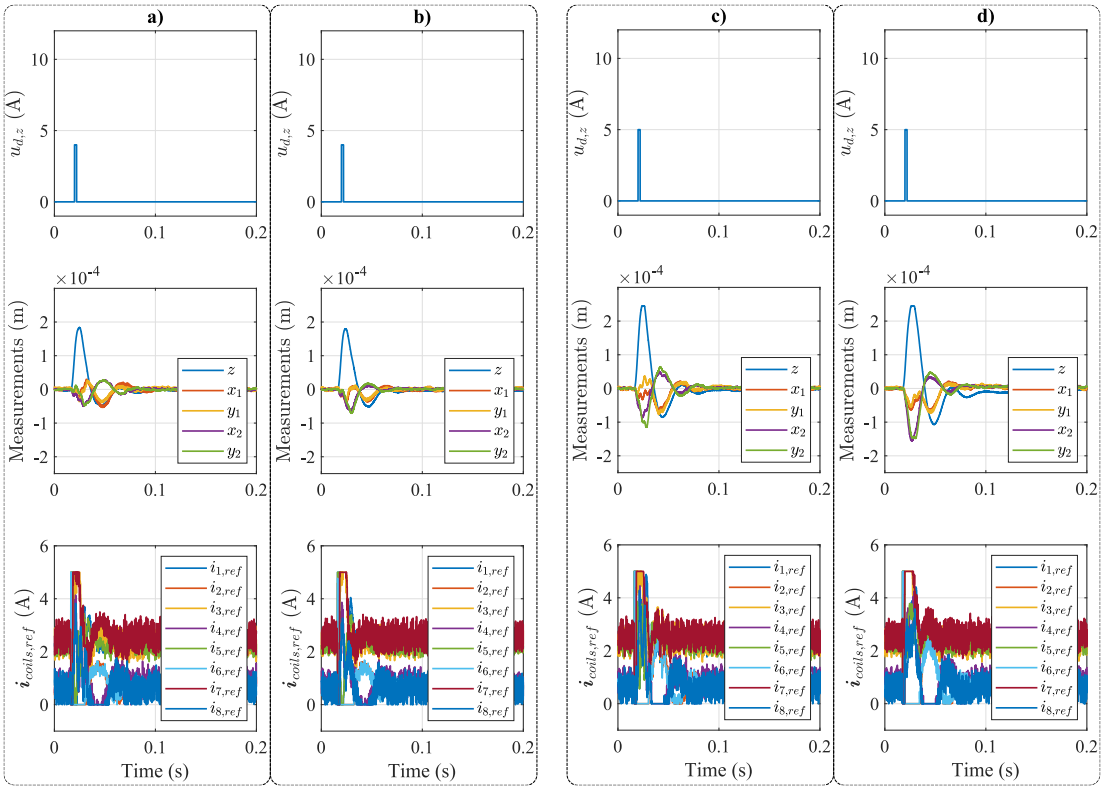

Figure 4.19: OF-MPC and PID comparison when an short-time impact force is applied in axial direction when using a) OF-MPC and b) PIDs. A response to a higher disturbance is present in c) for an OF-MPC and in d) for PIDs. Both OF-MPC and PIDs controllers are tuned with $\alpha_{z,x_1,y_1,x_2,y_2} = 0.2$.

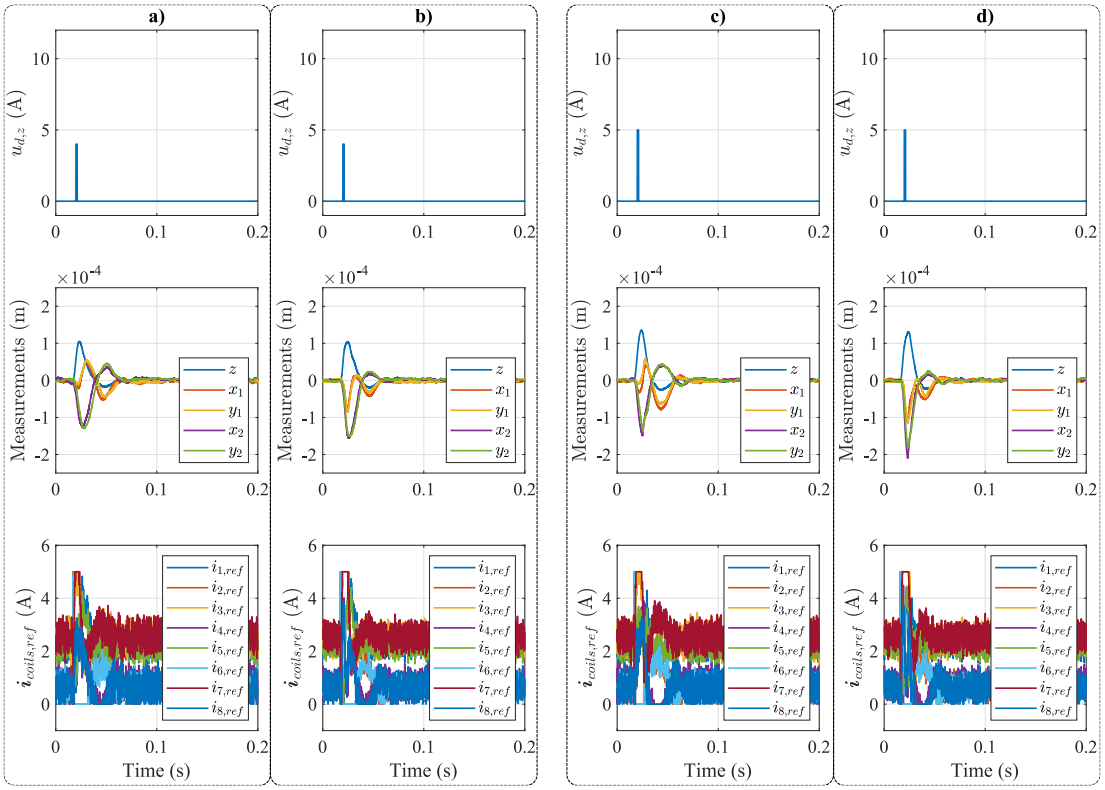

Figure 4.20: OF-MPC and PID comparison when an short-time impact force is applied in axial direction when using a) OF-MPC and b) PIDs. A response to a higher disturbance is present in c) for an OF-MPC and in d) for PIDs. Both OF-MPC and PIDs controllers are tuned with $\alpha_z = 0.4$, $\alpha_{x_1,y_1,x_2,y_2} = 0.2$.

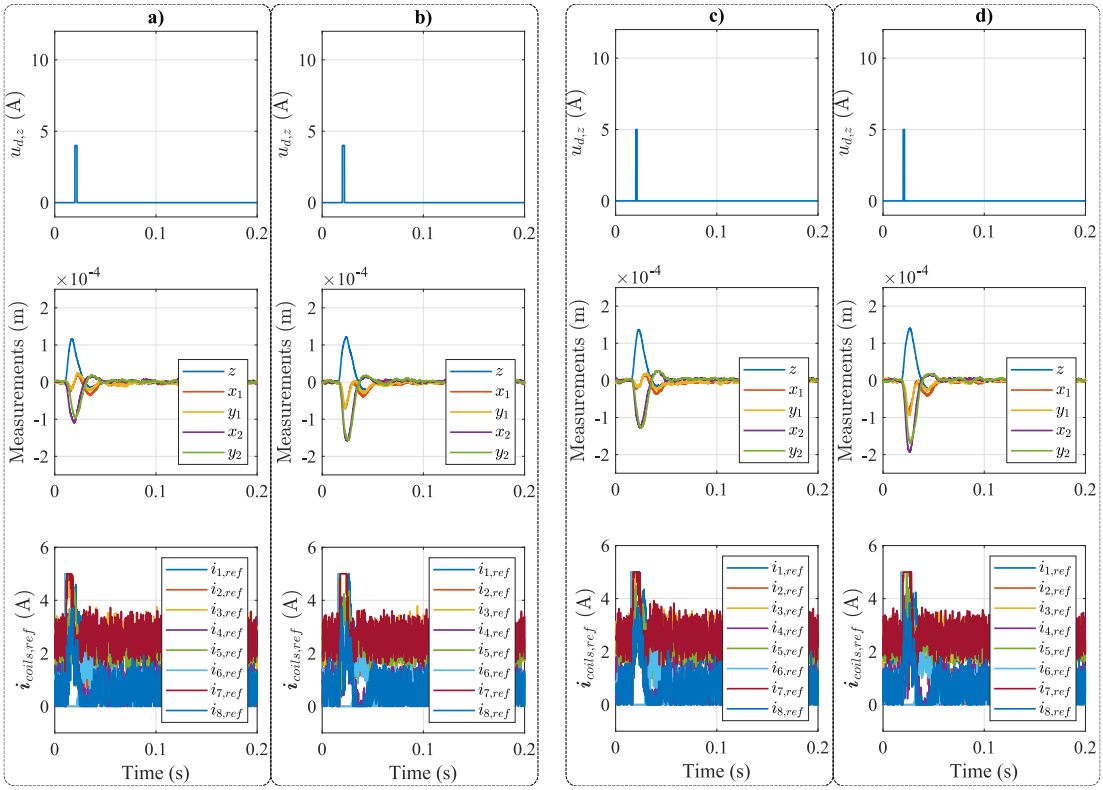

Figure 4.21: OF-MPC and PID comparison when an short-time impact force is applied in axial direction when using a) OF-MPC and b) PIDs. A response to a higher disturbance is present in c) for an OF-MPC and in d) for PIDs. Both OF-MPC and PIDs controllers are tuned with $\alpha_z = 0.4$, $\alpha_{x_1,y_1,x_2,y_2} = 0.3$.

4.7.5 Rotordynamics analysis

The effectiveness of the controller during rotation was validated by running the plant up to maximum spin speed $\Omega = 20000$ rpm. Note that the OF-MPC is based on a linearized plant model obtained at standstill operation (i.e., $\Omega = 0$ rad/s) as detailed in Section (4.5.1). This means that the variation of the plant due to the gyroscopic effects is not known by the controller. Nevertheless, the OF-MPC performed properly within the speed range of interest. Waterfall plots in run-down mode together with the unbalance responses and tachometer profile are reported in Appendix A.6. The unbalance forces resulted very small due to proper machining quality and balancing of the rotor, and hence no additional control action was advised during operation at different speeds.

Something important to remark is that the augmented state estimator used by the OF-MPC is not dedicated to estimate the unbalance forces. The rotor unbalance causes force disturbances that vary harmonically with the rotational speed of the machine while OF-MPC estimates low-frequency load variations, "persistent" additive disturbances lumping all into plant-model mismatch estimate. The determination of rotor balancing grade (see: ISO 1940, [91, Table 28.1]) is not the scope of this work. During the control design phase proposed in this thesis, it is assumed that the rotor balancing grade has a proper quality grade as suggested by the ISO standard 1940.

4.8 Conclusions

The possibility to optimally handle the plant-model mismatch together with the coil current limitation in cone-shaped AMB systems is offered by the offset-free model predictive control (OF-MPC). It guarantees zero-offset tracking adding integral action from the knowledge of the plant-model mismatch, while the controller design is an automated design procedure based on the trade-off between the control effort and the error in the controlled variables. The results demonstrate the potential of OF-MPC for cone-shaped AMB systems since the coupling of radial and axial control actions, and the low force generation capability in axial direction, can be addressed in a clear and systematic way. OF-MPC resulted a promising constrained optimal control technique that overcomes decentralized PID controllers in terms of axial disturbance rejection. It is an important contribution considering the low force generation capability of conical bearings.

In this chapter, the control algorithm was described in detail showing how to: reduce the computational burden of the control problem, generate an OF-MPC solver from a C code generation tool (CVXGEN) and design properly the plant state estimator. The performance of the control strategy was successfully validated with experimental results, and the tuning procedure is based only on the parameters (α_j, ρ) therefore, this work could serve as an easy-to-follow methodology for the implementation of model predictive control on magnetic bearing systems.

Chapter 5

Thesis conclusions and future work

5.1 Design Flow of OF-MPC for AMB systems

Chart 5.1 presents a work flow proposed in this thesis to design the OF-MPC for AMB systems, specially for conical-shaped AMB systems. The main points in the design flow are covered below.

5.1.1 Nonlinear plant modeling

A nonlinear plant model is required not only to obtain a linearized internal model of the OF-MPC but also to perform preliminary nonlinear simulations and hence for testing the OF-MPC in a more realistic scenario. The internal model of the controller is obtained by linearizing the plant model at a nominal bias current on each coil. The coil currents are assumed to be controlled by inner current loops with closed-loop dynamics much faster than the mechanical ones (hence current dynamics are neglected in the plant modeling phase).

5.1.2 Model augmentation and target selector

The linear model of the plant is augmented with a disturbance model to capture the plant-model mismatch. To this aim infinitely many choices are available. In this work, the so called *input disturbance model* is proposed. It consists of adding an integrating state that enters the system at the same place as the inputs. According to reference [53], several studies have pointed out that such a disturbance model is an appropriate choice for efficiently rejecting unmeasured disturbances (see [81, 44]). Some limitations in the location of the external disturbance in the model must be considered: (i) the number of external disturbances that can be added can not be higher than the number of measurements of the system and (ii) the augmented state matrix must have full row rank. The latter will guarantee a unique solution of the state and input targets.

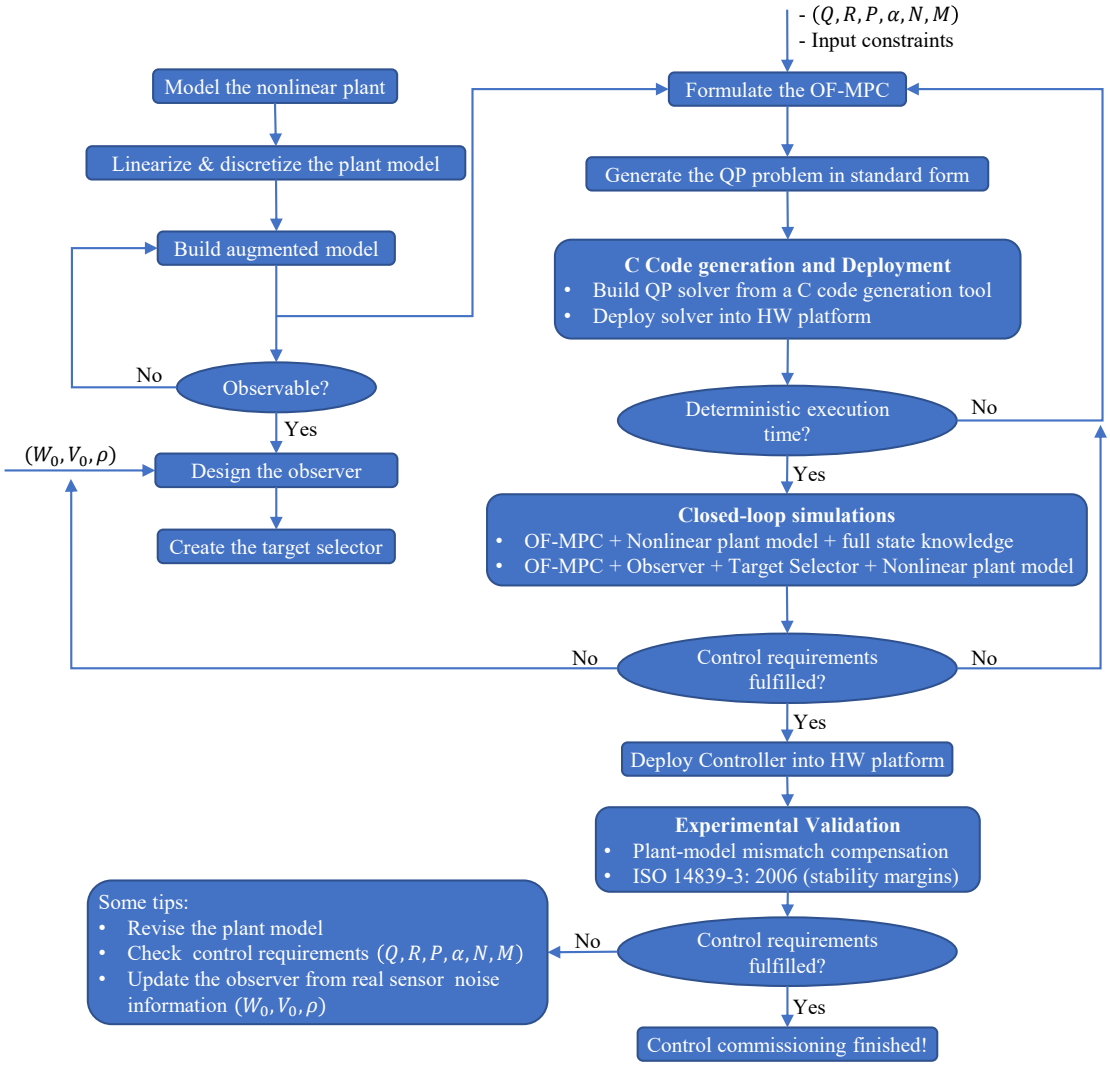

Figure 5.1: Proposed OF-MPC design flow for AMB systems.

An interesting feature of the OF-MPC for AMBs is obtained when the external disturbances added to the model are selected to be the disturbance forces. The point is that, at steady state, the disturbance estimate becomes a representation of the wight force compensated by the controller. This feature is important since the engineer can get more insight into the real plant operation based on an information which is intrinsically offered by the controller. Note that the disturbance estimate lumps also the plant-model mismatch and any other persistent external disturbance of the process. Any change in the plant operation will be reflected in the disturbance estimate in terms of external forces along the rotor motion directions.

5.1.3 Design of the augmented estimator

There is much already said when the linear plant model is only affected by white noise. Kalman filter approach is the more suitable solution in these cases. However, the difficulty arises when the plant model mismatch is not only due to white noise and hence the model drifts from the plant at steady-state.

State feedback control techniques are usually avoided because of the deterioration of the state estimate in presence of plant-model mismatch. That mismatch is expected from the OF-MPC controller but what about the state estimator? By augmenting the plant model, the plant model mismatch can be lumped into the new disturbance states. However, tuning the estimator from the augmented model is not trivial. A simple tuning rule proposed in [53] in applied here for the single-degree-of-freedom system (see Section 3.4). A more robust approach proposed by Doyle in [84] was preferred for the conical-shaped bearing example (see Section 4.5.3) in which a single parameter (ρ) is enough to handle effectively the trade-off between noise rejection and margin recovery.

5.1.4 Of-MPC formulation

The plant-model mismatch is compensated in a systematic and elegant way when using an OF-MPC control technique. Furthermore, the limitation in control inputs and system states are optimally handled. The latter is a remarkable feature of the OF-MPC for example in conical bearings (usually underactuated in term of actuation forces) and/or when the physical limitation of the AMB plant deserve more attention (frequent lifts up, mobile applications, etc.).

The OF-MPC formulation presented in this work, have been limited to input constraints and nothing was said about the inclusion of state constraints. The point is that more constraints are added to the problem, harder is to solve it in a deterministic time. One way to solve faster the OF-MPC problem is to remove unnecessary or "less important" constraints. That is why state constraints are usually avoided. The fact is that, since the objective function of the OF-MPC formulation produce a trade-off between inputs effort and state deviations, there might be no need of inequality constraints on the states to guarantee good control performance. Furthermore, adding inequality constraints in the states means to waste time in the update of the inequality matrices of the QP problem every time step. I personally consider that the online update of the QP matrices should be avoided for code robustness and well justified if done. The real-time update of the QP matrices could be required, for instance, in cases in which the gyroscopic effect can not be neglected.

Mixed optimization proved sufficient to guarantee good stability properties (see conical bearings application in Chapter 4). Matrices Q and R are used to properly weight the trade-off between the rotor clearance and available bearing capacity. They are selected in such a way that the rotor response consumes 25 % of the available clearance and, at the same time, for the control effort to be 20 % of the available bearing

capacity (in terms of coil current). A variation of the controller aggressiveness around this nominal requirement is proposed with the tuning parameter α.

Blocking moves

In MPC practice, to limit the computation burden it is often useful to limit the number of degrees of freedom by "blocking" control moves after a certain input horizon M, $1 \leq M < N$. It resulted strictly necessary to applying OF-MPC for the conical-shaped bearing. The control signal is frozen and held constant and equals to the input target $\boldsymbol{u}_t$ after prediction time $M-1$. It was done following the approach presented in [48, § 5]. However, there are other ways to freeze the control action (see Appendix A.6 in reference [54]). The analysis of AMB control performance and QP Hessian matrix properties when applying a different freezing rule is left for future works.

5.1.5 C code generation tools

For small systems (few states and inputs), the explicit MPC variant can result the best candidate. There exist some tools for MPC design, evaluation and deployment such as Hybrid Toolbox [92], Multiparametric Toolbox [93] and MPC Toolbox 5.0 (available from R2014b). During the progress of this work, some attempts to use those tools for finding an explicit variant of the OF-MPC for the conical bearing system where done. Unfortunately, it resulted in very long memory size requirements. The fact is that, to the best of the author knowledge, the most convenient approach (i.e., explicit or online MPC) to embed the OF-MPC controller for AMB systems is not well defined and a comparison of online/explicit MPC variant is not the scope of this research. Nevertheless, the online OF-MPC methodology presented in this work, proved to be a significant contribution in the filed of constrained optimal control for active magnetic bearings.

Matlab has many parser solvers that can facilitate the simulation of the controller in PC environment but these solvers are not suitable for deployment into a microcontroller. Matlab offers today some tools to generate C code from Simulink (Simulink Coder) or scripts (Matlab coder) environments but there is no possibility today to create custom online MPC solvers that can be embedded into a hardware platform. Only explicit MPC solvers (as explained above). In this work, two matlab independent approaches to generate a custom MPC solver were used: μAO-MPC [79] and CVXGEN [29].

μAO-MPC is a python module in which the the user writes the MPC problem and then a fast QP solver written in C is generated. However, when using μAO-MPC the user is forced to fix the control moves to the prediction horizon ($M = N$) i.e., there is no possibility to reduce the control moves and make the solver even much faster. Furthermore, the speed of converge of the solver is strictly related with the condition number of the Hessian matrix in the QP problem it generates. In this work, it proved to be sufficient for the single-axis AMB system of Chapter 3 but not suitable for the

OF-MPC formulation proposed in the cone-shaped AMB system.

A more generic C code generation tool is CVXGEN. The user can formulate not only standard MPC controllers but any convex QP problem. CVXGEN was used in Chapter 4 for the OF-MPC implementation on the Conical-shaped AMB system. Figure 5.2 shows a work flow followed to create a custom OF-MPC solver. CVXGEN is a well known tool in the research and industry. For example, the aerospace transportation company SpaceX uses the QP code generation tool CVXGEN [29] to land its rockets [94].

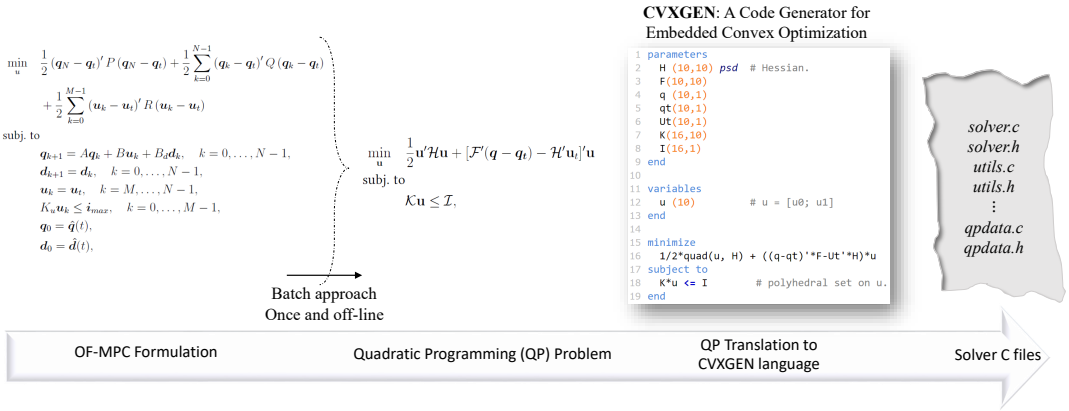

Figure 5.2: Implementation steps from: OF-MPC formulation to C code generation. This figure makes reference to the OF-MPC implemented on the cone-shaped AMB system.

Matlab integrated with external C code generators

Matlab is one of the most famous engineering tool for modeling and simulation of dynamics systems. Something interesting is the possibility it offers to run C code. CVXGEN creates also a Matlab MEX interface for use with each custom solver, making it easy to test and use high-speed solvers in simulations and data analysis. The C code generated in CVXGEN can be also implemented in Simulink environment as an *S-Function* as depicted in Figure 5.3. When using CVXGEN integrated with Matlab, the same C code of the solver that will be deployed into the microcontroller is used for the simulations. This integration offers a preliminary evaluation of both the closed-loop control performance and the C code generated by CVXGEN. This integration saves time, and becomes much more interesting and advantageous when the microcontroller can be deployed directly from Matlab environment.

5.2 Future work

- **Explicit versus online OF-MPC**: A discussion is still open about the comparison of explicit (i.e., look-up tables with optimal inputs as a function of plant state) and

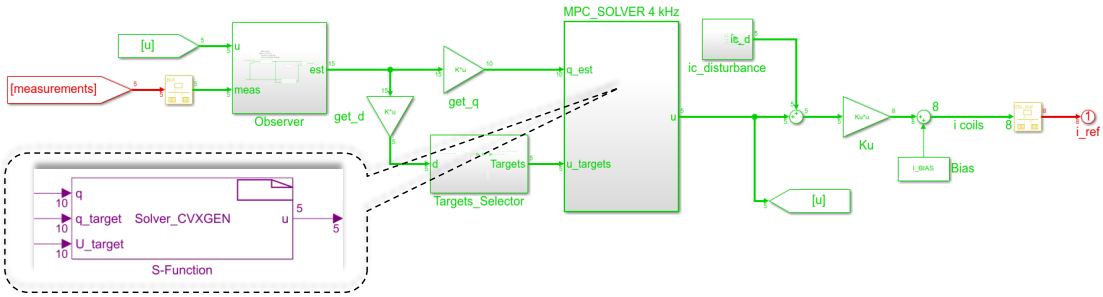

Figure 5.3: OF-MPC controller generated by CVXGEN and implemented in Matlab/Simulink environment. Matlab simulations can be performed using the same solver that will be deployed into the real hardware.

online OF-MPC variants for AMB systems.

- **Nonlinear OF-MPC**: AMB systems are strongly nonlinear systems. Even if the linear OF-MPC formulation proved sufficient to guarantee a proper close-loop behavior, future work can be conducted to validate nonlinear OF-MPC variants [46].
- **Gyroscopic effects and OF-MPC design**: There are some AMB applications in which the gyroscopic effect can not be neglected during the control design phase. Hence, in case of using OF-MPC, an online reformulation of the QP problem as a function of the spin speed is required. The spin speed can be quantified in small steps or operating zones and then a straightforward algorithm can be implemented to update the internal model of the OF-MPC controller every time step the spin speed changes the zone. Future work will be done in this direction.

Appendix A

Appendix A. Cone-shaped AMB

A.1 Plant data

The rotor quotes are presented in Fig. A.1

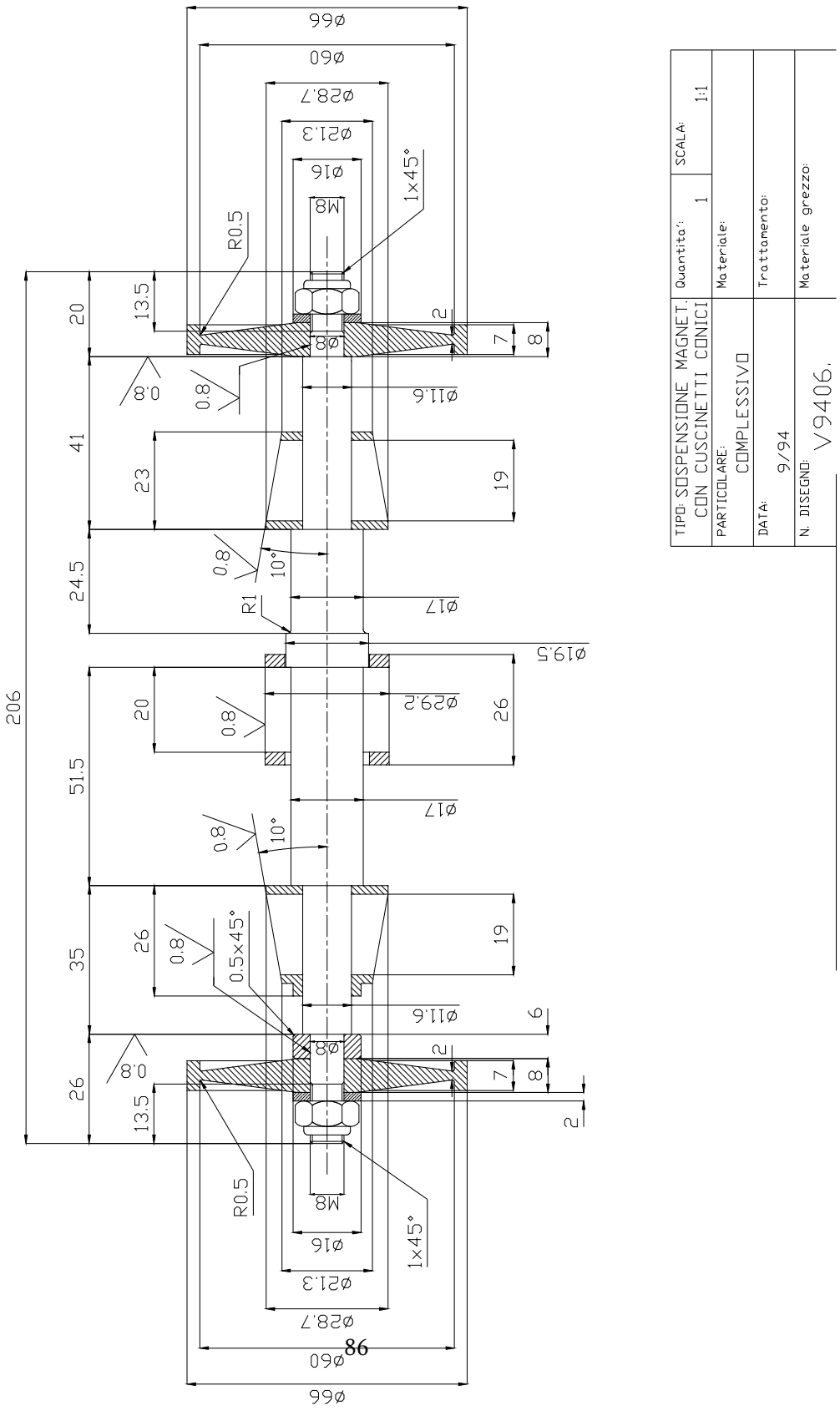

Figure A.1: Conical-shaped AMB Test tig. Rotor dimensions.

A.2 Nonlinear plant model in Matlab

```
function q = ConeShapedStateFcn(amb,q,u,d,Ts)
% ConeShapedStateFcn Discrete-time approximation to the cone ...
    shaped system.
% $\dot{\boldsymbol{\zeta}} = \boldsymbol{h}(\boldsymbol{\zeta}, \boldsymbol{i}, \boldsymbol{d}, \Omega)$
% Example state transition function for discrete-time nonlinear ...
    state
% estimators.
%
% Xk1 = ConeShapedStateFcn(X,U,Ts)
%
% Inputs:
%    q  - States at time step k X(k) = [z x y Theta_x Theta_y ...
    z_dot x y_dot Theta_x_dot Theta_y_dot]'
%    u  - input currents at time step u(k) = [i1   i2   i3   i4 ...
     i5   i6   i7   i8]'
%    d - Disturbances [Fz,Fx,Fy,M_x, M_y] on ...
    [z,x,y,Theta_x,Theta_y]
%    Ts - Sampling time
%
% Outputs:
%    Xk1 - Propagated states X[k+1]
%

% Euler integration of continuous-time dynamics x'=f(x,u,d) ...
    with sample time dt
dt = Ts; % [s] Sample time
q = q + ConeShapedStateFcnContinuous(amb,q,u,d)*dt;
end

function dqdt = ConeShapedStateFcnContinuous(amb,q,u,d)
%ConeShapedFcnContinuous
% X = [z x y Theta_x Theta_y z_dot x y_dot Theta_x_dot ...
    Theta_y_dot]'
% U = [ix1p ix1m iy1p iy1m ix2p ix2m iy2p iy2m]'
g     = 9.82;     %  [m/s2]
g0    = amb.g0;   % [m] Radial air gap
Beta  = amb.Beta; % [rad] Inclined angle of the magnetic core
% bt  = amb.bt;   % [m] distance between the two radial ...
    magnetic bearings
b1    = amb.b1;   % [m] distance between the radial magnetic ...
    bearing (1) and the center of gravity point of the rotor
b2    = amb.b2;   % [m] distance between the radial magnetic ...
    bearing (2) and the center of gravity point of the rotor
Rm    = amb.Rm;   % [m] Effective radius
m     = amb.m;    % [kg] rotor mass
Jp    = amb.Jp;   % [kgm2] polar moment of inertia
```

```
Jd    = amb.Jd;   % [kgm2] Diametrical moment of inertia
Omega = amb.Omega;% [rad/sec] spin speed

%% Force factors:
% |F| = mu0*S*N^2*i^2/(4*g^2)*cos(pi/8)
% |F| = K*i^2/g^2; K = mu0*S*N^2/4**cos(pi/8);
% F1(y2+,iy2+)
% F2(y2-,iy2-)
% F3(y1+,iy1+)
% F4(y1-,iy1-)
% F5(x2+,ix2+)
% F6(x2-,ix2-)
% F7(x1+,ix1+)
% F8(x1-,ix1-)
%%%%%%%%%%%%%%%%%%%%%%%%%%%%%%%%%%%%%%%%%%%%%%%%%%%%%
% U = [ix1- ix1+ iy1- iy1+ ix2- ix2+ iy2- iy2+]'  %%%
% U = [i8   i7   i4   i3   i6   i5   i2   i1]'    %%%
%%%%%%%%%%%%%%%%%%%%%%%%%%%%%%%%%%%%%%%%%%%%%%%%%%%%%
% Force constant:
K = amb.K; %
%%%%%%%%%%%%

% q = [z x y Theta_x Theta_y z_dot x y_dot Theta_x_dot ...
    Theta_y_dot]'

z = q(1);
x = q(2);
y = q(3);
theta_x = q(4);
theta_y = q(5);

i1 = u(1);
i2 = u(2);
i3 = u(3);
i4 = u(4);
i5 = u(5);
i6 = u(6);
i7 = u(7);
i8 = u(8);

% forces on Y2 pole face area:
F1 = K*i1^2/(g0-z*sin(Beta)-cos(Beta)*(y + b2*theta_x))^2;
F2 = K*i2^2/(g0-z*sin(Beta)+cos(Beta)*(y + b2*theta_x))^2;
% forces on Y1 pole face area:
F3 = K*i3^2/(g0+z*sin(Beta)-cos(Beta)*(y - b1*theta_x))^2;
F4 = K*i4^2/(g0+z*sin(Beta)+cos(Beta)*(y - b1*theta_x))^2;
% forces on X2 pole face area:
F5 = K*i5^2/(g0-z*sin(Beta)-cos(Beta)*(x - b2*theta_y))^2;
F6 = K*i6^2/(g0-z*sin(Beta)+cos(Beta)*(x - b2*theta_y))^2;
% forces on X1 pole face area:
```

```
F7 = K*i7^2/(g0+z*sin(Beta)-cos(Beta)*(x + b1*theta_y))^2;
F8 = K*i8^2/(g0+z*sin(Beta)+cos(Beta)*(x + b1*theta_y))^2;

% disturbance forces:
Fz        = d(1);
Fx        = d(2)-m*g*cos(pi/4);
Fy        = d(3)-m*g*cos(pi/4);
M_x       = d(4);
M_y       = d(5);

% AMB Model with nonlinear dynamics:
dqdt = [q(6);... z
q(7);... x
q(8);... y
q(9);... Theta_x
q(10);... Theta_y
((F1+F2+F5+F6)*sin(Beta)-(F3+F4+F7+F8)*sin(Beta)+ Fz)/m;... z_dot
((F5-F6+F7-F8)*cos(Beta) + Fx)/m;... x_dot
((F1-F2+F3-F4)*cos(Beta) + Fy)/m;... y_dot
(((F1-F2)*b2+(F4-F3)*b1)*cos(Beta)+(F2-F1+F3-F4)*Rm*sin(Beta)+M_x)/Jd ...
   -Jp*Omega*theta_y_dot/Jd;... theta_x_dot
(((F6-F5)*b2+(F7-F8)*b1)*cos(Beta)+(F5-F6+F8-F7)*Rm*sin(Beta) + ...
   M_y)/Jd + Jp*Omega*theta_x_dot/Jd]; % Theta_y_dot
end
```

A.3 Jacobians and linear modeling

$$\% \ \dot{\zeta} \doteq \underbrace{\left.\frac{\partial h}{\partial \zeta}\right|_0}_{\bar{A}} (\zeta - \zeta_0) + \underbrace{\left.\frac{\partial h}{\partial i}\right|_0}_{\bar{B}_i} (i - i_0) + \underbrace{\left.\frac{\partial h}{\partial d}\right|_0}_{\bar{B}_d} (d - d_0)$$

```

clear all
close all
clc
load('amb.mat')

%%%%%%%%%%%%%%%%%%%%%%%%
% Electromagnetic Forces
% |F| = K*i^2/g^2;
% F1(y2+,iy2+), force on AMB2, y+ diretion
% F2(y2-,iy2-), force on AMB2, y- diretion
% F3(y1+,iy1+), force on AMB1, y+ diretion
% F4(y1-,iy1-), force on AMB1, y- diretion
% F5(x2+,ix2+), force on AMB2, x+ diretion
% F6(x2-,ix2-), force on AMB2, x- diretion
% F7(x1+,ix1+), force on AMB7, x+ diretion
```

```
% F8(x1-,ix1-), force on AMB8, x- diretion
%%%%%%%%%%%%%%%%%%%%%%

% states and control inputs:
% X = [z x y theta_x theta_y z_dot x y_dot theta_x_dot ...
    theta_y_dot]'
% U = [i1 ... i8]'

%% symbolic variables decalaration:

% sym states:
syms z x y theta_x theta_y z_dot x_dot y_dot theta_x_dot ...
    theta_y_dot

% sym input currents:
syms i1 i2 i3 i4 i5 i6 i7 i8

% sym disturbance forces:
syms Fz Fx Fy Ftheta_x Ftheta_y

% intermediate equations
% forces on Y2 pole face area:
F1 = K*i1^2/(g0-z*sin(Beta)-cos(Beta)*(y + b2*theta_x))^2;
F2 = K*i2^2/(g0-z*sin(Beta)+cos(Beta)*(y + b2*theta_x))^2;
% forces on Y1 pole face area:
F3 = K*i3^2/(g0+z*sin(Beta)-cos(Beta)*(y - b1*theta_x))^2;
F4 = K*i4^2/(g0+z*sin(Beta)+cos(Beta)*(y - b1*theta_x))^2;
% forces on X2 pole face area:
F5 = K*i5^2/(g0-z*sin(Beta)-cos(Beta)*(x - b2*theta_y))^2;
F6 = K*i6^2/(g0-z*sin(Beta)+cos(Beta)*(x - b2*theta_y))^2;
% forces on X1 pole face area:
F7 = K*i7^2/(g0+z*sin(Beta)-cos(Beta)*(x + b1*theta_y))^2;
F8 = K*i8^2/(g0+z*sin(Beta)+cos(Beta)*(x + b1*theta_y))^2;

% AMB Model with nonlinear dynamics:
g =  [z_dot;... z
x_dot;... x
y_dot;... y
theta_x_dot;... theta_x
theta_y_dot;... theta_y
((F1+F2+F5+F6)*sin(Beta)-(F3+F4+F7+F8)*sin(Beta))/m+Fz/m;... z_dot
(F5-F6+F7-F8)*cos(Beta)/m+Fx/m;... dx
(F1-F2+F3-F4)*cos(Beta)/m+Fy/m;... dy
(((F1-F2)*b2+(F4-F3)*b1)*cos(Beta)+(F2-F1+F3-F4)*Rm*sin(Beta)+M_x)/Jd ...
    -Jp*Omega*theta_y_dot/Jd;... theta_x_dot
(((F6-F5)*b2+(F7-F8)*b1)*cos(Beta)+(F5-F6+F8-F7)*Rm*sin(Beta) + ...
    M_y)/Jd + Jp*Omega*theta_x_dot/Jd]; % Theta_y_dot

%% Symbolic coninuous Jacobians:
```

```
J_A = jacobian(g,[z; x; y; theta_x; theta_y; z_dot; x_dot; ...
    y_dot; theta_x_dot; theta_y_dot]);
J_B = jacobian(g,[i1; i2; i3; i4; i5; i6; i7; i8]);
J_Bd = jacobian(g,[Fz; Fx; Fy; Ftheta_x;  Ftheta_y]);

%% states at steady state: (when zero air gap deviation)
z=0; x=0; y=0;  theta_x=0;  theta_y=0; z_dot=0;  x_dot=0;  ...
    y_dot=0;  theta_x_dot=0;  theta_y_dot=0;

%% currents at steady state:
i1=amb.i0(1); i2=amb.i0(2); i3=amb.i0(3); i4=amb.i0(4); ...
    i5=amb.i0(5); i6=amb.i0(6); i7=amb.i0(7); i8=amb.i0(8);

%% disturbance forces at steady state:
% Fz=0; Fx=amb.m*g*cos(pi/4); Fy=amb.m*g*cos(pi/4); Ftheta_x=0; ...
    Ftheta_y=0;
Fz=0; Fx=0; Fy=0; Ftheta_x=0; Ftheta_y=0; % Assuming zero ...
    external forces at steady state.
%% Linearizing the plant at the opertating point:
A = double(subs(J_A))
B = double(subs(J_B))
Bd = double(subs(J_Bd))
```

A.4 QP matrices from the OF-MPC formulation

```
function [ H, F ] = getHF( A,B,Q,R,P,N,M)
% get H anf F matrices for the QP problem that corresponds to ...
    OF-MPC problem
% min_u  (1/2)u'Hu' + [F'(q - q_t) - H'u_t]'u
%
% Inputs:
%       A: state matrix
%       B: Input matrix
%       Q: Weight on the state
%       P: terminal weight
%       R: Weight on ths inputs
%       N: Prediction horizon
%       M: Control horizon

[n,m] = size(B);        % n: number of states
% m: number of inputs

Su = zeros(n*N,m*M);    % see Su in Chapter 2.

for j=1:1:M
Su_col = [];
```

```
for i=0:1:N-j
Su_col = [Su_col ;A^i*B];
end
Su(1+(j-1)*n:end,1+(j-1)*m:j*m) = Su_col;
end

Sx = [];
for i = 1:N
Sx = [Sx; A^i];
end

% weights matrices:
QQ = [];
for i=1:N-1
QQ = blkdiag(QQ,Q);
end

QQ = blkdiag(QQ,P);

RR = [];
for i=1:M
RR = blkdiag(RR,R);
end


H = Su'*QQ*Su + RR;
F = Sx'*QQ*Su;
end
```

A.5 OF-MPC as a QP problem written in CVXGEN code

```
%# QP problem written in CVXGEN for
%# the Conical-shaped AMB system with
%# Control horizon  M = 2.
%
% min_u  (1/2)u'Hu' + [F'(q - q_t) - H'u_t]'u
%
%% Code starts here:
parameters
H (10,10) psd  # Hessian.
F(10,10)
q (10,1)
qt(10,1)
Ut(10,1)
K(16,10)
I(16,1)
```

```
16 end
17
18 variables
19 u (10)          # u = [u0; u1]
20 end
21
22 minimize
23 1/2*quad(u, H) + ((q-qt)'*F-Ut'*H)*u
24 subject to
25 K*u ≤ I           # polyhedral set on u.
26 end
27 %# That's it! :)
```

A.6 Waterfall plots on the cone-shaped AMB system with OF-MPC control

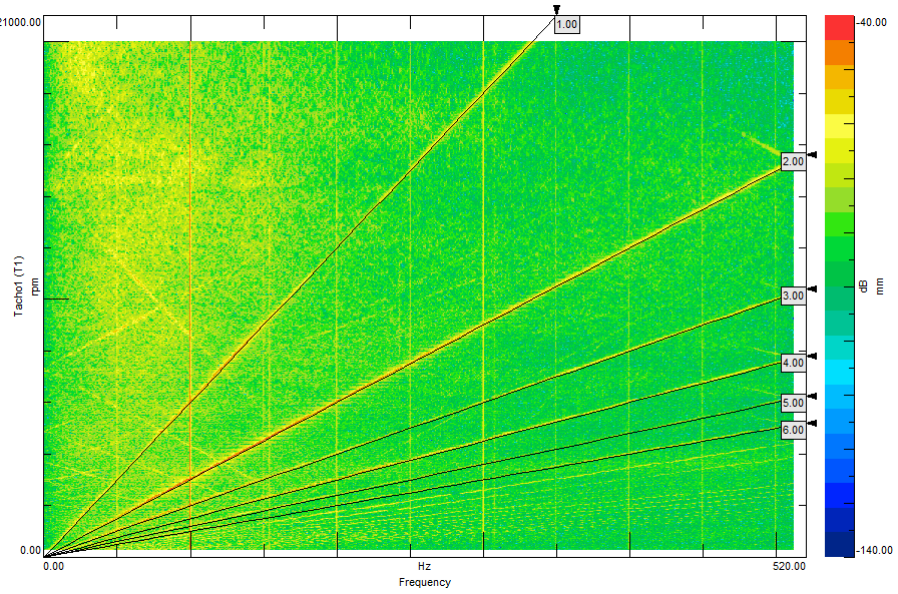

Figure A.2: Waterfall plot: x_1. OF-MPC agresiveness: $\alpha_{z,x_1,y_1,x_2,y_2} = 0.5$, state estimator with $\rho = 1$.

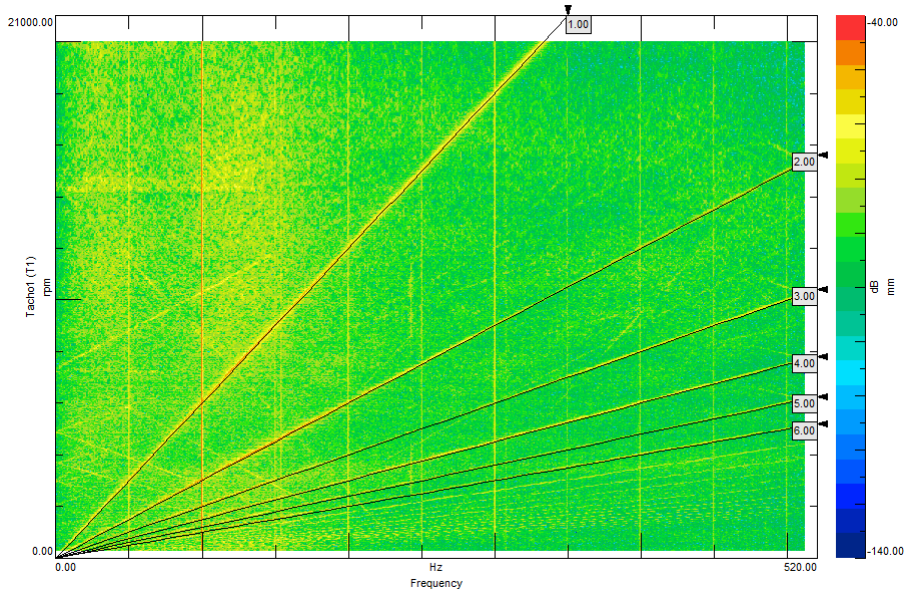

Figure A.3: Waterfall plot: y_1. OF-MPC agresiveness: $\alpha_{z,x_1,y_1,x_2,y_2} = 0.5$, state estimator with $\rho = 1$.

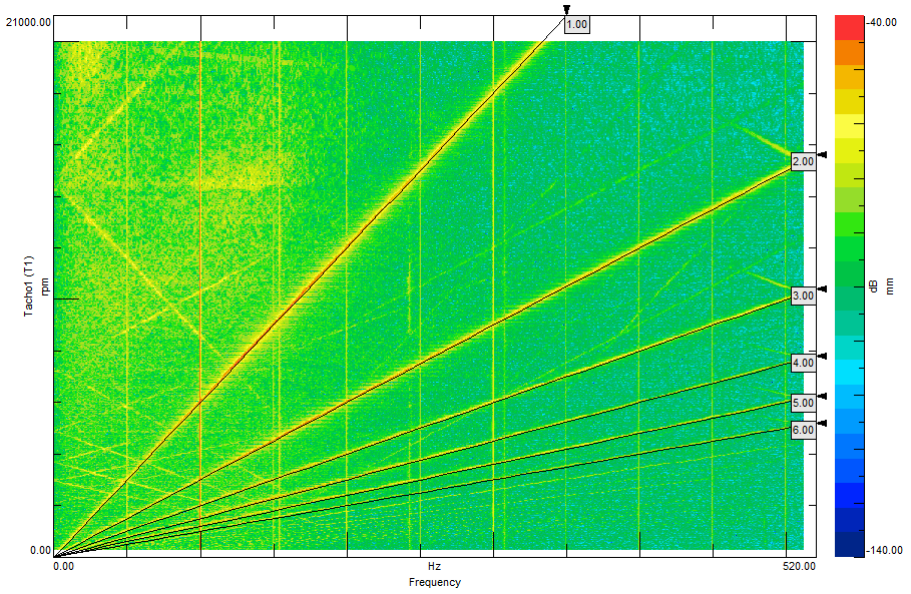

Figure A.4: Waterfall plot: x_2. OF-MPC agresiveness: $\alpha_{z,x_1,y_1,x_2,y_2} = 0.5$, state estimator with $\rho = 1$.

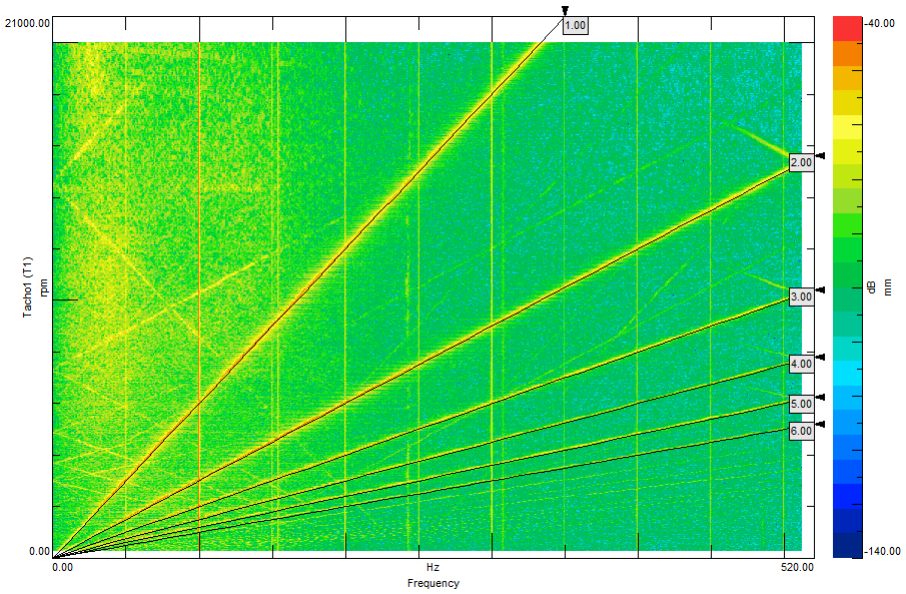

Figure A.5: Waterfall plot: y_2. OF-MPC agresiveness: $\alpha_{z,x_1,y_1,x_2,y_2} = 0.5$, state estimator with $\rho = 1$.

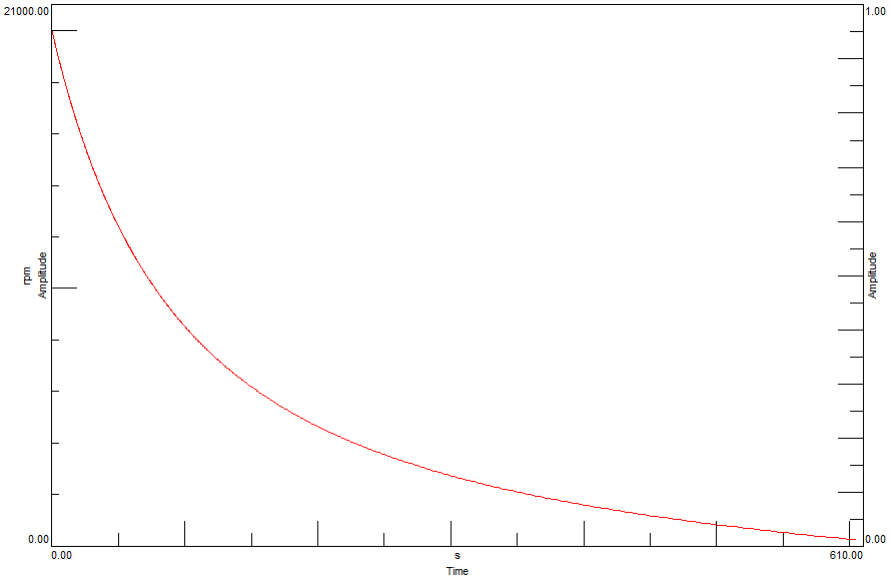

Figure A.6: Tachometer profile during a free run-down test.

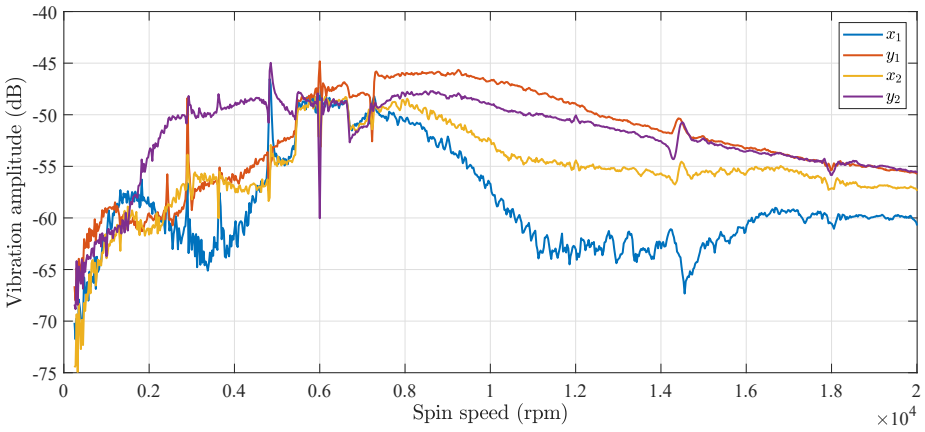

Figure A.7: Unbalance response in $(x_1,\ y_1,\ x_2,\ y_2)$. OF-MPC set with $\alpha_{z,x_1,y_1,x_2,y_2} = 0.5$ and state estimator with $\rho = 1$. The dB values refer to the rotor vibration measured in mm.

Bibliography

[1] Hannes Bleuler et al. *Magnetic bearings: theory, design, and application to rotating machinery*. Springer Science & Business Media, 2009.

[2] Eric H. Maslen and Jerzy T. Sawicki. "Mu-synthesis for magnetic bearings: Why use such a complicated tool?" In: *ASME 2007 international mechanical engineering congress and exposition*. American Society of Mechanical Engineers Digital Collection. 2007, pp. 1103–1112.

[3] Roger Fittro and Carl Knospe. "/spl mu/control of a high speed spindle thrust magnetic bearing". In: *Proceedings of the 1999 IEEE International Conference on Control Applications (Cat. No. 99CH36328)*. Vol. 1. IEEE. 1999, pp. 570–575.

[4] Roger Fittro, Carl Knospe, and L. Scott Stephens. "μ synthesis applied to the compliance minimization of an active magnetic bearing HSM spindle's thrust axis". In: *Machining science and technology* 7.1 (2003), pp. 19–51.

[5] Florian Lösch, Conrad Gähler, and Raoul Herzog. "Low Order μ-Synthesis Controller Design for a Large Boiler Feed Pump Equipped with Active Magnetic Bearings". In: *Proceedings of the 1999 IEEE International Conference on Control Applications*. Vol. 1. 1999, pp. 564–569.

[6] Toru Namerikawa and Masyuki Fujita. "Uncertainty structure and μ-synthesis of a magnetic suspension system". In: *IEEJ Transactions on Electronics, Information and Systems* 121.6 (2001), pp. 1080–1087.

[7] Hannes Bleuler. "Decentralized control of magnetic rotor bearing systems". PhD thesis. ETH Zurich, 1984.

[8] Liangliang Chen et al. "Vibration control for active magnetic bearing high-speed flywheel rotor system with modal separation and velocity estimation strategy". In: *Journal of Vibroengineering* 17.2 (2015), pp. 757–775.

[9] Thomas Schuhmann, Wilfried Hofmann, and Ralf Werner. "Improving operational performance of active magnetic bearings using Kalman filter and state feedback control". In: *IEEE Transactions on Industrial Electronics* 59.2 (2011), pp. 821–829.

[10] Veena Janardhanan and Shyju Mathew. "Improvement of operational performance of active magnetic bearing using nonlinear LQG controller". In: *International Journal of Engineering Research & Technology* 4.7 (2015), pp. 1187–1191.

[11] Mahdi Darbandi et al. "Linear output feedback control of a three-pole magnetic bearing". In: *IEEE/ASME Transactions on Mechatronics* 19.4 (2013), pp. 1323–1330.

[12] Sigurd Skogestad and Ian Postlethwaite. *Multivariable feedback control: analysis and design*. Vol. 2. Wiley New York, 2007.

[13] Fumio Matsumura et al. "State of the Art of Magnetic Bearings: Overview of Magnetic Bearing Research and Applications". In: *JSME International Journal Series C Mechanical Systems, Machine Elements and Manufacturing* 40.4 (1997), pp. 553–560.

[14] Weiyu Zhang and Huangqiu Zhu. "Radial magnetic bearings: An overview". In: *Results in physics* 7 (2017), pp. 3756–3766.

[15] David Q. Mayne. "Model predictive control: Recent developments and future promise". In: *Automatica* 50.12 (2014), pp. 2967–2986.

[16] S. Joe Qin and Thomas A. Badgwell. "A survey of industrial model predictive control technology". In: *Control Engineering Practice* 11.7 (2003), pp. 733–764.

[17] Régis Campos Fama et al. "Predictive control of a magnetic levitation system with explicit treatment of operational constraints". In: *Proceedings of the 18th International Congress of Mechanical Engineering, Ouro Preto, MG,(paper 0560)*. 2005.

[18] Rubens Junqueira Magalhães Afonso and Roberto Kawakami Harrop Galvão. "Predictive control of a magnetic levitation system with infeasibility handling by relaxation of output constraints". In: *ABCM Symposium Series in Mechatronics*. Vol. 3. 2007, pp. 11–18.

[19] Mariana Santos Matos Cavalca, Roberto Kawakami Harrop Galvão, and Takashi Yoneyama. "Robust model predictive control for a magnetic levitation system employing linear matrix inequalities". In: *ABCM Symposium Series in Mechatronics*. Vol. 4. 2009.

[20] Andreas Ulbig et al. "Explicit nonlinear predictive control for a magnetic levitation system". In: *Asian Journal of Control* 12.3 (2010), pp. 434–442.

[21] Thomas Bächle, Sebastian Hentzelt, and Knut Graichen. "Nonlinear model predictive control of a magnetic levitation system". In: *Control Engineering Practice* 21.9 (2013), pp. 1250–1258. ISSN: 0967-0661. DOI: http://dx.doi.org/10.1016/j.conengprac.2013.04.009. URL: http://www.sciencedirect.com/science/article/pii/S0967066113000828.

[22] Martin Klaučo, Martin Kalúz, and Michal Kvasnica. "Real-time implementation of an explicit MPC-based reference governor for control of a magnetic levitation system". In: *Control Engineering Practice* 60 (2017), pp. 99–105.

[23] Cishen Zhang et al. "Model-based predictive control for a compact and efficient flywheel energy storage system with magnetically assisted bearings". In: *2004 IEEE 35th Annual Power Electronics Specialists Conference (IEEE Cat. No. 04CH37551)*. Vol. 5. IEEE. 2004, pp. 3573–3579.

[24] Yao-Wen Tsai et al. "Model Predictive Control Nonlinear System of Active Magnetic Bearings for a Flywheel Energy Storage System". In: *AETA 2015: Recent Advances in Electrical Engineering and Related Sciences*. Springer, 2016, pp. 541–551.

[25] Jie Zhao et al. "Control of a constrained flexible rotor on active magnetic bearings". In: *IFAC-PapersOnLine* 48.28 (2015), pp. 156–161.

[26] Alexander Domahidi, Eric Chu, and Stephen Boyd. "ECOS: An SOCP solver for embedded systems". In: *2013 European Control Conference (ECC)*. IEEE. 2013, pp. 3071–3076.

[27] Bartolomeo Stellato et al. "OSQP: An operator splitting solver for quadratic programs". In: *2018 UKACC 12th International Conference on Control (CONTROL)*. IEEE. 2018, pp. 339–339.

[28] Yang Wang and Stephen Boyd. "Fast evaluation of quadratic control-Lyapunov policy". In: *IEEE Transactions on Control Systems Technology* 19.4 (2010), pp. 939–946.

[29] Jacob Mattingley and Stephen Boyd. "CVXGEN: A code generator for embedded convex optimization". In: *Optimization and Engineering* 13.1 (2012), pp. 1–27.

[30] Eric Chu et al. "Code generation for embedded second-order cone programming". In: *2013 European Control Conference (ECC)*. IEEE. 2013, pp. 1547–1552.

[31] Goran Banjac et al. "Embedded code generation using the OSQP solver". In: *2017 IEEE 56th Annual Conference on Decision and Control (CDC)*. IEEE. 2017, pp. 1906–1911.

[32] Abdelfatah M. Mohamed and Fawzi P. Emad. "Conical magnetic bearings with radial and thrust control". In: *Proceedings of the 28th IEEE Conference on Decision and Control,* IEEE. 1989, pp. 554–561.

[33] Shilei Xu and Jiancheng Fang. "A novel conical active magnetic bearing with claw structure". In: *IEEE Transactions on Magnetics* 50.5 (2013), pp. 1–8.

[34] Heng Zhou et al. "A novel 6/4 conical bearingless switched reluctance motor". In: *2015 18th International Conference on Electrical Machines and Systems (ICEMS)*. IEEE. 2015, pp. 1807–1811.

[35] Arvind Katyayn and Praveen Kumar Agarwal. "Comparative analysis of conical and conventional active magnetic bearings for complete support of a 5-dof rotor system". In: *2017 International Conference on Advances in Mechanical, Industrial, Automation and Management Systems (AMIAMS)*. IEEE. 2017, pp. 53–58.

[36] Y. Jing, Y. Lie, and X. Jing. "Coupled dynamics and control of a rotor-conical magnetic bearing system". In: *Proceedings of the Institution of Mechanical Engineers, Part J: Journal of Engineering Tribology* 220.7 (2006), pp. 581–586.

[37] Chongwon Lee and Ho-seop Jeong. "Dynamic modeling and optimal control of cone-shaped active magnetic bearing systems". In: *Control Engineering Practice* 4.10 (1996), pp. 1393–1403.

[38] Angelo Bonfitto et al. "Turbomolecular pumps on conical active magnetic bearings". In: *Mechanical Engineering Journal* 4.5 (2017), pp. 16–00569.

[39] Lih-Chang Lin and Tzyh-Biau Gau. "Feedback linearization and fuzzy control for conical magnetic bearings". In: *IEEE Transactions on Control Systems Technology* 5.4 (1997), pp. 417–426.

[40] Shi-Jing Huang and Lih-Chang Lin. "Fuzzy modeling and control for conical magnetic bearings using linear matrix inequality". In: *Journal of Intelligent and Robotic systems* 37.2 (2003), pp. 209–232.

[41] Urban Maeder, Francesco Borrelli, and Manfred Morari. "Linear Offset-free Model Predictive Control". In: *Automatica* 45.10 (Oct. 2009), pp. 2214–2222. ISSN: 0005-1098. DOI: 10.1016/j.automatica.2009.06.005. URL: http://dx.doi.org/10.1016/j.automatica.2009.06.005.

[42] Gabriele Pannocchia. "Offset-free tracking MPC: A tutorial review and comparison of different formulations". In: *2015 European Control Conference (ECC)*. IEEE. 2015, pp. 527–532.

[43] Gabriele Pannocchia and James B. Rawlings. "Disturbance models for offset-free model-predictive control". In: *AIChE Journal* 49.2 (2003), pp. 426–437. ISSN: 1547-5905. DOI: 10.1002/aic.690490213. URL: http://dx.doi.org/10.1002/aic.690490213.

[44] Gabriele Pannocchia and Eric C Kerrigan. "Offset-free control of constrained linear discrete-time systems subject to persistent unmeasured disturbances". In: *42nd IEEE International Conference on Decision and Control (IEEE Cat. No. 03CH37475)*. Vol. 4. IEEE. 2003, pp. 3911–3916.

[45] Francesco Borrelli and Manfred Morari. "Offset free model predictive control". In: *2007 46th IEEE Conference on Decision and Control*. IEEE. 2007, pp. 1245–1250.

[46] Manfred Morari and Urban Maeder. "Nonlinear offset-free model predictive control". In: *Automatica* 48.9 (2012), pp. 2059–2067.

[47] Angelo Bonfitto et al. "Offset-Free Model Predictive Control for Active Magnetic Bearing Systems". In: *Actuators*. Vol. 7. 3. Multidisciplinary Digital Publishing Institute. 2018, p. 46.

[48] Graham Goodwin, María M Seron, and José A De Doná. *Constrained control and estimation: an optimisation approach*. Springer Science & Business Media, 2006.

[49] Thomas A. Badgwell and Kenneth R. Muske. "Disturbance model design for linear model predictive control". In: *Proceedings of the 2002 American Control Conference (IEEE Cat. No.CH37301)*. Vol. 2. May 2002, 1621–1626 vol.2. DOI: 10.1109/ACC.2002.1023254.

[50] Gabriele Pannocchia. "Robust disturbance modeling for model predictive control with application to multivariable ill-conditioned processes". In: *Journal of Process Control* 13.8 (2003), pp. 693–701. ISSN: 0959-1524. DOI: https://doi.org/10.1016/S0959-1524(02)00134-8. URL: http://www.sciencedirect.com/science/article/pii/S0959152402001348.

[51] Thomas A. Meadowcroft, George Stephanopoulos, and Coleman Brosilow. "The modular multivariable controller: I: Steady-state properties". In: *AIChE Journal* 38.8 (1992), pp. 1254–1278.

[52] Francesco Borrelli, Alberto Bemporad, and Manfred Morari. *Predictive Control for Linear and Hybrid Systems*. Cambridge University Press, 2017. ISBN: 9781107652873. URL: https://books.google.it/books?id=VswfvgAACAAJ.

[53] Gabriele Pannocchia, Nabil Laachi, and James B Rawlings. "A candidate to replace PID control: SISO-constrained LQ control". In: *AIChE Journal* 51.4 (2005), pp. 1178–1189.

[54] Alberto Bemporad and Panagiotis Patrinos. "Simple and certifiable quadratic programming algorithms for embedded linear model predictive control". In: *IFAC Proceedings Volumes* 45.17 (2012), pp. 14–20.

[55] James Blake Rawlings, David Q Mayne, and Moritz Diehl. *Model Predictive Control: Theory, Computation, and Design*. Nob Hill Publishing, 2017.

[56] Akira Chiba et al. *Magnetic bearings and bearingless drives*. Elsevier, 2005.

[57] Xinwei Song et al. "Axial flow blood pumps". In: *ASAIO journal* 49 (2003), pp. 355–364.

[58] Alexei Filatov, Larry Hawkins, and Patrick McMullen. "Homopolar Permanent-Magnet-Biased Actuators and Their Application in Rotational Active Magnetic Bearing Systems". In: *Actuators*. Vol. 5. 4. Multidisciplinary Digital Publishing Institute. 2016, p. 26.

[59] Shyh-Leh Chen and Cheng-Chi Weng. "Robust control of a voltage-controlled three-pole active magnetic bearing system". In: *IEEE/ASME Transactions on Mechatronics* 15.3 (2010), pp. 381–388.

[60] Myounggyu D. Noh and Eric H. Maslen. "Self-sensing magnetic bearings using parameter estimation". In: *IEEE Transactions on Instrumentation and Measurement* 46.1 (1997), pp. 45–50.

[61] Takeshi Mizuno and Hannes Bleuler. "Self-sensing magnetic bearing control system design using the geometric approach". In: *Control Engineering Practice* 3.7 (1995), pp. 925–932.

[62] Angelo Bonfitto, Andrea Tonoli, and Mario Silvagni. "Sensorless active magnetic dampers for the control of rotors". In: *Mechatronics* 47 (2017), pp. 195–207.

[63] Shuliang Lei and Alan Palazzolo. "Control of flexible rotor systems with active magnetic bearings". In: *Journal of Sound and Vibration* 314.1-2 (2008), pp. 19–38.

[64] Zhaohui Ren and Lyndon S Stephens. "Closed-loop performance of a six degree-of-freedom precision magnetic actuator". In: *IEEE/ASME Transactions on Mechatronics* 10.6 (2005), pp. 666–674.

[65] Herbert Grabner, Siegfried Silber, and Wolfgang Amrhein. "Bearingless torque motor-modeling and control". In: *Proceedings of the 13th International Symposium on Magnetic Bearings (ISMB), Arlington, VA, USA*. 2012, pp. 6–9.

[66] Siegfried Silber et al. "Design aspects of bearingless slice motors". In: *IEEE/ASME transactions on mechatronics* 10.6 (2005), pp. 611–617.

[67] Eric Maslen and Dominick Montie. "Sliding mode control of magnetic bearings: A hardware perspective". In: *Journal of engineering for gas turbines and power* 123.4 (2001), pp. 878–885.

[68] Selim Sivrioglu and Kenzo Nonami. "Sliding mode control with time-varying hyperplane for AMB systems". In: *IEEE/ASME Transactions On Mechatronics* 3.1 (1998), pp. 51–59.

[69] Kenzo Nonami, Weidong He, and Hidekazu Nishimura. "Robust control of magnetic levitation systems by means of Hinf control/μ-synthesis". In: *JSME international journal. Ser. C, Dynamics, control, robotics, design and manufacturing* 37.3 (1994), pp. 513–520.

[70] Aleksander B. Hać and Masayoshi Tomizuka. "Application of learning control to active damping of forced vibration for periodically time variant systems". In: *Journal of Vibration and Acoustics* 112.4 (1990), pp. 489–496.

[71] Felix Betschon and Carl R. Knospe. "Reducing magnetic bearing currents via gain scheduled adaptive control". In: *IEEE/ASME transactions on mechatronics* 6.4 (2001), pp. 437–443.

[72] Jeen-Gwo Tsao, Ling-Tarng Sheu, and Li-Farn Yang. "Adaptive synchronization control of the magnetically suspended rotor system". In: *Dynamics and Control* 10.3 (2000), pp. 239–253.

[73] Amor Chowdhury and Andrej Sarjaš. "Finite element modelling of a field-sensed magnetic suspended system for accurate proximity measurement based on a sensor fusion algorithm with unscented Kalman filter". In: *Sensors* 16.9 (2016), p. 1504.

[74] Luis M. Castellanos et al. "Identification of Force-Displacement and Force-Current Factors in an Active Magnetic Bearing System". In: *Proceedings of the 18th Annual IEEE International Conference on Electro Information Technology, Rochester, MI, USA*. 2018, pp. 3–5.

[75] James B Rawlings. "Tutorial overview of model predictive control". In: *IEEE control systems magazine* 20.3 (2000), pp. 38–52.

[76] Xue Wang et al. "Design and application of offset-free model predictive control disturbance observation method". In: *Journal of Control Science and Engineering* 2016 (2016).

[77] Seok-Kyoon Kim et al. "Offset-free model predictive control for the power control of three-phase AC/DC converters". In: *IEEE Transactions on Industrial Electronics* 62.11 (2015), pp. 7114–7126.

[78] Frank A. Bender et al. "Modeling and offset-free model predictive control of a hydraulic mini excavator". In: *IEEE Transactions on Automation Science and Engineering* 14.4 (2017), pp. 1682–1694.

[79] Pablo Zometa, Markus Kögel, and Rolf Findeisen. "μAO-MPC: a free code generation tool for embedded real-time linear model predictive control". In: *2013 American Control Conference*. IEEE. 2013, pp. 5320–5325.

[80] Giancarlo Genta. *Vibration of structures and machines: practical aspects*. Springer Science & Business Media, 2012.

[81] Kenneth R. Muske and Thomas A. Badgwell. "Disturbance modeling for offset-free linear model predictive control". In: *Journal of Process Control* 12.5 (2002), pp. 617–632.

[82] Alberto Bemporad and Manfred Morari. "Robust model predictive control: A survey". In: *Robustness in identification and control*. Springer, 1999, pp. 207–226.

[83] Daniel Simon and Johan Löfberg. "Stability analysis of model predictive controllers using mixed integer linear programming". In: *2016 IEEE 55th Conference on Decision and Control (CDC)*. IEEE. 2016, pp. 7270–7275.

[84] John Doyle and Guter Stein. "Robustness with observers". In: *IEEE transactions on automatic control* 24.4 (1979), pp. 607–611.

[85] Brian Anderson and John Moore. *Optimal control: linear quadratic methods*. Courier Corporation, 2007.

[86] Alessandro Alessio and Alberto Bemporad. "A survey on explicit model predictive control". In: *Nonlinear model predictive control*. Springer, 2009, pp. 345–369.

[87] Yang Wang and Stephen Boyd. "Fast model predictive control using online optimization". In: *IEEE Transactions on control systems technology* 18.2 (2009), pp. 267–278.

[88] Jacob Mattingley, Yang Wang, and Stephen Boyd. "Code generation for receding horizon control". In: *2010 IEEE International Symposium on Computer-Aided Control System Design*. IEEE. 2010, pp. 985–992.

[89] Dan Simon. *Optimal state estimation: Kalman, H infinity, and nonlinear approaches*. John Wiley & Sons, 2006.

[90] Standard ISO. "Mechanical vibration-Vibration of rotating machinery equipped with active magnetic bearings-part 3: Evaluation of stability margin". In: *ISO 14839-3: 2006 (E)* (2004).

[91] Giancarlo Genta. *Vibration dynamics and control*. Springer, 2009.

[92] Alberto Bemporad. "Hybrid toolbox–User's guide". In: (2003).

[93] Michal Kvasnica et al. "Multi-parametric toolbox (MPT)". In: *International Workshop on Hybrid Systems: Computation and Control*. Springer. 2004, pp. 448–462.

[94] Lars Blackmore. "Autonomous precision landing of space rockets". In: *Frontiers of Engineering: Reports on Leading-Edge Engineering from the 2016 Symposium*. National Academies Press. 2017.

This Ph.D. thesis has been typeset by means of the TEX-system facilities. The typesetting engine was pdfLATEX. The document class was `toptesi`, by Claudio Beccari, with option `tipotesi=scudo`. This class is available in every up-to-date and complete TEX-system installation.